Extraneous argon in high-pressure metamorphic rocks: Distribution, origin and transport in the Cycladic Blueschist Unit (Greece)

Valentin Laurent, Benjamin Huet, Loic Labrousse, Laurent Jolivet, Patrick Monie, Romain Augier

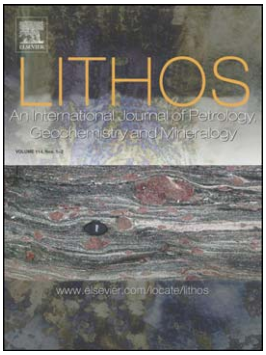

Extraneous argon in high-pressure metamorphic rocks: Distribution, origin and transport in the Cycladic Blueschist Unit (Greece)

Valentin Laurent, Benjamin Huet, Loïc Labrousse, Laurent Jolivet, Patrick Monie, Romain Augier

PII: S0024-4937(16)30446-7
DOI: doi:10.1016/j.lithos.2016.12.013
Reference: LITHOS 4174

To appear in: *LITHOS*

Received date: 13 July 2016
Accepted date: 15 December 2016

Please cite this article as: Laurent, Valentin, Huet, Benjamin, Labrousse, Loïc, Jolivet, Laurent, Monie, Patrick, Augier, Romain, Extraneous argon in high-pressure metamorphic rocks: Distribution, origin and transport in the Cycladic Blueschist Unit (Greece), *LITHOS* (2016), doi:10.1016/j.lithos.2016.12.013

Extraneous argon in high-pressure metamorphic rocks: Distribution, origin and transport in the Cycladic Blueschist Unit (Greece)

Valentin LAURENT[1,2,3], Benjamin HUET[4], Loïc LABROUSSE[5,6], Laurent JOLIVET[1,2,3], Patrick MONIE[7], Romain AUGIER[1,2,3]

[1]Université d'Orléans, ISTO, UMR 7327, 45071, Orléans, France

[2]CNRS/INSU, ISTO, UMR 7327, 45071 Orléans, France

[3]BRGM, ISTO, UMR 7327, BP 36009, 45060 Orléans, France

[4]Department of Geodynamics and Sedimentology, University of Vienna, Althanstrasse 14, 1090 Vienna, Austria. Now at Department of Hard Rock Geology, Geological Survey of Austria, Neulinggasse 38, 1030 Vienna, Austria

[5]UPMC Université Paris 06, UMR 7193, ISTeP, 4 place Jussieu, 75252 Paris cedex 05, France

[6]CNRS, UMR 7193, ISTeP, 4 place Jussieu, 75252 Paris cedex 05, France

[7]Géosciences Montpellier, UMR 5243, Université Montpellier, Place Bataillon, 34095 Montpellier, France

valentin.laurent@univ-orleans.fr (corresponding author), benjamin.huet@univie.ac.at, loic.labrousse@upmc.fr, laurent.jolivet@univ-orleans.fr, patrick.monie@gm.univ-montp2.fr, romain.augier@univ-orleans.fr

Abtract

The $^{40}Ar/^{39}Ar$ geochronological technique has significantly contributed to the study of crustal deformation. However, the frequent occurrence of extraneous argon in high-pressure terrains can make the interpretation of $^{40}Ar/^{39}Ar$ ages problematic. This contribution attempts to: i) characterize the distribution and origin of extraneous argon in the Cycladic Blueschist Unit (CBU, Greece) by applying the $^{40}Ar/^{39}Ar$ dating technique on three Cycladic islands, Syros, Tinos and Ios, which span a complete transect of the CBU and ii) discuss regional implications for the tectonometamorphic evolution of the CBU. Our results, combined with ages available in the literature, show that periods of peak-burial conditions (55-49 Ma) and syn- (45-38 Ma) to post-orogenic exhumation (37-21 Ma) are well constrained in the CBU by

the $^{40}Ar/^{39}Ar$ method. Moreover, Variscan apparent ages are preserved in the Cycladic basement of Ios, indicating that the $^{40}Ar/^{39}Ar$ system was not completely reset during the Eocene metamorphic episode. Additionally, our $^{40}Ar/^{39}Ar$ data show that the occurrence of extraneous argon is heterogeneously distributed in the CBU. While high-pressure rocks of Syros and Tinos are only locally affected, extraneous argon is clearly evidenced in the CBU of Ios, yielding geologically meaningless ages up to 900 Ma. On each island, the most affected ages were obtained in microstructures where fluid circulation is enhanced such as shear bands or strain shadows around garnets. We suggest that the Cycladic Basement, a polymetamorphic continental unit, behaved as an argon reservoir that has been mobilized by fluid circulation at the Eocene. These argon-enriched fluids have then heterogeneously contaminated metamorphic rocks when percolating through the CBU. Finally, we claim that a minimum closure temperature of 550°C must be accepted for the phengites of the CBU and conclude that volume diffusion is not the main process resetting the argon isotopic system in high-pressure rocks compare to recrystallization enhanced by fluid circulation and deformation.

1. Introduction

Extraneous argon is usually thought to represent a frequent drawback in dating high-pressure and low-temperature (HP-LT) metamorphic rocks with the $^{40}Ar/^{39}Ar$ method. By definition, extraneous argon is the additional ^{40}Ar leading to measured $^{40}Ar/^{36}Ar$ ratios in excess of atmospheric initial values (see Kelley, 2002 for a review). Two forms of extraneous argon have been identified in metamorphic rocks, i) inherited argon corresponds to *in situ* contamination of radiogenic ^{40}Ar deriving from K-rich minerals of the rock system (e.g.

Giorgis et al., 2000; Di Vincenzo et al., 2006), ii) excess argon is additional to atmospheric argon and corresponds to ^{40}Ar incorporated into the mineral lattice and/or as fluid inclusion by other processes than *in situ* radioactive decay of ^{40}K (i.e. from outside the system), for example by incorporation of external argon-enriched fluids (e.g. Qiu and Wijbrans, 2006; Warren et al., 2011). Units of oceanic affinity, which underwent a single HP metamorphic cycle in the subduction zone, are often less affected by the presence of inherited argon than polymetamorphic continental units (Arnaud and Kelley, 1995; Scaillet, 1996). The main reason is that felsic continental basement rocks do not easily record HP parageneses because they have often been dehydrated by earlier metamorphic reactions and thus need an external fluid infiltration to react and then to record metamorphism (Proyer, 2003). In the absence of a free aqueous fluid phase, phengite can trap inherited argon from the breakdown of precursor K-rich minerals (e.g. muscovite, K-feldspar), even if this breakdown occurred at temperature exceeding the range of commonly accepted closure temperature for argon diffusion in white micas (400-450 °C, e.g. Villa, 1998; Harrison et al., 2009) of several hundred degrees (e.g. Giorgis et al., 2000). On the contrary, mafic lithologies of oceanic affinity are often characterized by continuous dehydration reactions along the prograde path, releasing large amounts of fluids and allowing the system to evolve in open conditions (Scaillet, 1996; Itaya et al., 2011). Inherited argon released from mineral precursors may be evacuated by fluid circulation along damaged zones, resetting the argon isotopic system of each mineral phase. However, mafic lithologies characterized by small porosities maintained by low permeability during subduction can also retain *in situ* protolith-derived inherited argon under closed system conditions (Smye et al., 2013).

The Cycladic Blueschist Unit (CBU) is a HP-LT metamorphic belt that experienced a single burial and exhumation cycle in the Hellenic subduction zone. Previous $^{40}Ar/^{39}Ar$ data (Maluski et al., 1987; Bröcker et al., 1993, 2013; Putlitz et al., 2005; Lister and Forster, 2016)

show that this unit, largely composed of lithologies of oceanic affinity (metabasalts, metagabbros, metasediments; e.g. van der Maar, 1980; Melidonis, 1980), is poorly affected by the presence of extraneous argon, making the CBU an ideal case study to better understand the significance of $^{40}Ar/^{39}Ar$ ages in HP metamorphic context.

Our study aims at applying the $^{40}Ar/^{39}Ar$ dating technique on three Cycladic islands, Syros, Tinos and Ios, which span a complete transect of the CBU, from the basal thrust over the Cycladic Continental Basement (CCB) observed on Ios (Huet et al., 2009) to the upper detachments responsible for their exhumation, the Vari Detachment (Trotet et al., 2001; Soukis and Stöckli, 2013) and the North Cycladic Detachment System (Jolivet et al., 2010). The combination of our results with data available in the literature shows that periods of peak P-T conditions and syn- to post-orogenic exhumation are well constrained by $^{40}Ar/^{39}Ar$ conventional step-heating experiments on phengite single grains or populations. This evolution helps interpreting *in-situ* $^{40}Ar/^{39}Ar$ ages on phengites, which show a more complex signal. Our results imply that the presence of extraneous argon in the CBU is heterogeneous and closely correlated to the vicinity of the CCB, a continental unit affected by a polymetamorphic history. Finally, a synthesis of petrostructural and geochronological studies conducted in the Aegean domain combined with our new data allows proposing a geodynamic scenario of the tectonometamorphic evolution of this domain from late burial in the subduction channel to final exhumation.

2. Geological setting

2.1. Aegean domain

The tectonometamorphic evolution of the Aegean domain can be summarized in two main stages (Jolivet and Brun, 2010; Ring et al., 2010). First, from late Cretaceous to early Eocene, subduction and collision of Africa with Eurasia formed the Hellenides-Taurides chain

(Bonneau and Kienast, 1982). During this episode, the crust was thickened and HP-LT metamorphic units, such as the CBU, started to exhume between a top-to-the south thrust at the base and top-to-the east/northeast syn-orogenic detachments at the top (Trotet et al., 2001; Huet et al., 2009; Augier et al., 2015). Then, as a consequence of the acceleration of African slab rollback, post-orogenic extension affected the previously thickened crust from ca. 35 Ma in the Aegean Domain while the frontal zones were still under compression in Crete and the Peloponnese (Jolivet and Brun, 2010; Ring et al., 2010). In the Cyclades, back-arc extension was accommodated by regional-scale detachments such as the North Cycladic Detachment System (NCDS) or the West Cycladic Detachment System (WCDS) (Fig. 1a; Jolivet et al., 2010; Grasemann et al., 2012).

In this study, $^{40}Ar/^{39}Ar$ analyses were performed over three islands located in different positions of the Aegean domain: Tinos along the northern margin of the Cyclades, Syros in the centre and Ios in the south. They also show different structures recording different stages of the CBU evolution that is described in the following.

2.2. Geology of Syros

Located in the central part of the Aegean (Fig.1a), most of Syros surface exposes the CBU except for the southeast where the Vari Unit occurs (Fig. 1b). This unit, correlated to the Upper Cycladic Unit (UCU) where HP rocks have not been recognized, is composed of greenschist rocks and the Vari orthogneiss (Fig. 1b; Soukis and Stöckli, 2013; Laurent et al., 2016). The CBU stacks in Syros can be internally subdivided in three subunits, all bounded by top-to-the east shear zones and characterized by their lithology and predominant metamorphic facies that are from bottom to top (Fig. 1b, Laurent et al., 2016):

1) Posidonia Subunit, composed of the structurally lower gneiss of Komito overlain by albitic micaschists with intercalated boudins of metabasite and thin marble layers. This subunit has been pervasively overprinted in greenschist-facies conditions and only few blueschist- and eclogite-facies parageneses are observed within the core of metabasite boudins. The Achladi-Delfini Shear Zone separates the Posidonia Subunit from the upper Chroussa Subunit.

2) Chroussa Subunit, composed of a lithostratigraphic sequence of alternating micaschists, thick marble layers and metabasites. In this subunit, some areas are overprinted in the greenschist-facies, while other places show well-preserved eclogite- and blueschist-facies parageneses. The Kastri Shear Zone separates the Chroussa Subunit from the upper Kampos Subunit.

3) Kampos Subunit, which is mainly composed of a mélange of metabasites wrapped in serpentinites and minor metasediments. Eclogite- and blueschist-facies parageneses are spectacularly preserved and mostly escaped significant retrogression. The top-to-the east Vari Detachment caps the Kampos Subunit, and at larger scale separates the top of the CBU on Syros from the upper Vari Unit (Trotet et al., 2001; Soukis and Stöckli, 2013; Laurent et al., 2016).

Eclogite-facies parageneses are recognized within all three subunits of the CBU (Laurent et al., 2016). Despite their contrasting degree of retrogression, all subunits reached similar HP-LT metamorphic peak conditions at ca. 20 kbar and 550 °C (Trotet et al. 2001). Exhumation of the CBU in Syros was accommodated along large-scale shear zones by a top-to-the east/northeast sense of shear from the depth of the eclogite-facies all the way to the depth of the greenschist-facies (Trotet et al., 2001; Laurent et al., 2016). Studies attempting to date the maximum burial led to ca. 53-42 Ma ages (Tomaschek et al., 2003; Putlitz et al., 2005; Lagos et al., 2007; Lister and Forster, 2016). The final, mostly syn-kinematic

retrogression in the greenschist-facies conditions has been dated as late as at 25 to 21 Ma (Bröcker et al., 2013). These ages are presented with more details in the discussion.

2.3. Geology of Tinos

Tinos Island is located in the northern part of the Cyclades, 15 km northeast of Syros (Fig. 1a). This island is mainly composed of the CBU except for the Upper unit that is composed of serpentinite, metagabbros and minor metasediments (Fig. 1c; Melidonis, 1980; Avigad and Garfunkel, 1989). The Upper unit belongs to the UCU that was metamorphosed in the amphibolite- and greenschist-facies at ca. 70 Ma and escaped significant record of the alpine HP-LT event (Avigad and Garfunkel, 1989; Bröcker and Franz, 1998; Katzir et al., 1996). The Tinos Detachment, belonging to the NCDS, separates this unit from the lower CBU (Fig. 1c, e.g. Jolivet and Patriat, 1999).

CBU in Tinos is represented by a sequence of metapelites, marbles and metabasites (Fig. 1c). The structurally lowest rocks are dolomitic marbles, which were previously interpreted either as the base of the CBU (Mélidonis 1980; Parra et al., 2002; Bröcker and Franz, 2005) or as part of the external Gavrovo-Tripolitza Nappe also cropping out in Evia and continental Greece (Avigad and Garfunkel, 1989). A gradient of greenschist-facies retrogression is observed when approaching the Tinos Detachment, from preserved eclogites and blueschists to the southwest toward strongly retrograded rocks to the northeast (Jolivet and Patriat, 1999; Parra et al., 2002). Additionally, a gradient of finite deformation is observed with evolution from a coaxial deformation at the base of the CBU toward a highly non-coaxial deformation at the top, associated with top-to-the-northeast sense of shear within the Tinos Detachment (Jolivet and Patriat, 1999; Mehl et al., 2005). Metamorphic peak P-T conditions in the CBU were estimated at 18-15 kbar for 500-550 °C, whereas initiation of

greenschist-facies overprint is estimated at 7-9 kbar and 450-500 °C (Bröcker et al, 1993; Parra et al., 2002). $^{40}Ar/^{39}Ar$ and Rb-Sr ages on phengites constrain the HP metamorphic episode between 55-40 Ma and the period of retrogression in the greenschist-facies between 25 and 18 Ma (Bröcker et al., 1993; Bröcker and Franz, 1998).

Finally, a Miocene granodiorite (17-14 Ma; e.g. Altherr et al., 1982; Bröcker and Franz, 2000; Brichau et al., 2007), observed in the east of Tinos (Fig. 1c), seals the ductile deformation. This late-tectonic intrusion through the Tinos Detachment induced contact metamorphism in both the CBU and the UCU (Avigad and Garfunkel, 1989; Bröcker and Franz, 2000).

2.4. Geology of Ios

The geological structure of Ios is classically described as a dome structure cored by the lower CCB and mantled by the CBU (Fig. 1d, e.g. van der Maar, 1980; Huet et al., 2009).

The CCB is mainly composed of a variably deformed and metamorphosed Variscan granite core surrounded by garnet-micaschists (Fig. 1d, van der Maar, 1980). The amphibolite-facies metamorphism, dated at ca. 310 Ma in the garnet-micaschist series, relates to the pre-alpine history of the CCB (van der Maar, 1980; Henjes-Kunst and Kreuzer, 1982; Baldwin and Lister, 1998). Even though HP-LT mineralogical index such as glaucophane or clinopyroxene-garnet association have been described (van der Maar, 1980; Henjes-Kunst and Kreuzer, 1982), the peak P-T metamorphic conditions are poorly constrained with estimates ranging from 25 kbar – 540 °C (Perraki and Mposkos, 2001) to 11 kbar – 475 °C (Gupta and Bickle, 2004).

The overlying CBU is composed of marble, metapelite and metabasite (Fig. 1d, van der Maar, 1980). HP-LT metamorphic rocks such as eclogite and blueschist are locally

preserved and are also overprinted in the greenschist-facies conditions (van der Maar, 1980; van der Maar and Jansen, 1983). Peak metamorphic conditions of 18.5 ± 3 kbar for 510 ± 20 °C (Huet, 2010) were constrained between 50 and 40 Ma by K-Ar and $^{40}Ar/^{39}Ar$ dating (van der Maar and Jansen, 1983; Baldwin and Lister, 1998). Using the same radiochronometers, the greenschist retrogression was dated between 25-30 Ma and correlated to the regional Oligo-Miocene LP-HT event (van der Maar and Jansen, 1983; Baldwin and Lister, 1998).

The contact between the CCB and the CBU was first described as a top-to-the south extensional shear zone, the South Cycladic Shear Zone (SCSZ, Lister et al., 1984). More recently, two main tectonometamorphic events have been described (Huet et al., 2009; Augier et al., 2015), i) a first penetrative, top-to-the south sense of shear was contemporaneous with overthrusting of the CBU on the CCB at ca. 35 Ma, ii) a second extensional top-to-the north shearing has been observed mainly in the CBU correlated with the Oligo-Miocene post-orogenic extension stages (Huet et al., 2009).

3. Analytical methods

$^{40}Ar/^{39}Ar$ dating combined direct *in-situ* analyses of phengite on polished 0.5 mm thick rock-sections and conventional laser-probe step-heating technique performed on phengite single grains and concentrates. Single grains of mica were handpicked in fraction 0.5-1 mm. Only single grains with no apparent deformation and inclusion were kept for further processing (Fig. 2). For dating populations, phengites were concentrated from the fraction 0.25-0.5 mm using a Frantz magnetic separator. Separates were then washed in acetone, ethanol and distilled water and dried at 80 °C in oven before packing into aluminium foils for irradiation. All samples were irradiated at McMaster (Hamilton, Canada) and analysed at Géosciences Montpellier (Université de Montpellier 2, France, see Monié and

Agard (2009) and Augier et al. (2005) for analytical details). Irradiation flux was monitored using the sanidine FCT standard with an age of 28.02 ± 0.28 Ma (Renne, 1998). The $^{40}Ar/^{39}Ar$ isotopic data are presented in supplementary material.

Grains that were not irradiated were mounted with double-stick conductive carbon tape. They were then imaged with a scanning electron microscope (SEM) and mineral chemical compositions were determined using a CAMECA SX100 electron probe micro-analyser at ISTEP laboratory (Paris, France, see Yamato et al. (2007) for analytical details). Cores and rims of eight grains per sample were analysed. The chemical composition of populations and *in-situ* dated phengites was analysed in thin-sections realised with the mirror-half of rock section used for *in-situ* dating, allowing correlation between microstructural position, chemistry and ages. The phengite chemistry is presented on X_{Mg}-Si (per formula unit) diagrams.

4. Sampling strategy, samples description and phengite chemistry

Syros is the island where HP parageneses are best preserved from greenschist-facies retrogression and where peak metamorphic conditions were dated with U/Pb, Lu/Hf and Rb-Sr geochronology (Tomaschek et al., 2003; Lagos et al., 2007; Cliff et al., 2016). Samples from this island are therefore likely to provide constraints on the HP evolution of the CBU and the behaviour of the K/Ar system at HP conditions. Conversely, rocks from Tinos were selected along the greenschist-facies strain gradient record in the footwall of the NCDS to constrain the age of the syn-kinematic retrogression during back-arc extension. Sampling on Tinos therefore offers the opportunity to bring further time-constraints on the NCDS evolution, from initiation to deactivation, and better understand the K/Ar system in such an environment. Rocks from Ios were selected in the vicinity of the contact between the CBU and the CCB, allowing dating first the overthrusting of the CBU on the CCB and second,

constraining its late-orogenic top-to-the north reactivation. Moreover, the CCB is mainly composed of continental basement rocks and thus the potential link between these lithologies and the presence of extraneous argon in phengites was studied in details. In the following, a petrostructural description of each dated sample is presented. Mineralogy of all analysed samples is presented in Table 1.

4.1. Syros

Eight samples were selected among rocks collected on Syros. These samples are all located on the geological map and on a synthetic cross-section (Figs. 1b, 3a). S07-14 and S07-16 samples were selected in the northern part of Syros where HP parageneses are best preserved (Fig. 1b).

Samples S07-01, S07-02, S07-04, S07-04bis and S07-Jojo were sampled in the southern coast of Syros, near Cape Katerghaki (see location in Fig. 1b). Along this outcrop, retrogression of eclogite in blueschist-facies conditions is associated with top-to-the east shearing (Laurent et al., 2016). Phengite grains from S07-01 micaschist show dispersed chemical compositions (Fig. 3c). S07-02 is a blueschist-facies metabasite showing homogeneous phengite composition (Fig. 3c). S07-04 and S07-04bis are eclogites that are slightly retrogressed in blueschist-facies conditions. Phengite composition of S07-04 shows a systematic decrease of X_{Mg} from core to rim (Fig. 3c). Sample S07-Jojo is an eclogite that is crosscut by blueschist-facies top-to-the east shear bands consisting of glaucophane, quartz, calcite and phengite (Fig. 3b, Table 1). Phengite composition is similar in the eclogitic foliation and shear bands (Fig. 3c).

Sample S07-17 is a metapelite collected near Komito (see location in Fig. 1b) and corresponds to the basal part of the CBU where greenschist-facies retrogression is pervasive

(Fig. 3a). The analysed phengites show homogeneous chemical composition with some phengite cores showing lower Si value (Fig. 3c).

4.2. Tinos

Sixteen samples from Tinos were analysed and dated. Most of them were collected on the same outcrops as those studied by Parra et al. (2002) for determining the P-T path of the CBU on Tinos. These samples are all located on a geological map and a synthetic cross-section of the island (Figs. 1c, 4a).

T07-07 and T07-09, respectively a micaschist and a calcschist (Table 1), were sampled along the southwest coast of Tinos (Fig. 4a). In thin section, T07-07 shows discrete top-to-the northeast shear bands marked by chlorite and phengite. Phengite composition within the foliation and within shear bands differs significantly (Fig. 4d). Analysed single grains of T07-09 show homogeneous chemical composition from core to rim except for one core analysis (Fig. 4d).

T07-10a, T07-10b, T07-11, T07-13, T07-14 and T07-15bis were sampled along the road south of the Isternia Pass, in an outcrop where HP parageneses are well preserved (Figs. 4a, 4b, Table 1). Sample T07-10a is a vein transposed into the foliation and deformed by top-to-the northeast shear bands. Chemical analyses of phengites indicate constant composition of single grains (Fig. 4d). Sample T07-10b is a micaschist hosting the T07-10a vein and is intensely affected by top-to-the northeast shearing. Chemical analyses indicate that phengite have homogeneous compositions from core to rim (Fig. 4d). Sample T07-11 is a blueschist-facies metabasite, in which phengite shows homogeneous composition except for one core analysis (Fig. 4d). T07-13 is a blueschist-facies metabasite showing minor shearing deformation. Chemical composition of phengite is constant in this sample except for one core

analysis (Fig. 4d). T07-14 is also a blueschist-facies metabasite affected by strong top-to-the-northeast shear deformation. Garnet and glaucophane is partially replaced by chlorite, showing retrogression in greenschist-facies conditions (see detailed mineralogy in Table 1). Phengite grains show identical composition from core to rim (Fig. 4d). Sample T07-15bis is a micaschist where strain shadows around garnets indicate top-to-the NE sense of shear. Chemical analyses show that Si content of phengite is higher in the foliation and pressure shadows than in shear bands (Fig. 4d).

T07-16 sample corresponds to a HP-micaschist partially overprinted in the greenschist-facies conditions collected at the boundary between well preserved and completely overprinted HP metamorphic rocks (Fig. 5d). Here again, the greenschist-facies retrogression appears coeval with top-to-the northeast shearing. Chemical composition of phengite grains is constant from core to rim. However, recrystallized phengites in micro-scale shear bands have lower Si and X_{Mg} values (Fig. 5e).

T07-25 is a micaschist sampled near Kato Pyrgos (see location on Fig. 4a). Chemical analyses of phengite grains show scattered Si and X_{Mg} values without clear core-rim zonation (Fig. 5e).

Samples T07-24, T07-22, T07-19 and T07-18 come from Planitis islet just below the contact between the CBU and Upper Unit (Fig. 5a). These samples were collected within the detachment zone and are affected by intense top-to-the northeast shearing. T07-24 is a micaschist sampled at the top of a thick marble layer (Fig. 5a). Rims of phengite grains have homogeneous composition while core compositions are more dispersed (Fig. 5e). T07-22 is an intensely sheared vein sampled a few meters below the detachment (Fig. 5a). Analysed phengites have homogeneous Si content and more dispersed X_{Mg} values (Fig. 5e). T07-19 is a micaschist collected two meters below the detachment plane (Fig. 5a). Foliation-forming phengites or phengite inclusions in pyrite crystals have distinct composition from

recrystallized newly-formed phengites in shear bands (Fig. 5e). T07-18 is a marble sampled in the Upper Unit, ca. 10 meters above the detachment (Fig. 5a). Slightly distinct compositions have been analysed for phengites in foliation and in shear bands (Fig. 5e).

Sample T07-27 is a micaschist collected near Kolympitra Bay (see location in Fig. 1c) and is structurally located at ca. 100 meters below the detachment plane. It belongs to a level of interbedded metasediments within intensely folded marbles (Fig. 5b). Core-rim analyses of phengite grains show heterogeneous compositions (Fig. 5e).

Sample T07-30 was collected at the top of the granodioritic intrusion of Tinos (Fig. 1c). Here, aplitic sills are injected within the foliation of rocks of the Upper Unit and deformed by syn-kinematic normal faults (Fig. 5c). This sample shows no apparent shear deformation.

4.3. Ios

Four samples have been dated in Ios. They are located on a geological map of the island and a synthetic cross-section (Figs. 1d, 6a).

I07-23 is a micaschist sampled from the CCB, a few meters below the contact with the CBU (Fig. 6a). In this outcrop, top-to-the south sense of shear is partly overprinted by late extensional top-to-the north shear bands. Analysed grains of white mica show variable chemical compositions defining two distinct groups, muscovites with a low Si content and phengites with higher Si content (Fig. 6b). Muscovites are likely to be inherited from the ante-alpine amphibolite-facies metamorphism recorded in the CCB (Henjes-Kunst and Kreuzer, 1982), while phengites are associated with alpine deformation (Huet et al., 2009).

I07-122 is a micaschist collected in the CBU, tens of meters above the contact with the CCB, and affected by top-to-the south shear bands (Fig. 6a). Chemical composition of

phengites is correlated to their microstructural position (Fig. 6b). Phengites with high Si content are located within the foliation and those with intermediate Si are observed within shear bands in association with paragonite.

Samples I07-15 and I07-18 were collected in the CBU, in blueschist-facies mafic boudins affected by top-to-the south shearing (Fig. 6a). Chemical analyses of these samples indicate that white micas have paragonite composition except for one core analysis of I07-15 that corresponds to phengite composition with low Na content (Fig. 6b).

5. $^{40}Ar/^{39}Ar$ results

5.1. Syros

Two single grains of S07-14 were analysed by $^{40}Ar/^{39}Ar$ step-heating yielding reproducible age patterns (Fig. 7a). The age spectrum of the single grain S07-$14_{(1)}$ shows a plateau age of 49.44 ± 2.62 Ma for 70% of ^{39}Ar released (Fig. 7a). Consistently, all temperature steps of the single grain S07-$14_{(2)}$ yield a flat age spectrum characterized by a plateau age of 50.84 ± 0.84 Ma (Fig. 7a). $^{40}Ar/^{39}Ar$ step-heating experiments on a concentrate of S07-16 yield a decreasing age spectrum defining a flat portion at 55.04 ± 0.56 Ma for 75% of ^{39}Ar released (Fig. 7a). The inverse isochron yields an age of 56.70 ± 1.30 Ma with an atmospheric initial $^{40}Ar/^{36}Ar$ of 312.3 ± 14.0 (MSWD = 26.27). The high MSWD value is the consequence of very low error on the different isotopic ratios and of the high radiogenic content. The presence of a significant atmospheric component released during the first heating steps is common in $^{40}Ar/^{39}Ar$ analyses, a component that is weakly bound to the mineral surface and possibly in fluid inclusions (Qiu and Wijbrans, 2006).

One single grain of S07-01, S07-04 and S07-04bis samples and two single grains of S07-02 were analysed by laser-heating experiments (Fig. 7a). While the first temperature steps of the age spectrum of S07-01 are discordant, a plateau age at 41.65 ± 0.95 Ma is

defined for about 70% of ^{39}Ar released (Fig. 7a). The important error on final temperature steps is linked to a high atmospheric contribution from mineral inclusions. All temperature steps of single grain S07-02$_{(1)}$ yield a flat age spectrum with a plateau age at 43.51 ± 0.56 Ma (Fig. 7a). The second single grain S07-02$_{(2)}$ yields a similar flat age spectrum characterized by a plateau age at 41.95 ± 0.77 Ma for 90% of ^{39}Ar released (Fig. 7a). While the first temperature steps of the age spectrum of S07-04 are contaminated by weakly bound excess argon, the remaining 90% of ^{39}Ar released gives a plateau age of 44.89 ± 0.65 Ma (Fig. 7a). The age spectrum of S07-04bis yields apparent ages ranging from 44 to 40 Ma with the last four steps defining a plateau age of 40.29 ± 0.73 Ma for 85% of ^{39}Ar released (Fig. 7a).

S07-Jojo sample was analysed by the ^{40}Ar/^{39}Ar *in-situ* laser ablation technique (Fig. 7b). Most of measured ^{40}Ar/^{39}Ar apparent ages are comprised between 50 and 47 Ma, without any distinction between phengites located in the eclogitic foliation or in the blueschist-facies shear band (Fig. 7b). Two apparent ages at 55.33 ± 3.48 Ma and 42.47 ± 2.03 Ma from the shear band fall out of this range. An inverse isochron, excluding these two points, yields an age of 48.5 ± 1.10 Ma with an atmospheric initial ^{40}Ar/^{36}Ar of 309.4 ± 42.2 (MSWD = 0.16, Fig. 7b).

One single grain separated from sample S07-17 and analysed by step-heating yields an age spectrum characterized by a significantly younger plateau age of 26.12 ± 0.52 Ma for 80% of ^{39}Ar released (Fig. 7a).

5.2 Tinos

One single grain of T07-10a and T07-10b, two distinct grains of T07-11 and T07-13 and three grouped grains of T07-14 were dated by ^{40}Ar/^{39}Ar step-heating technique (Fig. 8a). Additionally, *in-situ* laser ablation was conducted on a rock-section of sample T07-15bis (Fig. 8a). The single grain of T07-10a yields a flat age spectrum characterized by a plateau age of

34.48 ± 0.99 Ma for 100% of ^{39}Ar released in five steps (Fig. 8a). The single grain of T07-10b yields a slightly increasing age spectrum at the end of degassing and a plateau age of 44 Ma for about 65% of ^{39}Ar released (Fig. 8a). Two steps have a large analytical error due to an imprecise evaluation of ^{36}Ar and therefore of the atmospheric contribution in these steps. The resolution of the single phengite grain T07-11$_{(1)}$ age spectrum is limited by degassing of 72% of the total ^{39}Ar released during a single step. However, a plateau age of 47.67 ± 0.77 Ma is calculated for the three last temperature steps (90% of ^{39}Ar released). From the same sample, the single grain T07-11$_{(2)}$ yields a flat age spectrum characterized by a well-defined plateau age of 42.09 ± 0.60 Ma for 95% of the total ^{39}Ar released (Fig. 8a). These data show an age scatter of ca. 5 Ma between the two dated single grains of T07-11, probably reflecting the presence of different phengite generations in this sample. The single phengite grain of T07-13$_{(1)}$ yields a flat age spectrum characterized by a plateau age of 40.43 ± 1.53 Ma defined by the seven last temperature steps (60% of the total ^{39}Ar released, Fig. 8a). Consistently, four temperature steps of the single grain T07-13$_{(2)}$ define a plateau age of 38.89 ± 0.48 Ma for 70% of the total ^{39}Ar released (Fig. 8a). The three grouped grains of T07-14 yield a complex age spectrum with two flat segments and apparent ages ranging from 55 to 34 Ma (except the two first steps that show strong atmospheric contribution from the mineral surface, Fig. 8a). The first low temperature step shows ages at 42 ± 2 Ma while the last temperature steps define a low-quality plateau age of 48.37 ± 1.35 Ma for 53% of the total ^{39}Ar released. T07-15bis sample was analysed by ^{40}Ar/^{39}Ar *in-situ* laser ablation technique (Fig. 8b). In strain shadows around garnet, apparent ages range from ca. 90 to 49 Ma, while within foliation apparent ages are comprised between 58 and 44 Ma. Additionally, apparent ages ranging from 49 to 40 Ma were measured within shear bands, showing that no clear correlation between measured age and microstructural location is observed in this sample (Fig. 8b). Excluding the three ages older than 50 Ma, an inverse isochron yields an age of 41.5 ± 1.5 Ma with an initial

$^{40}Ar/^{36}Ar$ of 368.8 ± 24.7 (MSWD = 0.53, Fig. 8b) suggesting that some excess argon contaminated the sample.

Two single grains of T07-16 were dated by $^{40}Ar/^{39}Ar$ step-heating in addition to direct *in-situ* laser ablation on phengites. Each single grain yields a flat age spectrum and consistent plateau ages of 41.78 ± 0.86 Ma (90% of the total ^{39}Ar released) and 41.96 ± 0.83 Ma (100% of the total ^{39}Ar released, Fig. 8a). *In-situ* experiments yield apparent ages ranging from 53 to 41 Ma for phengites located in strain shadows of garnet and comprised between 50 to 41 Ma for phengites within foliation (Fig. 8c). In shear bands, *in-situ* apparent ages range from 50 to 35 Ma. No clear correlation between the microstructures and $^{40}Ar/^{39}Ar$ ages is observed (Fig. 8c), apart for younger apparent ages measured in shear bands.

$^{40}Ar/^{39}Ar$ step-heating experiments on sample T07-07 and T07-09 were conducted respectively on a concentrate and one single grain (Fig. 8a). The concentrate yields a hump-shaped age spectrum with apparent ages ranging from 27 to 23 Ma. Chemical compositions from this sample show two distinct groups (foliation and shear bands, Fig. 4d). The variation in $^{40}Ar/^{39}Ar$ apparent ages may reflect outgassing of phengite with different compositions (Wijbrans and McDougall, 1986). Due to this potential mixing, we interpret the maximum age (27 Ma) as providing a minimum age for phengite in foliation and minimum age (23 Ma) as providing maximum age for phengite in shear bands. The resolution of the single grain T07-09 age spectrum is limited by the first temperature step, which liberates a large gas amount corresponding to 80% of the total ^{39}Ar released (Fig. 8a). This anomalous behaviour could relate to high paragonite content as suggested by one chemical composition of core-analysed white mica within this sample (Fig. 4d). The low K-content and poor resolution of this age spectrum make questionable the age of 37.53 ± 1.30 Ma defined by the first temperature step (Fig. 8a) that is significantly older than ages obtained from the concentrate.

One single grain and a population from T07-25 were dated by $^{40}Ar/^{39}Ar$ step-heating

(Fig. 9a). The single grain yields a slightly discordant concave age spectrum with an age of 31.84 ± 0.46 Ma integrated on 90% of ^{39}Ar released (Fig. 9a). The analysis of the concentrate yields a more complex age spectrum characterized by a sharp decrease of apparent ages over the first four temperature steps and then a progressive age increase from 34 to 26 Ma (Fig. 9a). A partially flat segment provides an age of 30.50 ± 0.34 Ma, consistent with the minimum of the single grain age spectrum. Analyses of phengite chemical compositions from this sample show distinct core-rim compositions and several phengite generations can also be expected (Fig. 5e).

Single grains from T07-24, T07-27 and T07-22 and one concentrate of T07-18 were dated by ^{40}Ar/^{39}Ar step-heating (Fig. 9a). Additionally, ^{40}Ar/^{39}Ar *in-situ* laser ablation experiments were conducted on T07-18 and T07-19 (Figs. 9b, 9c). The single grain of T07-24 yields a flat age spectrum characterized by a well-defined plateau age of 23.77 ± 0.94 Ma for 90% of total ^{39}Ar released (Fig. 9a). The single grain of T07-27 also yields a flat age spectrum with a plateau age of 31.47 ± 0.82 Ma for 95% of ^{39}Ar released (Fig. 9a). Degassing of the single grain T07-22 gives for the third step a large gas yield corresponding to 85% of the total ^{39}Ar released (Fig. 9a). The analysis of the concentrate of T07-18 yields a complex age spectrum characterized by a sharp decrease of apparent ages during the first temperature steps and then a progressive increase of apparent ages ranging from 26 to 41 Ma with an intermediate flat segment at 41.12 ± 0.42 Ma (60% of total ^{39}Ar released, Fig. 9a). Phengite chemical compositions from this sample show distinct values from foliation to shear bands showing the presence of two phengite generations (Fig. 5e). The variation in ^{40}Ar/^{39}Ar apparent ages may reflect outgassing of these two generations. ^{40}Ar/^{39}Ar *in-situ* experiment of T07-18 yields apparent ages ranging from 44 to 42 Ma for phengites within foliation and 66 to 14 Ma for phengites within shear bands. While *in-situ* apparent ages of phengites within foliation can be correlated with the plateau age of 41.12 ± 0.42 Ma obtained for this sample,

no clear correlation between microstructures and $^{40}Ar/^{39}Ar$ ages is observed (Fig. 9b). *In-situ* experiments of T07-19 yield apparent ages ranging from 40 to 21 Ma for phengites located within foliation and 44 to 28 Ma for phengites within shear bands (Fig. 9c). Again, no clear correlation between microstructures and $^{40}Ar/^{39}Ar$ ages is observed.

Finally, one single biotite grain of T07-30 was dated by $^{40}Ar/^{39}Ar$ step-heating in order to constrain cooling age of the granodioritic intrusion of Tinos. A plateau age of 13.90 ± 2.40 Ma is calculated for 90% of total ^{39}Ar released (Fig. 9a).

5.3 Ios

One single grain of I07-23 was dated by $^{40}Ar/^{39}Ar$ step-heating. The age spectrum has a hump-shaped profile subdivided in three distinct segments (Fig. 10a). The first three temperature steps yield apparent ages around 187 Ma, the next seven steps define a plateau age of 282.57 ± 3.79 Ma for 53% of total ^{39}Ar released and finally, the two last temperature steps give apparent ages ranging from 264 to 261 Ma. This kind of profile is reminiscent of that produced by Wijbrans and McDougall (1986) and suggests the preservation of inherited muscovite associated with the growth of Alpine fine-grained white micas. The minimum cooling age of 282 Ma obtained for the intermediate segment is reasonably consistent with the age of the Variscan events determined on Ios (305-295 Ma, Henjes-Kunst and Kreuzer, 1982).

$^{40}Ar/^{39}Ar$ *in-situ* experiments were conducted on I07-122 and yield apparent ages ranging from 90 to 27 Ma for phengites within the foliation and 939 to 69 Ma for phengites within shear bands (Fig. 10b). Measured apparent ages in shear bands are generally older than in foliation, reflecting the presence of extraneous argon in phengites within shear bands. The origin of extraneous argon is discussed in the following section.

Single phengite grains of I07-15 and I07-18 were dated by $^{40}Ar/^{39}Ar$ step-heating (Fig.

10a). The single grain I07-15 yields an age spectrum characterized by a plateau age of 41.00 ± 1.72 Ma for 83% of total ^{39}Ar released (Fig. 10a). Single grain I07-18 yields an age spectrum characterized by a plateau at 48.46 ± 0.82 Ma for 65% of total ^{39}Ar released and a slight decrease of apparent ages at the end of degassing (Fig. 10a).

6. Discussion

6.1 Internal consistency of the ^{40}Ar/^{39}Ar age results and comparison with previous geochronological studies

Timing of the tectonometamorphic evolution of the CBU, CCB and the UCU of Syros, Tinos and Ios have been investigated using mostly of the existing geochronological methods such as U/Pb (Keay, 1998; Bröcker and Enders, 1999; Tomaschek et al., 2003; Bröcker and Keasling, 2006; Brichau et al., 2007), Lu/Hf (Lagos et al., 2007), Sm-Nd (Dragovic et al., 2015), ^{40}Ar/^{39}Ar (Maluski et al., 1987; Bröcker et al., 1993, 2004, 2013; Baldwin, 1996; Baldwin and Lister, 1998; Tomaschek et al., 2003; Putlitz et al., 2005; Zeffren et al., 2005; Brichau et al., 2007; Forster and Lister 2009; Rogowitz et al., 2015; Lister and Forster, 2016), Rb-Sr (Altherr et al., 1982; Henjes-Kunst and Kreuzer, 1982; Bröcker and Franz, 1998, 2000, 2005; Bröcker and Enders, 2001; Bröcker et al., 2004, 2013; Thomson et al., 2009), fission track and (U-Th)/He thermochronology (Altherr et al., 1982; Hejl et al., 2008; Ring et al., 2003; Brichau et al., 2007; Thomson et al., 2009; Soukis and Stöckli, 2013). Data are all compiled in the figure 11. When enough data exist, each ^{40}Ar/^{39}Ar age ($t_0 \pm \sigma_0$) is represented by a curve defined by a normalized probability law following the equation:

$$p(t) = \frac{1}{\sigma_0\sqrt{2\pi}} \exp((t - t_0)^2/{\sigma_0}^2)$$

where t_0 is the absolute age and σ_0 is the uncertainty on the age. The corresponding frequencies are then summed to provide a single curve. Moreover, maximum and minimum ages given by hump-shaped ^{40}Ar/^{39}Ar spectra are represented by blue squares connected by

dashed lines (Fig. 11). Geochronological constraints available for Ios result mainly from $^{40}Ar/^{39}Ar$ studies on phengite, with few age constraints provided by other methods. Moreover, a majority of $^{40}Ar/^{39}Ar$ studies on concentrates yielded complex age spectra reflecting mixture of mineral generations (Fig. 11). Finally, samples used to date the overthrusting of the CBU onto the CCB on Ios show the presence of extraneous argon preventing any geological interpretation but improving our understanding of argon behaviour in HP metamorphic rocks (Fig. 10).

6.1.1 Time-constraints on peak-burial conditions during subduction

Three age ranges have been previously proposed for peak metamorphism (Fig. 11), i) between 80 and 75 Ma (U/Pb ages on zircon, Bröcker and Enders, 1999; Bröcker and Keasling, 2006), ii) between 53 and 50 Ma (U/Pb ages on zircon, $^{40}Ar/^{39}Ar$ in phengites and Lu/Hf on garnet, Tomaschek et al., 2003; Lagos et al., 2007; Lister and Forster, 2016), iii) between 52 and 42 Ma ($^{40}Ar/^{39}Ar$ ages on phengites, Putlitz et al., 2005).

Based on our results and studies of Tomaschek et al. (2003), Lagos et al. (2007), and Lister and Forster (2016) on Syros and Dragovic et al. (2015) on Sifnos, we propose that timing of peak metamorphism in the Cyclades is comprised between 55 and 49 Ma. Indeed, the distribution of $^{40}Ar/^{39}Ar$ ages obtained on phengite single grains and populations shows two peaks at 55 and 49 Ma (Fig. 11). Moreover, dating of samples S07-14 and S07-16 from Syros with well-preserved HP assemblages (Table 1) was conducted in order to constrain the age of peak metamorphism in the CBU and yield consistent plateau ages at ca. 55 and 50 Ma (Fig. 7). Besides, Lu/Hf ages at 52.2 ± 0.3 Ma, 51.4 ± 0.4 Ma and 50 ± 2 Ma are also associated with eclogite parageneses and show no chemical and isotopic disturbance related to an earlier event (Lagos et al., 2007). Cretaceous and Eocene U/Pb ages were determined on

zircons of the same sample (Tomaschek et al., 2003). Cretaceous ages were correlated with pristine zircons interpreted to reflect the age of the magmatic protolith, while Eocene ages were correlated to skeletal zircons interpreted to date recrystallization at peak metamorphic conditions (Tomaschek et al., 2003). Finally, Sm-Nd age constraints on garnet from Sifnos, the other Cycladic island where HP parageneses are well preserved (e.g. Trotet et al., 2001; Dragovic et al., 2012; Roche et al., 2016), support this timing of peak metamorphism (Dragovic et al., 2015).

The age of peak metamorphism is more difficult to constrain on Tinos and Ios because HP parageneses are more overprinted than in Syros. $^{40}Ar/^{39}Ar$ ages ranging from 50 to 48 Ma were obtained in the less retrograded metamorphic rocks both on phengite single grains and populations, which can be interpreted as the age of peak metamorphism or the early exhumation path in Tinos and Ios (Figs. 8, 10). This age seems robust because it overlaps within error the age measured in Syros for the peak of metamorphism. However, additional radiochronologic constraints using different isotopic methods should be conducted to better constrain this age on Tinos and Ios.

Finally, no absolute age data allows estimating the period of peak metamorphism in the CCB. A large age range between 60 and 40 Ma has been proposed (Baldwin and Lister, 1998). Paleogeographic reconstructions show that ages obtained in the CBU allow constraining maximal age for peak metamorphism in the CCB (e.g. Huet et al., 2009; Jolivet and Brun, 2010).

6.1.2 Time-constraints on exhumation in the subduction and back-arc zones

On Syros and Tinos, distribution of $^{40}Ar/^{39}Ar$ and Rb-Sr ages in the CBU shows a clear correlation between the preservation of HP parageneses and ages older than ca. 35 Ma

(Figs. 1, 3, 4). $^{40}Ar/^{39}Ar$ apparent ages from phengite single grains in blueschist-facies rocks of Syros range from 45 to 40 Ma (Figs. 3, 7). In Tinos, $^{40}Ar/^{39}Ar$ ages ranging from 45 to 38 Ma correspond in a large majority to single grains and populations of phengites from blueschist-facies rocks (Figs. 4, 8). This range of ages has been also found just below and above the Tinos detachment (Figs. 4, 9). Finally, not excluding the possibility of extraneous argon, the two blueschist-facies samples I07-18 (garnet-bearing blueschist) and I07-15 (albite-epidote blueschist) from the CBU in Ios show consistent plateau ages at 48.46 ± 0.82 Ma and 41.00 ± 1.72 Ma constraining respectively the transition from eclogite- to blueschist-facies and blueschist- to greenschist-facies P-T conditions (Figs. 6, 10).

The meaning of $^{40}Ar/^{39}Ar$ ages younger than peak metamorphism is debated (e.g. Bröcker et al., 2013). They can be interpreted as cooling ages controlled by Fick diffusion law or as recrystallization ages. Previous studies in the CBU argued that $^{40}Ar/^{39}Ar$ ages younger than peak metamorphism constrain recrystallization or neo-crystallization during exhumation and not solely cooling ages (e.g. Baldwin and Lister, 1998; Cossette et al., 2015; Rogowitz et al., 2015; Lister and Forster, 2016). For example, Cossette et al. (2015) provided *in situ* Ar/Ar laser ablation analyses on white micas collected below a crustal-scale detachment exposed on Kea and Serifos islands (CBU, Greece). Both calcite- and quartz-rich lithologies were analysed in order to evaluate whether a correlation can be drawn between Ar/Ar ages, deformation and lithology. Their results show that older ages of 44-36 Ma are obtained in non-deformed phengites from calcite-rich samples, where deformation was partitioned in calcite, are consistent with the timing of HP metamorphism. On the contrary, younger ages of 25-18 Ma are measured in quartz-rich samples, where phengites appear completely newly-crystallized. This age is correlated with the timing of the Miocene ductile extension related to the activity of the detachment. Additionally, the recent work of Cliff et al. (2016) on Syros argued that Rb-Sr dating in phengites microsampled from blueschist-facies extensional

fabrics, which have a closure temperature higher than peak metamorphic temperature, constrain recrystallization during exhumation in the blueschist-facies P-T conditions between 42 and 30 Ma. Our results confirm this interpretation and suggest that ages determined in HP rocks of the CBU ranging from 45 to 38 Ma are meaningful, constraining the first exhumation steps from eclogite to blueschist-facies P-T conditions, accommodated by top-to-the northeast extensional shearing on top of the CBU and top-to-the south thrusting over the CCB.

In this study, $^{40}Ar/^{39}Ar$ ages associated with greenschist-facies parageneses range between 37 and 23 Ma except for T07-16 and T07-22 samples from Tinos, which preserve ages ranging from 53 to 38 Ma (Figs. 7, 8, 9). These results are consistent with previous Rb-Sr and $^{40}Ar/^{39}Ar$ studies (Bröcker et al., 1993, 2004, 2013; Bröcker and Franz, 1998). Indeed, two distinct $^{40}Ar/^{39}Ar$ and Rb-Sr age clusters are observed (Fig. 11): i) $^{40}Ar/^{39}Ar$ ages at ca. 32 Ma and, ii) Rb-Sr ages comprised between 24 and 22 Ma. Most of Rb-Sr ages from Tinos were measured in intensely sheared samples located below the detachment, allowing constraining the final increment of deformation associated with the Tinos Detachment. These results are consistent with the plateau age at 26.12 ± 0.52 Ma in S07-17 and the youngest *in-situ* $^{40}Ar/^{39}Ar$ ages in T07-19 ranging from 21 to 28 Ma (Fig. 9).

Emplacement of the syn-kinematic granodioritic intrusion exposed in Tinos was dated at 14.5 ± 0.3 Ma by U/Pb analyses on zircon (Keay 1998; Brichau et al., 2007). Besides, cooling is constrained by mid- to low-temperature thermochronology with ages comprised between 14 and 8 Ma (Fig. 11, Altherr et al., 1982; Hejl et al., 2008; Ring et al., 2003; Brichau et al., 2007; Thomson et al., 2009; Soukis and Stöckli, 2013). The ca. 14 Ma $^{40}Ar/^{39}Ar$ age obtained in this study, consistent with earlier studies yielding similar to younger ages (Figs. 9, 11, Altherr et al., 1982; Avigad, 1998), therefore record an increment of fast cooling.

6.2. Keys for the interpretation of *in-situ* $^{40}Ar/^{39}Ar$ ages

All *in-situ* $^{40}Ar/^{39}Ar$ apparent ages obtained in this study are summarized in Fig. 12. These ages were obtained from phengites located in three different microstructural positions: i) within foliation, ii) within strain shadows of garnets and iii) within shear bands. A major observation is the lack of obvious correlation between apparent ages and microstructural location. For example, in S07-Jojo and T07-16, apparent ages correspond to well-defined isochrons (Figs. 7, 8). While in S07-Jojo homogeneous $^{40}Ar/^{39}Ar$ apparent ages are consistent with homogeneous chemical composition of phengite, for T07-16 phengite composition within shear-bands can be distinguished from within foliation and strain shadows of garnets (Fig. 8). In I07-122, T07-15bis, T07-18 and T07-19, oldest apparent ages were obtained within shear bands or garnet strain shadows, contradicting the relative chronology established in the field and by thin-section observation (Figs. 8, 9, 10). This discrepancy is even more clearly marked in I07-122 sample where meaningless apparent ages of 413 Ma and 940 Ma were obtained within shear bands (Fig. 10). In this case, it is therefore difficult to establish unambiguous relationship between microstructures, phengite chemical composition and *in-situ* $^{40}Ar/^{39}Ar$ apparent ages at centimetre to millimetre-scale.

Two interpretations can explain the homogeneous distribution of apparent ages and compositions in S07-Jojo, i) measured ages are meaningful and phengites that crystallized either in the foliation or in shear bands are coeval recording different thermochemical equilibria (in the presence and absence of fluids for instance) ii) Deformation and fluid circulation, channelized within shear bands during blueschist-facies deformation, homogenized compositions and reset $^{40}Ar/^{39}Ar$ isotopic record in phengites within shear bands and within the close eclogitic foliation. Because $^{40}Ar/^{39}Ar$ step-heating experiments on single grain and bulk phengites clearly distinguish eclogite-facies peak metamorphism (55-49

Ma) from retrograde blueschist-facies deformation (49-38 Ma) at the island-scale (Fig. 11), the second hypothesis was preferred. In addition, the outcrop where sample S07-Jojo was sampled shows an east-west gradient of retrogression from eclogite to blueschist-facies associated with top-to-the east sense of shear (Fig. 3, Laurent et al., 2016). This interpretation explains the overall range of apparent $^{40}Ar/^{39}Ar$ ages (42-55 Ma, Fig. 7) as the consequence of heterogeneous fluid circulation and resetting of $^{40}Ar/^{39}Ar$ isotopic system rather than by the presence of excess argon, which is not identified in Syros. Preservation of old ages due to inefficient removal of grain boundary Ar by the grain boundary fluids has been also described in the Alps (Warren et al., 2012). Heterogeneous fluid circulation and recrystallization can also be involved in T07-16 for which $^{40}Ar/^{39}Ar$ apparent ages, ranging from 53 to 38 Ma, have no consistent distribution (Fig. 8). Following this interpretation, older $^{40}Ar/^{39}Ar$ apparent ages constrained the period of peak metamorphism at 55-49 Ma while the youngest estimate the age of syn-blueschist retrograde deformation between 45 and 38 Ma.

Apparent $^{40}Ar/^{39}Ar$ ages of phengite older than 60-55 Ma, with a questionable geological significance in the CBU, seem to be the consequence of the presence of excess argon. These old apparent ages are correlated with microstructures that favoured fluid circulation, such as shear bands or strain shadows around garnets (Figs. 10, 12). Following this observation, fluid circulation seems to be able to transport excess argon in significant quantities.

Finally, the chemical composition of micaschists in the CBU is characterized by high Na-content evidenced by the systematic presence of Na-rich phengites, paragonite or albite (Trotet et al., 2001; Parra et al., 2002). This specific composition could involve a more complex behaviour of argon isotopes trapping and transport, explaining why other *in-situ* $^{40}Ar/^{39}Ar$ studies on non-sodic HP-LT micaschist report a clearer relationship between microstructures and $^{40}Ar/^{39}Ar$ apparent ages (e.g. Agard et al., 2002; Augier et al., 2005).

6.3. Origin of extraneous argon

Extraneous argon is heterogeneously distributed in phengites from the CBU. Our results suggest that metamorphic rocks of Syros do not seem affected by extraneous argon while HP units in Tinos are only locally affected, with maximum $^{40}Ar/^{39}Ar$ apparent ages of 90 Ma measured in strain shadows around garnets (Figs 8, 12). Conversely, phengites are most affected by extraneous argon in Ios, with meaningless apparent ages measured in shear bands up to 900 Ma (Fig. 10). Two hypotheses may explain this observation: i) an open fluid circulation system allowed evacuating inherited argon from the CBU of Syros and to a lesser extent in Tinos, while a closed system in Ios has preserved inherited argon in the CBU, ii) during mylonitization of the orthogneiss in the CCB, recrystallization of the Variscan K-feldspar and/or its transformation to phengite (Huet et al., 2009) released ^{40}Ar and the CCB thus behaved as a reservoir of inherited argon mobilized by fluid circulation during the Alpine metamorphic episode. These argon-enriched fluids have then heterogeneously contaminated metamorphic rocks when percolating the CBU. In our interpretation, the heterogeneous presence of extraneous argon in the CBU is the consequence of the second hypothesis because our results show evidences of contamination by excess argon preferentially located in domains of large fluid infiltration (Figs. 10, 12). The most contaminated samples were found on Ios because of the proximity with the CCB (Fig. 6a). In addition, our data show that Variscan apparent ages at 282.57 ± 3.79 Ma are preserved in the CCB (Fig. 10a), indicating that the $^{40}Ar/^{39}Ar$ system was not completely reset during the Eocene HP-LT metamorphic episode.

6.4. Closure temperature of the K/Ar system in high-pressure phengites

Considering reconstructed P-T paths of the CBU in Syros (Trotet et al., 2001; Lister and Forster, 2016) or in Sifnos (Groppo et al. 2009; Dragovic et al., 2012), the maximum temperature (Tmax) reached by HP-LT metamorphic rocks is ca. 550 °C. Moreover, the P-T evolution followed by the CBU during first exhumation steps is rather isothermal, at least for the most retrograded units (Trotet et al., 2001; Groppo et al., 2009; Dragovic et al., 2012). Using the closure temperature concept, rocks derived from Syros should all yield a consistent age for a given grain size corresponding to the time span elapsed from the bulk cooling through ca. 400-450 °C (Villa, 1998; Harrison et al., 2009) preventing the discrimination of former events. Our results and previously published data (Tomaschek et al., 2003; Putlitz et al., 2005; Lagos et al., 2007; Lister and Forster, 2016) show that this is not the case and argon diffusion at these HP conditions seems to be minor. Therefore, phengites of the CBU must have been more retentive to argon diffusion and a minimum closure temperature of 550 °C corresponding to Tmax should be accepted for phengites of the CBU. Our results suggest that reset of the argon isotopic system in HP metamorphic context, at least in the CBU, is controlled by recrystallization enhanced by fluid circulation and deformation (Villa, 1998; Di Vincenzo et al., 2006; Lister et al., 2016).

Another argument showing that the closure temperature of argon in HP phengites could be higher than traditionally accepted is the comparison between $^{40}Ar/^{39}Ar$ and Rb-Sr ages. Indeed, on each Cycladic Island studied here, Rb-Sr ages are a few millions years younger than $^{40}Ar/^{39}Ar$ ages (Fig. 11). A similar situation has been reported in different HP-LT metamorphic belts (e.g. Li et al., 1994; Di Vincenzo et al., 2006; Bröcker et al., 2013) and it was also observed at sample-scale on Tinos (Bröcker et al., 2004). It is often interpreted as an argument for the presence of extraneous argon in phengites. Our study shows that in the

CBU, particularly on Syros, this argument cannot be used. Older $^{40}Ar/^{39}Ar$ ages are better explained by a minimum closure temperature of argon in HP phengites of 550 °C, equivalent or even higher than the one accepted for the Rb-Sr dating method in phengite (ca. 500 ± 50 °C; Blanckenburg et al., 1989). Consequently, inferring $^{40}Ar/^{39}Ar$ ages in HP phengites as geologically meaningless because Rb-Sr ages are younger is an interpretation that should be regarded with great care.

6.5. Regional implications: the tectonometamorphic evolution of the CBU

From examples of Syros, Tinos and Ios, and integrating data from the literature of the whole Aegean domain, we suggest geochronological constraints on the P-T-t-d evolution of metamorphic units, mainly focalized on the CBU. These time-constraints confirm the distinction between a first syn-orogenic step of exhumation within the subduction zone followed by post-orogenic exhumation contemporaneous of the formation of the Aegean Sea and accommodated by a crustal-scale system of detachments. The following discussion is illustrated by a series of geodynamic reconstructions in the form of N-S oriented cross-sections (Fig. 13).

6.5.1 From late-burial to peak metamorphic conditions

Peak-pressure P-T conditions of the CBU are rather homogeneous through the Cyclades. In Tinos (Parra et al., 2002), Andros (Huet et al., 2015), Syros (Trotet et al., 2001), Sifnos (Trotet et al., 2001; Groppo et al., 2009; Dragovic et al., 2012), Sikinos (Augier et al., 2015) and Ios (Huet et al., 2009), these conditions are all comprised between 18-22 kbar and 500-550 °C. The period of peak-pressure in the CBU has been constrained in Syros, Sifnos,

Tinos and Ios at 55-49 Ma (Bröcker et al., 1993; Baldwin, 1996; Tomaschek et al., 2003; Lagos et al., 2007; Dragovic et al., 2015; Lister and Forster, 2016).

Different conditions were determined for the peak-pressure of the CCB with about 15 kbar – 550 °C in Naxos (Avigad, 1998; Duchene et al., 2006), 19 kbar – 530 °C in Samos (Feenstra et al., 2007), 11 kbar – 475 °C for Sikinos (Gupta and Bickle, 2004) and ca. 16.5 kbar – 500 °C for Ios (Huet et al., 2009). This dispersion contrasts with the homogeneity of conditions in the CBU albeit the highest peak conditions determined in Samos and Ios are close to those determined for the CBU. Few geochronological constraints exist for the age of peak-pressure in the CCB. In Naxos, U/Pb radiochronometric ages in zircon between 55 and 45 Ma were interpreted as dating peak metamorphism (Martin et al., 2006). In Ios, the period of peak pressure in the CCB is difficult to constrain by $^{40}Ar/^{39}Ar$ method because of excess argon (Fig. 10). Nevertheless, ages similar to those determined in Naxos (Martin et al., 2006) and in the CBU (50-55 Ma) were measured and can therefore be considered as a first approximation.

6.5.2 Syn-orogenic exhumation

Exhumation within the subduction channel in a high P-T ratio environment allowing partial retrogression of eclogites in the blueschist-facies is well documented on Syros, Tinos and Ios. On Syros and Tinos, syn-orogenic exhumation is controlled by top-to-the east/northeast sense of shear associated with the Vari Detachment (Trotet et al., 2001; Parra et al., 2002; Soukis and Stöckli, 2013; Laurent et al., 2016) and is constrained between 49 and 38 Ma (Fig. 11). On Ios, exhumation in the blueschist-facies is controlled by top-to-the south shearing associated with overthrusting of the CBU onto the CCB, which is constrained between a minimum age of 50 Ma and a maximum age of 25 Ma (Fig. 11, Forster and Lister,

2009; Huet et al., 2009). This crustal-scale structure extends over nearly 500 km from Olympos to Western-Turkey (Ring et al., 2007; Lacassin et al., 2007). Such HP-LT exhumation model of the CBU, accommodated by a general extrusion structure between a top-to-the northeast detachment at the top and top-to-the south thrust at the base, has also been proposed for Samos Island (Ring et al., 2007) or the Cyclades in a broad sense (Huet et al., 2009; Jolivet and Brun, 2010; Ring et al., 2010). On Samos, the activity of syn-orogenic structures in the blueschist-facies has been constrained between 42 and 32 Ma by $^{40}Ar/^{39}Ar$ and Rb-Sr geochronological methods on phengite, partly coeval with structures observed in the north and south of the Cyclades (Ring et al., 2007). Furthermore, tectonic structures with similar kinematics and P-T conditions were observed in Evia (Xypolias et al., 2012). Rb-Sr ages on HP-LT phengites of these structures are comprised between 33 and 21 Ma, which is diachronous compared to Samos and the rest of the Cyclades. However, it was shown in Tinos that the Rb-Sr phengite system could be partially or totally reset in the greenschist-facies without important reequilibration of the major element chemistry (Bröcker et al., 2004). It is therefore possible that HP tectonic structures observed in Evia are older than 33 Ma. Finally, the CBU are also exposed in the Olympos-Ossa-Pelion ranges (north Aegean Domain), between a top-to-the northeast detachment at the roof and a basal top-to-the southwest thrust, which were active in HP-LT conditions between 45 and 35 Ma (Lacassin et al., 2007).

The global structure of syn-orogenic exhumation of the CBU was similar in the whole Aegean domain with crustal-scale tectonic contacts initiated between 50-45 Ma and deactivated around 35-30 Ma (Fig. 13). In the Cyclades, these structures have accommodated about 30-25 km of vertical exhumation, exhuming the CBU at ca. 30 km deep into the crust, below the upper Pelagonian unit (Fig. 13).

6.5.3 Post-orogenic exhumation

A drastic change in kinematic boundary conditions occurs at ca. 35 Ma with a decrease of the absolute northward motion of Africa and the southward retreat of the subducting slab (Fig. 13, Jolivet and Faccenna, 2000). This drastic change marks the transition from syn-orogenic exhumation to post-orogenic extension and is recorded by a decreasing exhumation rate and an isobaric warming in Tinos (Parra et al., 2002) and Andros (Huet et al., 2015). The crustal geometry of tectonic structures accommodating the initiation of post-orogenic exhumation is poorly constrained. Little retrogression in greenschist-facies conditions is observed in Syros below the Vari Detachment (Laurent et al., 2016). Therefore, at least part of the Vari Detachment ceased to be active in HP-LT conditions, accommodating only the syn-orogenic exhumation (Fig. 13). Being a major inherited structure, the base of the UCU was reactivated by post-orogenic detachments such as the NCDS (Fig. 13, Jolivet et al., 2010).

In the western Cyclades, post-orogenic exhumation is accommodated by the WCDS (Fig. 13; Grasemann et al., 2012). The initiation of post-orogenic exhumation in the Cyclades is therefore diachronous, the NCDS (30-35 Ma, Jolivet et al., 2010) being activated before the WCDS (26-22 Ma, Grasemann et al., 2012). However, the last increments of ductile deformation recorded by $^{40}Ar/^{39}Ar$ and Rb-Sr radiochronometers are dated at 18-20 Ma both for the NCDS and WCDS (this study, Grasemann et al., 2012; Cossette et al., 2015). The latest ductile increments of activity of these two detachment systems is therefore synchronous, showing that for the last 5-8 Ma, top-to-the northeast and southwest shear directions coexist in the Cyclades (Fig. 13).

6.5.4 Syn-kinematic intrusions and final exhumation

Ductile detachments do not explain the final exhumation of the CBU above the brittle-ductile transition. Once plutonic intrusions were emplaced below the NCDS at about 12-16 Ma, deformation jumped on a structurally higher position along secondary detachments as observed in Tinos (Jolivet and Patriat, 1999; Brichau et al., 2007), Mykonos (Lecomte et al., 2010), Serifos (Rabillard et al., 2015) and Ikaria (Beaudoin et al., 2015; Laurent et al., 2015). The vertical exhumation until a few kilometres deep is therefore associated with upward migration of the actively deforming zone, which is a consequence of intrusions that lifts up the ductile–brittle transition (Fig. 13, Jolivet and Patriat, 1999).

Finally, the lack of clasts from the CBU and CCB in continental Miocene sedimentary basins (8-10 Ma) exposed in Mykonos, Naxos and Paros (Sanchez-Gomez et al., 2002) shows that the deeper metamorphic units have not reached the surface before ca. 8 Ma, corresponding to the youngest fission tracks ages measured in the Cyclades (Ring et al., 2010; Soukis and Stöckli, 2013). The final vertical exhumation was accommodated by brittle high-angle normal faults observed throughout the Aegean domain (Fig. 13). Pliocene paleogeographic reconstructions, after the Messinian salinity crisis, show that the current morphology in horst and grabens of the Cyclades would be posterior to 4 Ma (Hejl et al., 2008).

7. Conclusion

Our study shows that the timing of the tectonometamorphic evolution of the HP-LT CBU is well constrained by the $^{40}Ar/^{39}Ar$ dating technique, allowing the identification of phengites contaminated by extraneous argon. The distribution of extraneous argon is heterogeneous over the CBU, and seems to be linked with the vicinity of the Cycladic

Continental Basement where inherited argon has been preserved from the Variscan metamorphic episode. The main evidences of excess argon in the CBU were identified within microstructures where fluid circulation is favoured, showing that excess argon derived from the circulation of external argon-enriched fluids. Additionally, assuming a relatively isothermal exhumation of the CBU, we suggest a minimum closure temperature of 550 °C for phengite of the CBU and conclude that volume diffusion is a minor process resetting the argon isotopic system in high-pressure rocks compare to recrystallization enhanced by fluid circulation and deformation. Finally, our results support that HP units of oceanic affinity with a simple metamorphic history are less affected by the presence of extraneous argon than polymetamorphic continental units. Indeed, due to continuous dehydration reactions along the prograde path, oceanic units released large quantities of fluids allowing an evolution in open conditions resetting the argon isotopic system. These new ages and conclusions in terms of their geological significance are then used to describe the sequence of events that led to the formation and exhumation of the CBU.

Acknowledgments

This work has received funding from the ANR EGEO Project, from the European Research Council (ERC) under the seventh Framework Programme of the European Union (ERC Advanced Grant, grant agreement No 290864, RHEOLITH) and from the Institut Universitaire de France. It is a contribution of the Labex VOLTAIRE.

References

Agard, P., Monié, P., Jolivet, L., Goffé, B., 2002. Exhumation of the Schistes Lustrés complex: in situ laser probe $^{40}Ar/^{39}Ar$ constraints and implications for the Western

Alps. Journal of Metamorphic Geology 20, 599–618.

Altherr, R., Kreuzer, H., Wendt, I., Lenz, H., Wagner, G.A., Keller, J., Harre, W., Hohndorf, A., 1982. A late Oligocene/early Miocene high temperature belt in the Attic-Cycladic crystalline complex (SE Pelagonian, Greece). Geologisches Jahrbuch E 23, 97–164.

Arnaud, N.O., Kelley, S.P., 1995. Evidence for excess argon during high pressure metamorphism in the Dora Maira Massif (western Alps, Italy), using an ultra-violet laser ablation microprobe ^{40}Ar-^{39}Ar technique. Contributions to Mineralogy and Petrology 121, 1–11.

Augier, R., Agard, P., Monié, P., Jolivet, L., Robin, C., Booth-Rea, G., 2005. Exhumation, doming and slab retreat in the Betic Cordillera (SE Spain): in situ ^{40}Ar/^{39}Ar ages and P–T–d–t paths for the Nevado-Filabride complex. Journal of Metamorphic Geology 23, 357–381.

Augier, R., Jolivet, L., Gadenne, L., Lahfid, A., Driussi, O., 2015. Exhumation kinematics of the Cycladic Blueschists unit and back-arc extension, insight from the Southern Cyclades (Sikinos and Folegandros Islands, Greece), Tectonics, 34, 152-185, doi: 10.1002/2014TC003664.

Avigad, D., Garfunkel, Z., 1989. Low-angle faults above and below a blueschist belt—Tinos Island, Cyclades, Greece. Terra Nova 1, 182–187.

Baldwin, S.L., 1996. Contrasting P-T-t Histories for Blueschists from the Western Baja Terrane and the Aegean: Effects of Synsubduction Exhumation and Backarc Extension. Subduction top to bottom 135–141.

Baldwin, S.L., Lister, G.S., 1998. Thermochronology of the South Cyclades Shear Zone, Ios, Greece: Effects of ductile shear in the argon partial retention zone. Journal of Geophysical Research: Solid Earth 103, 7315–7336.

Beaudoin, A., Augier, R., Laurent, V., Jolivet, L., Lahfid, A., Bosse, V., Arbaret, L., Rabillard, A., Menant, A., 2015. The Ikaria high-temperature Metamorphic Core Complex (Cyclades, Greece): Geometry, kinematics and thermal structure. Journal of Geodynamics 92, 18–41. doi:10.1016/j.jog.2015.09.004

Blanckenburg, F. v, Villa, I.M., Baur, H., Morteani, G., Steiger, R.H., 1989. Time calibration of a PT-path from the Western Tauern Window, Eastern Alps: the problem of closure temperatures. Contributions to Mineralogy and Petrology 101, 1–11.

Bonneau, M., Kienast, J.R., 1982. Subduction, collision et schistes bleus; l'exemple de l'Egee (Grece). Bulletin de la société Géologique de France 785–791.

Brichau, S., Ring, U., Carter, A., Monié, P., Bolhar, R., Stockli, D., Brunel, M., 2007. Extensional faulting on Tinos island, Aegean sea, Greece: How many detachments? Tectonics 26.

Bröcker, M., Baldwin, S., Arkudas, R., 2013. The geological significance of 40Ar/39Ar and Rb–Sr white mica ages from Syros and Sifnos, Greece: a record of continuous (re) crystallization during exhumation? Journal of Metamorphic Geology 31, 629–646.

Bröcker, M., Bieling, D., Hacker, B., Gans, P., 2004. High-Si phengite records the time of greenschist facies overprinting: implications for models suggesting mega-detachments in the Aegean Sea. Journal of Metamorphic Geology 22, 427–442.

Bröcker, M., Enders, M., 2001. Unusual bulk-rock compositions in eclogite-facies rocks from Syros and Tinos (Cyclades, Greece): implications for U–Pb zircon geochronology. Chemical Geology 175, 581–603.

Bröcker, M., Enders, M., 1999. U–Pb zircon geochronology of unusual eclogite-facies rocks from Syros and Tinos (Cyclades, Greece). Geological Magazine 136, 111–118.

Bröcker, M., Franz, L., 2005. The base of the Cycladic blueschist unit on Tinos Island (Greece) re-visited: field relationships, phengite chemistry and Rb–Sr geochronology.

Neues Jahrbuch für Mineralogie-Abhandlungen: Journal of Mineralogy and Geochemistry 181, 81–93.

Bröcker, M., Franz, L., 2000. The contact aureole on Tinos (Cyclades, Greece): tourmaline-biotite geothermometry and Rb-Sr geochronology. Mineralogy and Petrology 70, 257–283.

Bröcker, M., Franz, L., 1998. Rb–Sr isotope studies on Tinos Island (Cyclades, Greece): additional time constraints for metamorphism, extent of infiltration-controlled overprinting and deformational activity. Geological Magazine 135, 369–382.

Bröcker, M., Keasling, A., 2006. Ionprobe U-Pb zircon ages from the high-pressure/low-temperature mélange of Syros, Greece: age diversity and the importance of pre-Eocene subduction. Journal of Metamorphic Geology 24, 615–631.

Bröcker, M., Kreuzer, H., Matthews, A., Okrusch, M., 1993. 40Ar/39Ar and oxygen isotope studies of polymetamorphism from Tinos Island, Cycladic blueschist belt, Greece. Journal of Metamorphic Geology 11, 223–240.

Cliff, R.A., Bond, C.E., Butler, R.W.H., Dixon, J.E., 2016. Geochronological challenges posed by continuously developing tectonometamorphic systems; insights from Rb–Sr mica ages from the Cycladic Blueschist Belt, Syros (Greece). Journal of Metamorphic Geology.

Cossette, É., Schneider, D.A., Warren, C.J., Grasemann, B., 2015. Lithological, rheological, and fluid infiltration control on 40Ar/39Ar ages in polydeformed rocks from the West Cycladic detachment system, Greece. Lithosphere 7, 189–205.

Di Vincenzo, G., Tonarini, S., Lombardo, B., Castelli, D., Ottolini, L., 2006. Comparison of 40Ar–39Ar and Rb–Sr data on phengites from the UHP Brossasco–Isasca Unit (Dora Maira Massif, Italy): implications for dating white mica. Journal of Petrology 47, 1439–1465.

Dragovic, B., Baxter, E.F., Caddick, M.J., 2015. Pulsed dehydration and garnet growth during subduction revealed by zoned garnet geochronology and thermodynamic modeling, Sifnos, Greece. Earth and Planetary Science Letters 413, 111–122.

Dragovic, B., Samanta, L.M., Baxter, E.F., Selverstone, J., 2012. Using garnet to constrain the duration and rate of water-releasing metamorphic reactions during subduction: An example from Sifnos, Greece. Chemical Geology 314, 9–22.

Duchene, S., Aissa, R., Vanderhaeghe, O., 2006. Pressure-temperature-time evolution of metamorphic rocks from Naxos (Cyclades, Greece): constraints from thermobarometry and Rb/Sr dating. Geodinamica Acta 19, 301–321.

Feenstra, A., Petrakakis, K., Rhede, D., 2007. Variscan relicts in Alpine high-P pelitic rocks from Samos (Greece): evidence from multi-stage garnet and its included minerals. Journal of Metamorphic Geology 25, 1011–1033.

Forster, M., Lister, G., 2009. Core-complex-related extension of the Aegean lithosphere initiated at the Eocene-Oligocene transition. Journal of Geophysical Research: Solid Earth 114.

Giorgis, D., Cosca, M., Li, S., 2000. Distribution and significance of extraneous argon in UHP eclogite (Sulu terrain, China): insight from in situ 40 Ar/39 Ar UV-laser ablation analysis. Earth and Planetary Science Letters 181, 605–615.

Grasemann, B., Schneider, D.A., Stöckli, D.F., Iglseder, C., 2012. Miocene bivergent crustal extension in the Aegean: Evidence from the western Cyclades (Greece). Lithosphere L164–1.

Groppo, C., Forster, M., Lister, G., Compagnoni, R., 2009. Glaucophane schists and associated rocks from Sifnos (Cyclades, Greece): New constraints on the P–T evolution from oxidized systems. Lithos 109, 254–273.

Gupta, S., Bickle, M.J., 2004. Ductile shearing, hydrous fluid channelling and high-pressure

metamorphism along the basement-cover contact on Sikinos, Cyclades, Greece. Geological Society, London, Special Publications 224, 161–175.

Harrison, T.M., Célérier, J., Aikman, A.B., Hermann, J., Heizler, M.T., 2009. Diffusion of 40 Ar in muscovite. Geochimica et Cosmochimica Acta 73, 1039–1051.

Hejl, E., Riedl, H., Weingartner, H., 2002. Post-plutonic unroofing and morphogenesis of the Attic–Cycladic complex (Aegea, Greece). Tectonophysics 349, 37–56.

Henjes-Kunst, F., Kreuzer, H., 1982. Isotopic dating of pre-alpidic rocks from the island of Ios (Cyclades, Greece). Contributions to Mineralogy and Petrology 80, 245–253.

Huet, B., 2010. Rhéologie de la lithosphère continentale: L'exemple de la Mer Egée. Université Pierre et Marie Curie-Paris VI.

Huet, B., Labrousse, L., Jolivet, L., 2009. Thrust or detachment? Exhumation processes in the Aegean: insight from a field study on Ios (Cyclades, Greece). Tectonics 28.

Huet, B., Labrousse, L., Monié, P., Malvoisin, B., Jolivet, L., 2015. Coupled phengite 40 Ar–39 Ar geochronology and thermobarometry: PTt evolution of Andros Island (Cyclades, Greece). Geological Magazine 152, 711–727.

Itaya, T., Tsujimori, T., Liou, J.G., 2011. Evolution of the Sanbagawa and Shimanto high-pressure belts in SW Japan: insights from K–Ar (Ar–Ar) geochronology. Journal of Asian Earth Sciences 42, 1075–1090.

Jolivet, L., Brun, J.-P., 2010. Cenozoic geodynamic evolution of the Aegean. International Journal of Earth Sciences 99, 109–138.

Jolivet, L., Faccenna, C., 2000. Mediterranean extension and the Africa-Eurasia collision. Tectonics 19, 1095–1106.

Jolivet, L., Lecomte, E., Huet, B., Denèle, Y., Lacombe, O., Labrousse, L., Le Pourhiet, L., Mehl, C., 2010. The north cycladic detachment system. Earth and Planetary Science Letters 289, 87–104.

Jolivet, L., Menant, A., Sternai, P., Rabillard, A., Arbaret, L., Augier, R., Laurent, V., Beaudoin, A., Grasemann, B., Huet, B., others, 2015. The geological signature of a slab tear below the Aegean. Tectonophysics. doi:10.1016/j.tecto.2015.08.004

Jolivet, L., Patriat, M., 1999. Ductile extension and the formation of the Aegean Sea. Geological Society, London, Special Publications 156, 427–456.

Keay, S., 1998. The geological evolution of the Cyclades, Greece: constraints from SHRIMP U-Pb geochronology. Australian National University.

Kelley, S., 2002. Excess argon in K–Ar and Ar–Ar geochronology. Chemical Geology 188, 1–22.

Lacassin, R., Arnaud, N., Leloup, P.-H., Armijo, R., Meyer, B., 2007. Syn-and post-orogenic exhumation of metamorphic rocks in North Aegean. eEarth 2, 51–63.

Lagos, M., Scherer, E.E., Tomaschek, F., Münker, C., Keiter, M., Berndt, J., Ballhaus, C., 2007. High precision Lu–Hf geochronology of Eocene eclogite-facies rocks from Syros, Cyclades, Greece. Chemical Geology 243, 16–35.

Laurent, V., Beaudoin, A., Jolivet, L., Arbaret, L., Augier, R., Rabillard, A., Menant, A., 2015. Interrelations between extensional shear zones and synkinematic intrusions: The example of Ikaria Island (NE Cyclades, Greece). Tectonophysics 651, 152–171. doi:10.1016/j.tecto.2015.03.020

Laurent, V., Jolivet, L., Roche, V., Augier, R., Scaillet, S., Cardello, G.L., 2016. Strain localization in a fossilized subduction channel: Insights from the Cycladic Blueschist Unit (Syros, Greece). Tectonophysics 672, 150–169. doi:10.1016/j.tecto.2016.01.036

Lecomte, E., Jolivet, L., Lacombe, O., Denèle, Y., Labrousse, L., Le Pourhiet, L., 2010. Geometry and kinematics of a low-angle normal fault on Mykonos island (Cyclades, Greece): Evidence for slip at shallow dip. Tectonics 29.

Li, S., Wang, S., Chen, Y., Liu, D., Qiu, J.I., Zhou, H., Zhang, Z., 1994. Excess argon in phengite from eclogite: Evidence from dating of eclogite minerals by Sm· Nd, Rb· Sr and 40Ar39Ar methods. Chemical Geology 112, 343–350.

Lister, G., Forster, M., 2016. White mica 40Ar/39Ar age spectra and the timing of multiple episodes of high-pressure metamorphic mineral growth in the Cycladic eclogite-blueschist belt, Syros, Aegean Sea, Greece. Journal of Metamorphic Geology.

Lister, G.S., Banga, G., Feenstra, A., 1984. Metamorphic core complexes of Cordilleran type in the Cyclades, Aegean Sea, Greece. Geology 12, 221–225.

Maluski, H., Bonneau, M., Kienast, J.R., 1987. Dating the metamorphic events in the Cycladic area; 39 Ar/40 Ar data from metamorphic rocks of the Island of Syros (Greece). Bulletin de la Société géologique de France 3, 833–842.

Martin, L., Duchêne, S., Deloule, E., Vanderhaeghe, O., 2006. The isotopic composition of zircon and garnet: a record of the metamorphic history of Naxos, Greece. Lithos 87, 174–192.

Mehl, C., Jolivet, L., Lacombe, O., 2005. From ductile to brittle: evolution and localization of deformation below a crustal detachment (Tinos, Cyclades, Greece). Tectonics 24.

Melidonis, N.G., 1980. The geological structure and mineral deposits of Tinos island (Cyclades, Greece). The geology of Greece 13, 1–80.

Monie, P., Agard, P., 2009. Coeval blueschist exhumation along thousands of kilometers: Implications for subduction channel processes. Geochemistry, Geophysics, Geosystems 10.

Parra, T., Vidal, O., Jolivet, L., 2002. Relation between the intensity of deformation and retrogression in blueschist metapelites of Tinos Island (Greece) evidenced by chlorite–mica local equilibria. Lithos 63, 41–66.

Perraki, M., Mposkos, E., 2001. New constraints for the Alpine HP metamorphism of the Ios

basement, Cyclades, Greece. Bull. Geol. Soc. Greece 34, 977–984.

Philippot, P., Rumble, D., 2000. Fluid-rock interactions during high-pressure and ultrahigh-pressure metamorphism. International Geology Review 42, 312–327.

Proyer, A., 2003. Metamorphism of pelites in NKFMASH–a new petrogenetic grid with implications for the preservation of high-pressure mineral assemblages during exhumation. Journal of metamorphic Geology 21, 493–509.

Putlitz, B., Cosca, M.A., Schumacher, J.C., 2005. Prograde mica 40 Ar/39 Ar growth ages recorded in high pressure rocks (Syros, Cyclades, Greece). Chemical Geology 214, 79–98.

Qiu, H.-N., Wijbrans, J.R., 2006. Paleozoic ages and excess 40 Ar in garnets from the Bixiling eclogite in Dabieshan, China: New insights from 40 Ar/39 Ar dating by stepwise crushing. Geochimica et Cosmochimica Acta 70, 2354–2370.

Rabillard, A., Arbaret, L., Jolivet, L., Le Breton, N., Gumiaux, C., Augier, R., Grasemann, B., 2015. Interactions between plutonism and detachments during Metamorphic Core Complex formation, Serifos Island (Cyclades, Greece). Tectonics.

Renne, P.R., Swisher, C.C., Deino, A.L., Karner, D.B., Owens, T.L., DePaolo, D.J., 1998. Intercalibration of standards, absolute ages and uncertainties in 40 Ar/39 Ar dating. Chemical Geology 145, 117–152.

Ring, U., Glodny, J., Will, T., Thomson, S., 2010. The Hellenic subduction system: high-pressure metamorphism, exhumation, normal faulting, and large-scale extension. Annual Review of Earth and Planetary Sciences 38, 45–76.

Ring, U., Thomson, S.N., Bröcker, M., 2003. Fast extension but little exhumation: the Vari detachment in the Cyclades, Greece. Geological Magazine 140, 245–252.

Ring, U., Will, T., Glodny, J., Kumerics, C., Gessner, K., Thomson, S., Güngör, T., Monié, P., Okrusch, M., Drüppel, K., 2007. Early exhumation of high-pressure rocks in

extrusion wedges: Cycladic blueschist unit in the eastern Aegean, Greece, and Turkey. Tectonics 26.

Roche, V., Laurent, V., Cardello, G.L., Jolivet, L., Scaillet, S., 2016. Anatomy of the Cycladic Blueschist Unit on Sifnos Island (Cyclades, Greece). Journal of Geodynamics 97, 62–87. doi:10.1016/j.jog.2016.03.008

Rogowitz, A., Huet, B., Schneider, D., Grasemann, B., 2015. Influence of high strain rate deformation on 40Ar/39Ar mica ages from marble mylonites (Syros, Greece). Lithosphere 7, 535–540.

Sanchez-Gomez, M., Avigad, D., Heimann, A., 2002. Geochronology of clasts in allochthonous Miocene sedimentary sequences on Mykonos and Paros islands: implications for back-arc extension in the Aegean Sea. Journal of the Geological Society 159, 45–60.

Scaillet, S., 1996. Excess 40 Ar transport scale and mechanism in high-pressure phengites: A case study from an eclogitized metabasite of the Dora-Maira nappe, western Alps. Geochimica et Cosmochimica Acta 60, 1075–1090.

Smye, A.J., Warren, C.J., Bickle, M.J., 2013. The signature of devolatisation: Extraneous ^{40}Ar systematics in high-pressure metamorphic rocks. Geochimica et Cosmochimica Acta 113, 94–112.

Soukis, K., Stockli, D.F., 2013. Structural and thermochronometric evidence for multi-stage exhumation of southern Syros, Cycladic islands, Greece. Tectonophysics 595, 148–164.

Thomson, S.N., Ring, U., Brichau, S., Glodny, J., Will, T.M., 2009. Timing and nature of formation of the Ios metamorphic core complex, southern Cyclades, Greece. Geological Society, London, Special Publications 321, 139–167.

Tomaschek, F., Kennedy, A.K., Villa, I.M., Lagos, M., Ballhaus, C., 2003. Zircons from

Syros, Cyclades, Greece—recrystallization and mobilization of zircon during high-pressure metamorphism. Journal of Petrology 44, 1977–2002.

Trotet, F., Vidal, O., Jolivet, L., 2001. Exhumation of Syros and Sifnos metamorphic rocks (Cyclades, Greece). New constraints on the PT paths. European Journal of Mineralogy 13, 901–902.

Van der Maar, P.A., 1980. The geology and petrology of Ios, Cyclades, Greece. Ann. Geol. Pays Hell 30, 206–224.

Van der Maar, P.A., Jansen, J.B.H., 1983. The geology of the polymetamorphic complex of Ios, Cyclades, Greece and its significance for the Cycladic Massif. Geologische Rundschau 72, 283–299.

Villa, I.M., 1998. Isotopic closure. Terra Nova-Oxford 10, 42–47.

Warren, C.J., Sherlock, S.C., Kelley, S.P., 2011. Interpreting high-pressure phengite 40Ar/39Ar laserprobe ages: an example from Saih Hatat, NE Oman. Contributions to Mineralogy and Petrology 161, 991–1009.

Warren, C.J., Smye, A.J., Kelley, S.P., Sherlock, S.C., 2012. Using white mica 40Ar/39Ar data as a tracer for fluid flow and permeability under high-P conditions: Tauern Window, Eastern Alps. Journal of Metamorphic Geology 30, 63–80.

Wijbrans, J.R., McDougall, I., 1986. 40Ar/39Ar dating of white micas from an Alpine high-pressure metamorphic belt on Naxos (Greece): the resetting of the argon isotopic system. Contributions to Mineralogy and Petrology 93, 187–194.

Whitney, D.L., Evans, B.W., 2010. Abbreviations for names of rock-forming minerals. American mineralogist 95, 185.

Xypolias, P., Iliopoulos, I., Chatzaras, V., Kokkalas, S., 2012. Subduction-and exhumation-related structures in the Cycladic Blueschists: Insights from south Evia Island (Aegean region, Greece). Tectonics 31.

Yamato, P., Agard, P., Goffé, B., De Andrade, V., Vidal, O., Jolivet, L., 2007. New, high-precision P–T estimates for Oman blueschists: implications for obduction, nappe stacking and exhumation processes. Journal of Metamorphic Geology 25, 657–682.

Zeffren, S., Avigad, D., Heimann, A., Gvirtzman, Z., 2005. Age resetting of hanging wall rocks above a low-angle detachment fault: Tinos Island (Aegean Sea). Tectonophysics 400, 1–25.

Figure captions:

Figure 1: Location of the studied area and dated samples. a) Simplified geological map of the Cyclades situating Syros, Tinos and Ios islands (after Jolivet et al., 2015). Major tectonic structures are represented such as the North Cycladic Detachment System (NCDS), the West Cycladic Detachment System (WCDS) and the Paros-Naxos Detachment (PND), as well as kinematic indicators. a, b, c) Geological map of respectively Syros (after Laurent et al., 2016), Tinos (modified after Mélidonis, 1980) and Ios (modified after Huet et al., 2009) showing the main tectonic structures and localizing the studied samples.

Figure 2: BSE secondary electron images of three phengite single grains. a, b) Phengite single grains separate from preserved HP-LT metamorphic rocks are little deformed and not interstratified with other mineral phases. c) In contrast, phengite single grains separate from intensely retrograded greenschist-facies rocks are in some cases interstratified with other phyllosilicates (light coloured, mostly chlorite).

Table 1: Lithology and mineralogy of dated samples. Mineral abbreviations are after Whitney and Evans (2010).

Figure 3: Description and phengite chemistry of Syros samples. a) Location of samples on a geological cross-section (after Laurent et al., 2016, see location on Fig. 1b). b) Synthetic 3D sketch of post-eclogitic deformation showing the structural position of S07-04, S07-04bis and S07-Jojo samples. c) Phengite chemistry of dated samples measured by electron microprobe. For single grain analyses, both core and rim chemical compositions have been measured.

Figure 4: Outcrop conditions and phengite chemistry of Tinos samples. a) Location of samples on a geological cross-section (after Mehl et al., 2005, see location on Fig. 1c). b) Detailed localization at outcrop-scale of dated samples. c) Synthetic 3D sketch showing the structural position and deformation of T07-07 and T07-09. d) Phengite chemistry of dated samples measured by electron microprobe. For single grain analyses, both core and rim chemical compositions have been measured.

Figure 5: Description and phengite chemistry of Tinos samples. a) Synthetic 3D sketch of the detachment plane in Planitis (see location in Fig. 1c) showing the structural position of dated samples. b, c) Detailed location at outcrop-scale of T07-27 and T07-30 samples. d) Synthetic 3D sketch showing the structural position and deformation of T07-16 sample. e) Phengite chemistry of dated samples measured by electron microprobe. For single grain analyses, both core and rim chemical compositions have been measured.

Figure 6: Description and phengite chemistry of Tinos samples. a) Location of samples on a geological cross-section (after Huet et al., 2009, see location on Fig. 1d). b) Phengite chemistry of dated samples measured by electron microprobe. For single grain analyses, both core and rim chemical compositions have been measured.

Figure 7: $^{40}Ar/^{39}Ar$ ages from Syros. a) Age spectra obtained on single grain and population of phengite. b) Distribution of *in-situ* apparent ages in phengitic micas from sample S07-Jojo and isochron plot.

Figure 8: $^{40}Ar/^{39}Ar$ ages from Tinos. a) Age spectra obtained on single grain and populations of phengite. b, c) Distribution of *in-situ* apparent ages in phengitic micas in T07-15bis and T07-16 samples and isochron plots.

Figure 9: $^{40}Ar/^{39}Ar$ ages from Tinos. a) Age spectra measured on single grains and concentrates of phengites. b, c) Distribution of *in-situ* apparent ages in phengites from samples T07-18 and T07-19.

Figure 10: $^{40}Ar/^{39}Ar$ ages from Ios. a) Age spectra obtained on single grains and populations of phengite. b) Distribution of *in-situ* apparent ages in phengitic micas from sample I07-122. The two oldest ages measured in shear bands (zone B of I07-122) are not represented in the diagram.

Figure 11: Synthetic diagram compiling geochronological data from Syros, Tinos and Ios islands (raw data are listed in supplementary material).

Figure 12: Summary of $^{40}Ar/^{39}Ar$ *in-situ* apparent ages measured in phengites. Grey-scale colour refers to the microstructural position of the analysed phengite. The two oldest ages measured in I07-122 (shear bands, zone B) are not represented. Note that no clear correlation between ages and microstructural position are observed.

Figure 13: Series of step-by-step north-south cross-sections from 50 Ma to 8 Ma showing the tectono-metamorphic evolution of the CBU. See text for details.

Supplementary data:

Table 2. $^{40}Ar/^{39}Ar$ isotope results of concentrates.

Table 3. $^{40}Ar/^{39}Ar$ isotope results of single grains.

Table 4. $^{40}Ar/^{39}Ar$ isotope results of *in-situ* laser ablation experiments.

Table 5. Synthesis of geochronological data measured on Syros.

Table 6. Synthesis of geochronological data measured on Tinos.

Table 7. Synthesis of geochronological data measured on Ios.

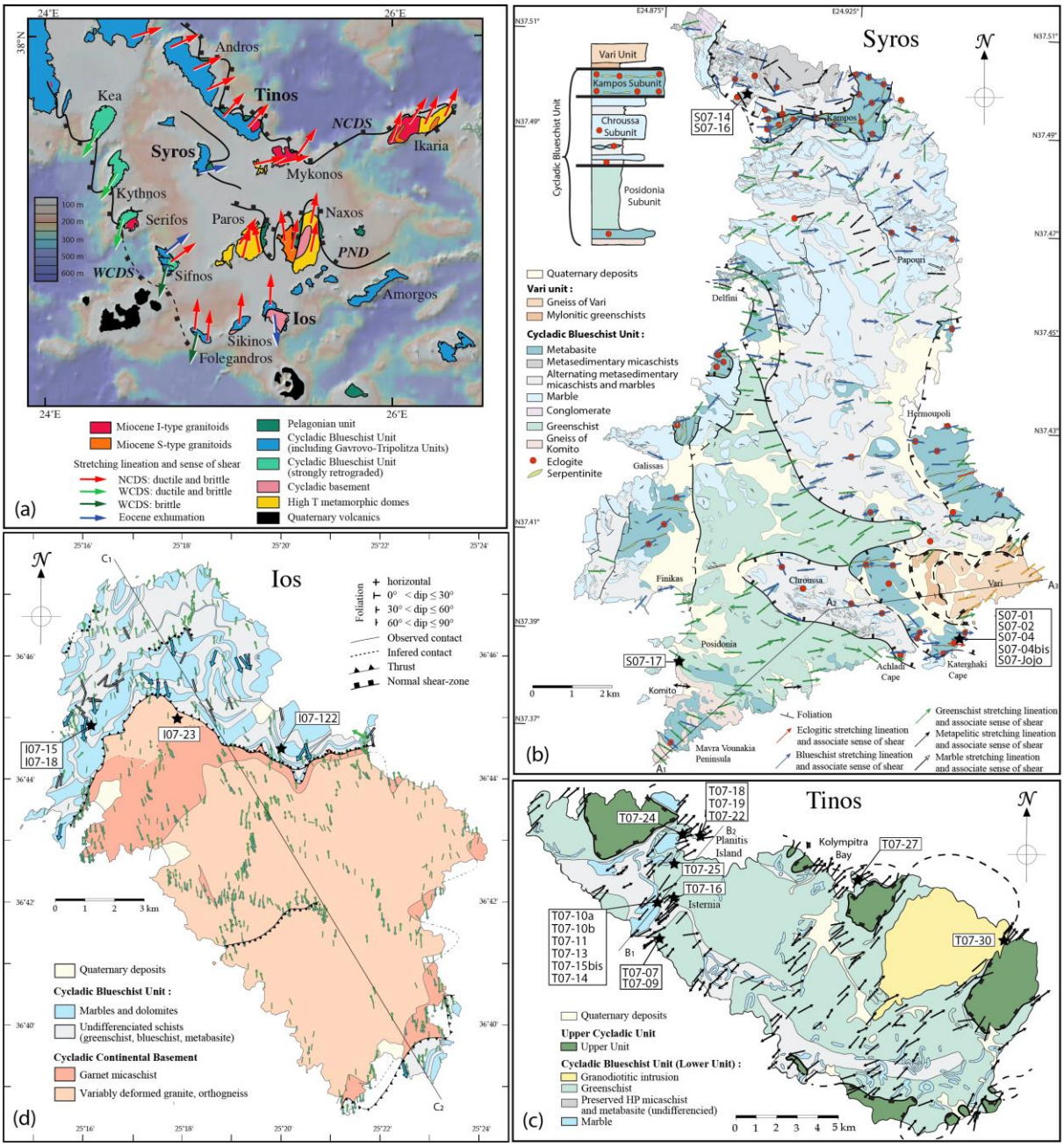
(a)
Andros
Tinos
Kea
Syros
NCDS
Ikaria
Mykonos
Kythnos
Serifos
Paros
Naxos
PND
WCDS
Sifnos
Amorgos
Ios
Sikinos
Folegandros
Miocene I-type granitoids
Miocene S-type granitoids
Stretching lineation and sense of shear
NCDS: ductile and brittle
WCDS: ductile and brittle
WCDS: brittle
Eocene exhumation
Pelagonian unit
Cycladic Blueschist Unit (including Gavrovo-Tripolitza Units)
Cycladic Blueschist Unit (strongly retrograded)
Cycladic basement
High T metamorphic domes
Quaternary volcanics
(b)
Syros
Vari Unit
Kampos Subunit
Chroussa Subunit
Posidonia Subunit
Cycladic Blueschist Unit
Quaternary deposits
Vari unit :
Gneiss of Vari
Mylonitic greenschists
Cycladic Blueschist Unit :
Metabasite
Metasedimentary micaschists
Alternating metasedimentary micaschists and marbles
Marble
Conglomerate
Greenschist
Gneiss of Komito
Eclogite
Serpentinite
S07-14
S07-16
Kampos
Papouri
Delfini
Hermoupoli
Galissas
Finikas
Chroussa
Vari
Posidonia
S07-17
Komito
Achladi Cape
Katerghaki Cape
S07-01
S07-02
S07-04
S07-04bis
S07-Jojo
Mavra Voumakia Peninsula
Foliation
Eclogitic stretching lineation and associate sense of shear
Blueschist stretching lineation and associate sense of shear
Greenschist stretching lineation and associate sense of shear
Metapelitic stretching lineation and associate sense of shear
Marble stretching lineation and associate sense of shear
(c)
Tinos
T07-18
T07-19
T07-22
T07-24
Planitis Island
Kolympitra Bay
T07-27
T07-25
T07-16
Istermia
T07-10a
T07-10b
T07-11
T07-13
T07-15bis
T07-14
T07-07
T07-09
T07-30
Quaternary deposits
Upper Cycladic Unit
Upper Unit
Cycladic Blueschist Unit (Lower Unit) :
Granodiotitic intrusion
Greenschist
Preserved HP micaschist and metabasite (undifferencied)
Marble
(d)
Ios
Foliation
horizontal
0° < dip ≤ 30°
30° < dip ≤ 60°
60° < dip ≤ 90°
Observed contact
Infered contact
Thrust
Normal shear-zone
I07-122
I07-23
I07-15
I07-18
Quaternary deposits
Cycladic Blueschist Unit :
Marbles and dolomites
Undifferenciated schists (greenschist, blueschist, metabasite)
Cycladic Continental Basement
Garnet micaschist
Variably deformed granite, orthogneiss

Figure 1

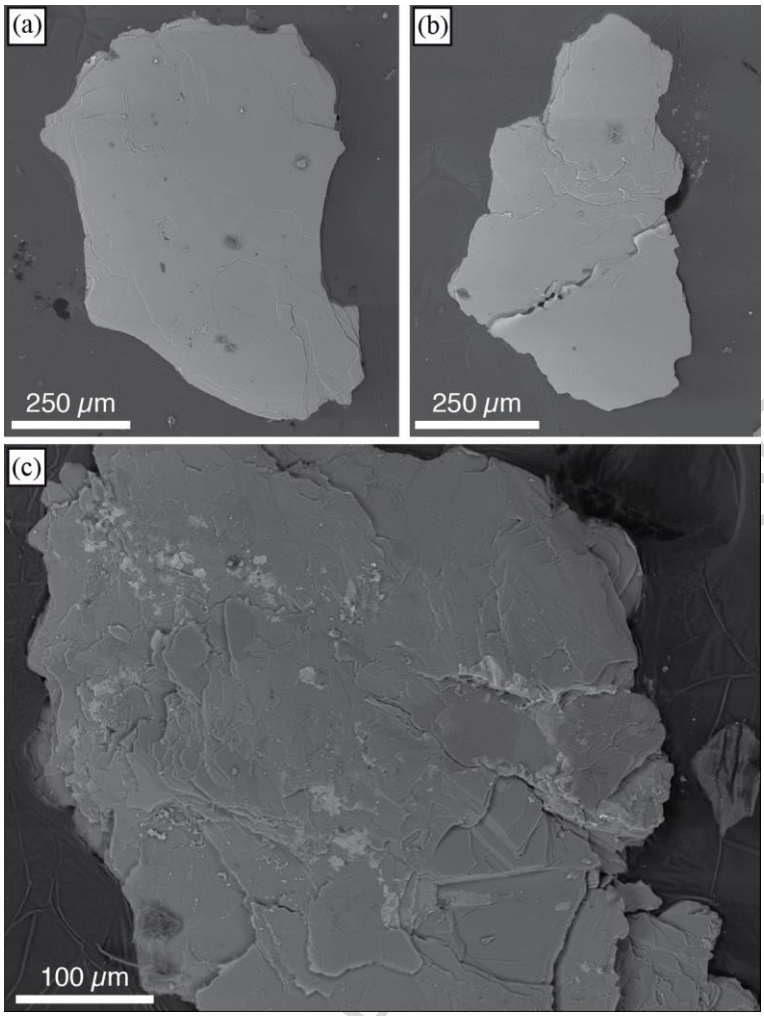

Figure 2

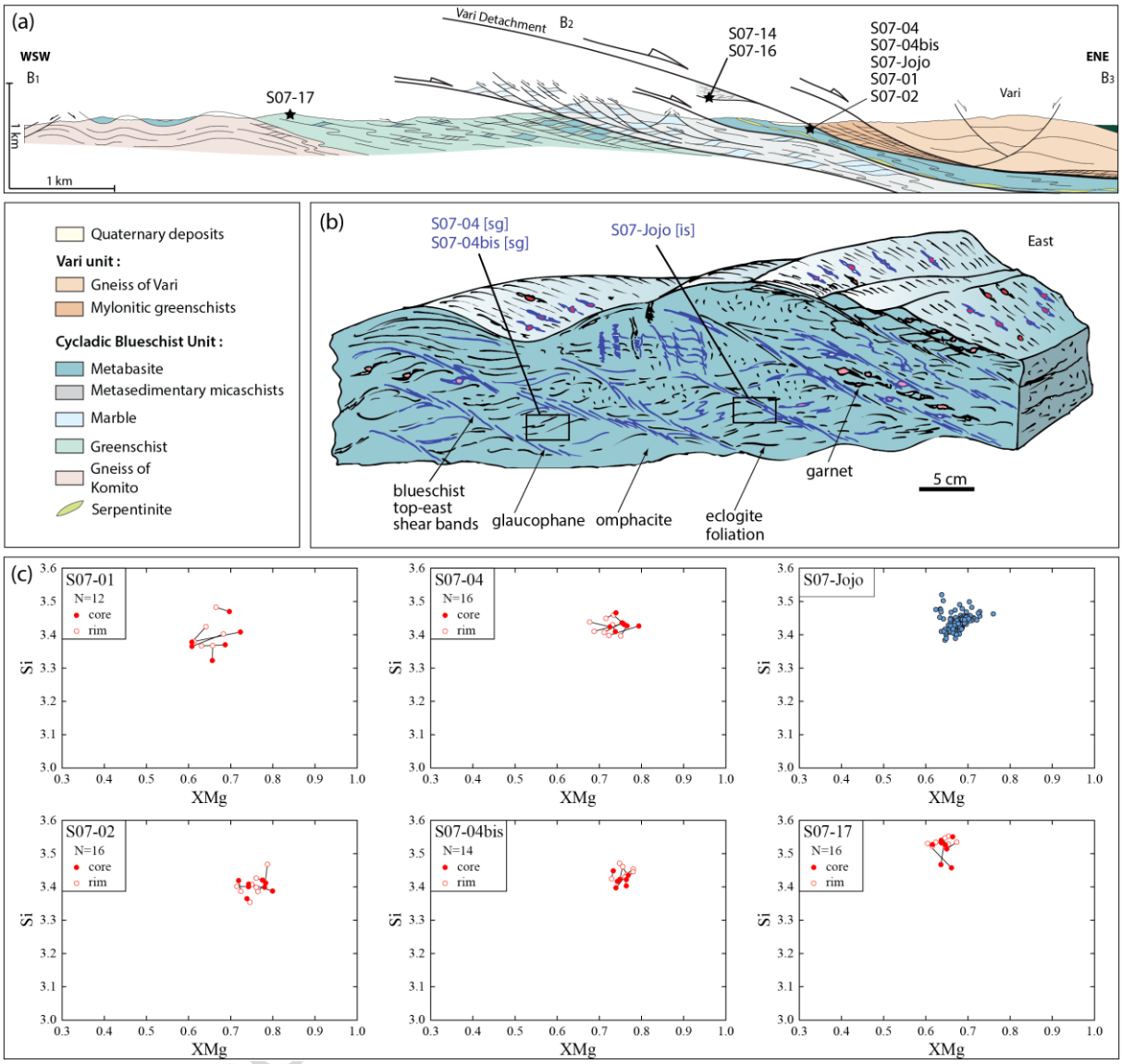

Figure 3

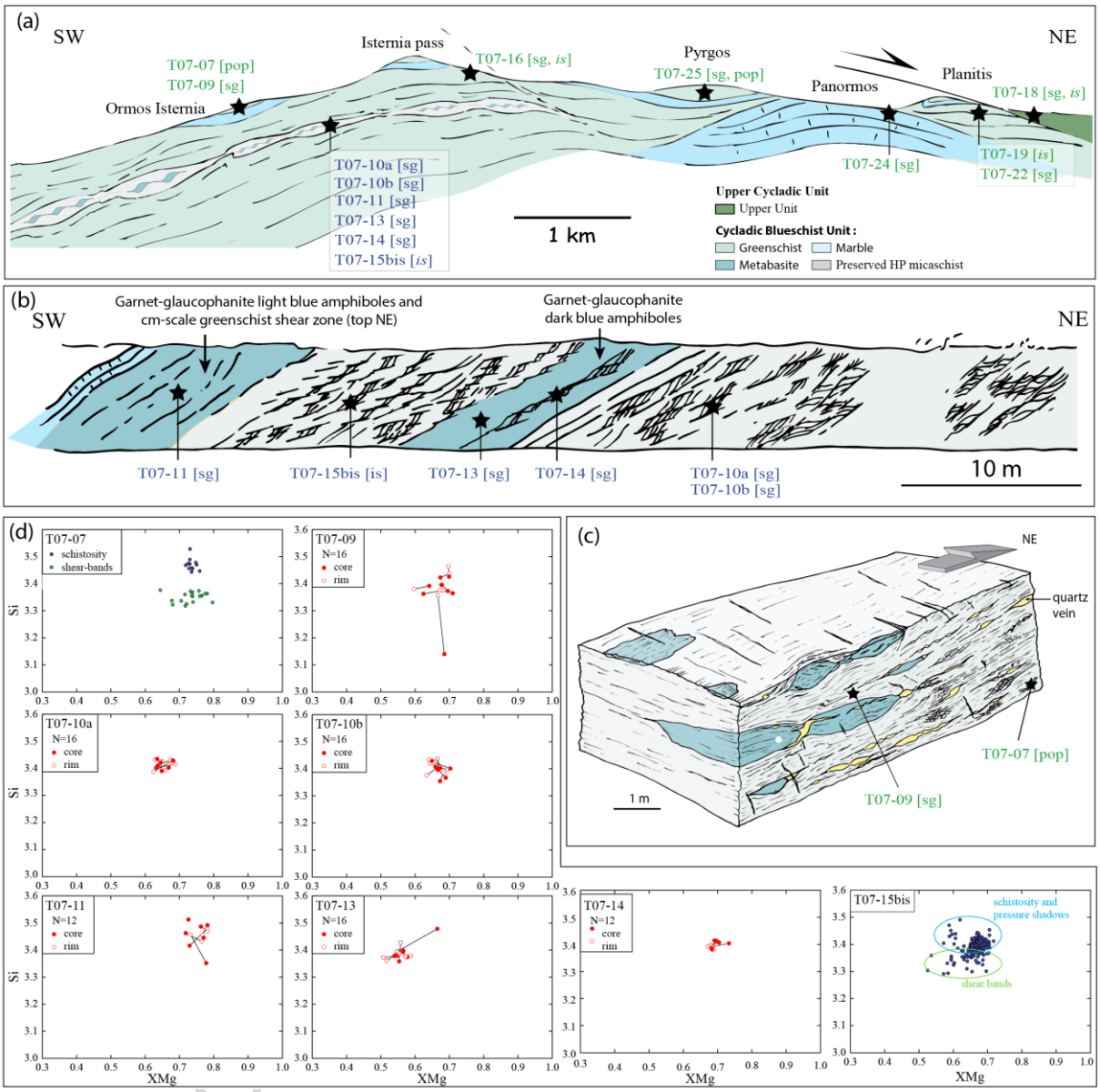

Figure 4

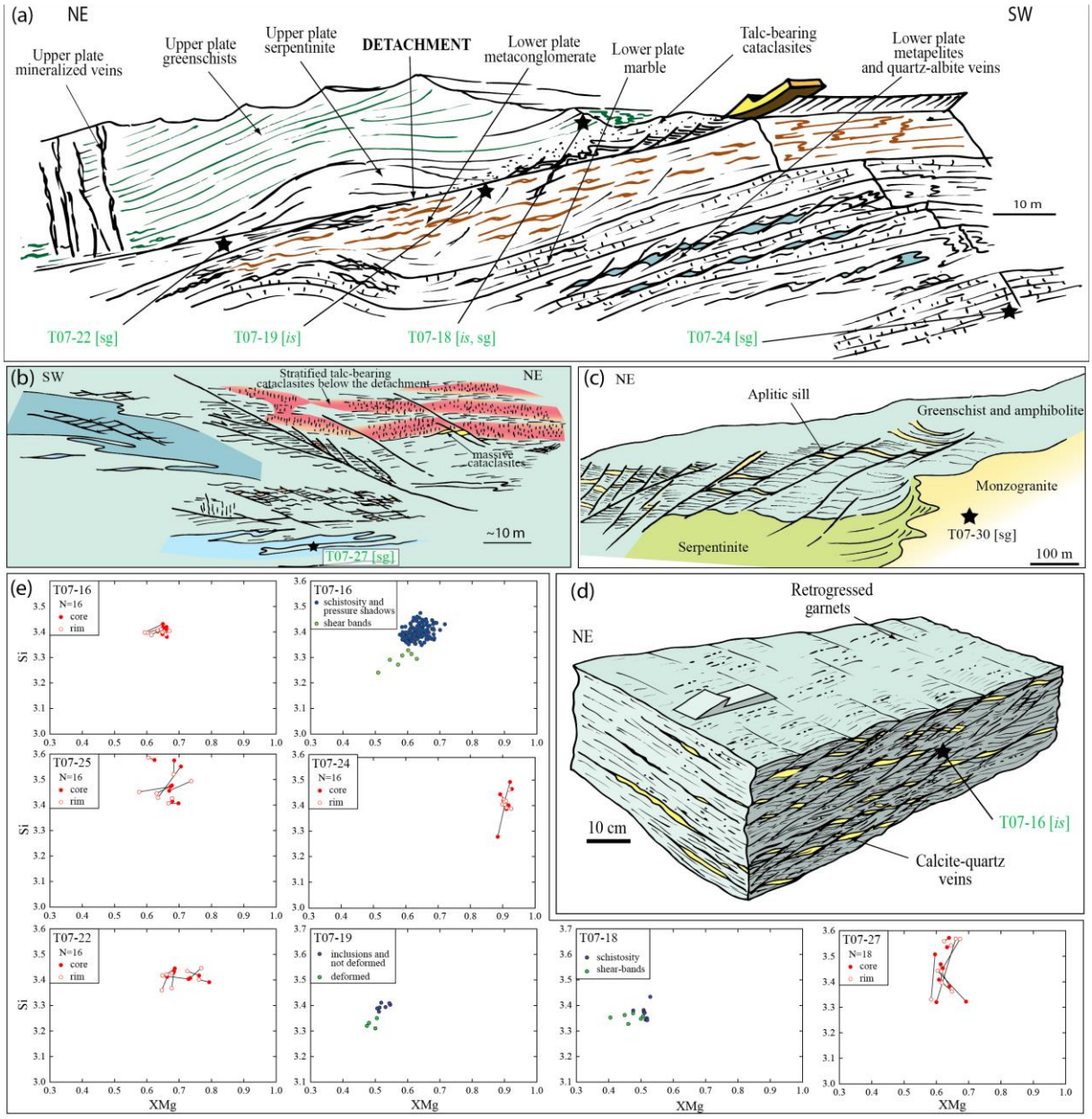

Figure 5

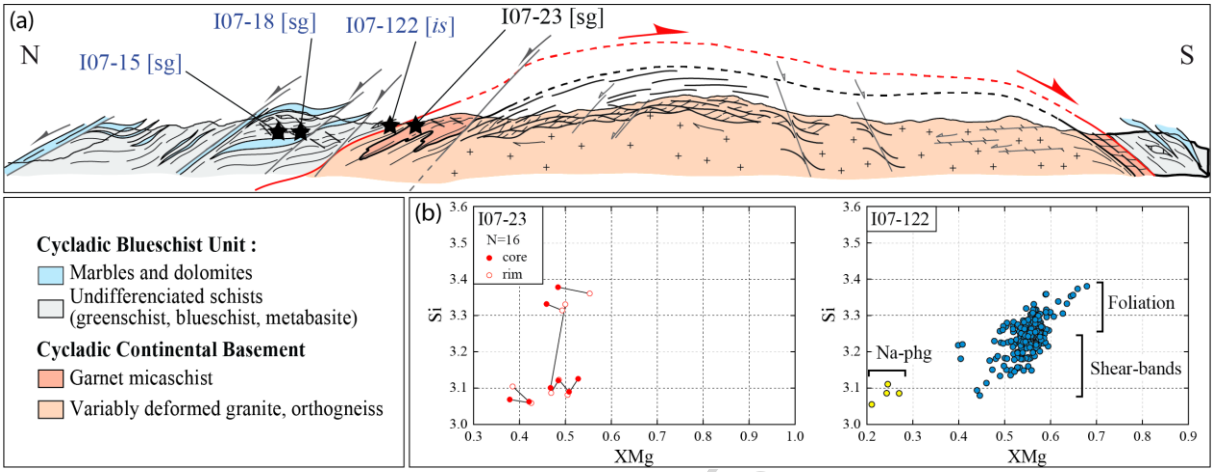

Figure 6

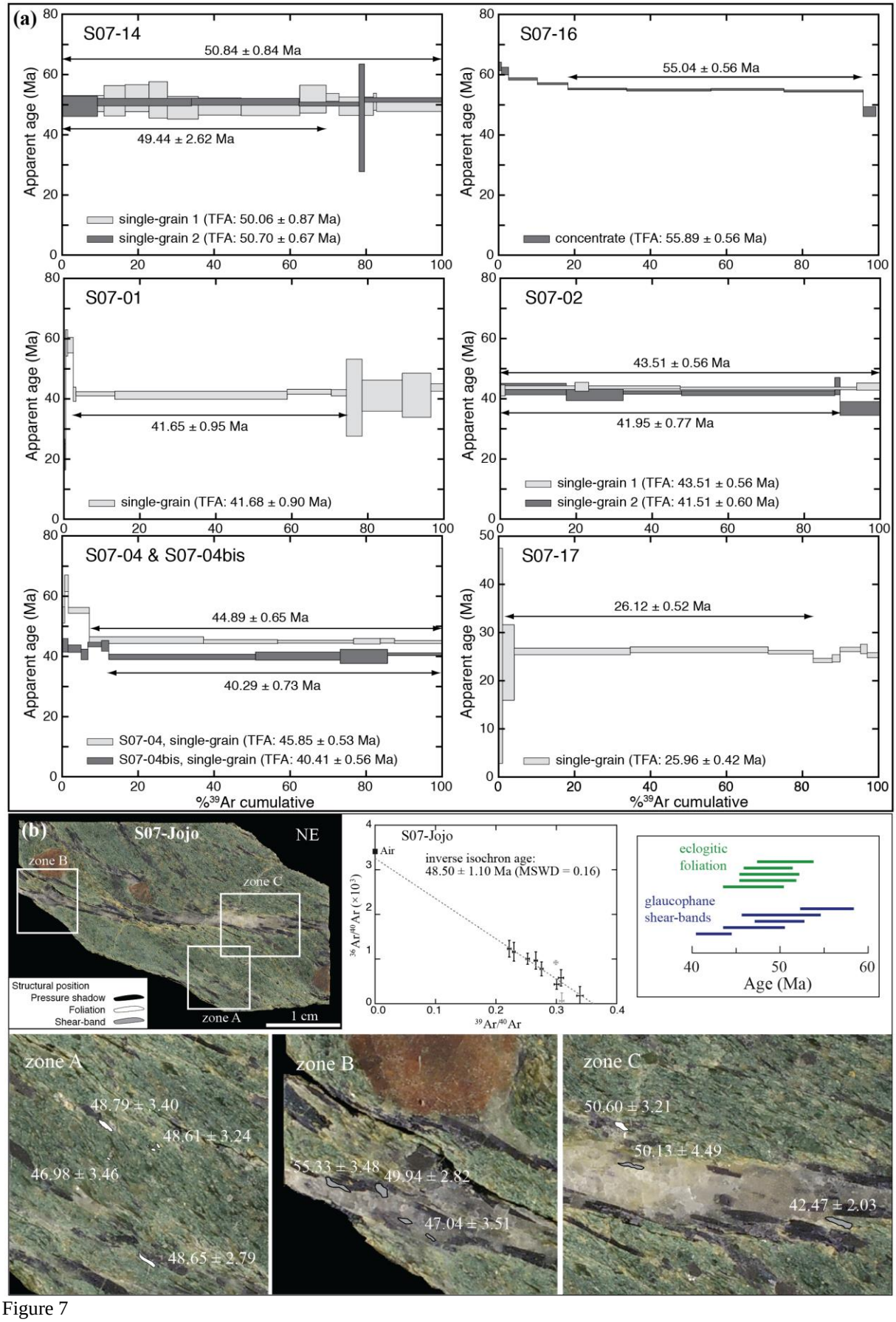
(a)
S07-14
50.84 ± 0.84 Ma
49.44 ± 2.62 Ma
single-grain 1 (TFA: 50.06 ± 0.87 Ma)
single-grain 2 (TFA: 50.70 ± 0.67 Ma)
S07-16
55.04 ± 0.56 Ma
concentrate (TFA: 55.89 ± 0.56 Ma)
S07-01
41.65 ± 0.95 Ma
single-grain (TFA: 41.68 ± 0.90 Ma)
S07-02
43.51 ± 0.56 Ma
41.95 ± 0.77 Ma
single-grain 1 (TFA: 43.51 ± 0.56 Ma)
single-grain 2 (TFA: 41.51 ± 0.60 Ma)
S07-04 & S07-04bis
44.89 ± 0.65 Ma
40.29 ± 0.73 Ma
S07-04, single-grain (TFA: 45.85 ± 0.53 Ma)
S07-04bis, single-grain (TFA: 40.41 ± 0.56 Ma)
S07-17
26.12 ± 0.52 Ma
single-grain (TFA: 25.96 ± 0.42 Ma)
Apparent age (Ma)
%39Ar cumulative
(b)
S07-Jojo
NE
zone B
zone C
zone A
1 cm
Structural position
Pressure shadow
Foliation
Shear-band
S07-Jojo
Air
inverse isochron age:
48.50 ± 1.10 Ma (MSWD = 0.16)
36Ar/40Ar (×10-3)
39Ar/40Ar
eclogitic foliation
glaucophane shear-bands
Age (Ma)
zone A
48.79 ± 3.40
48.61 ± 3.24
46.98 ± 3.46
48.65 ± 2.79
zone B
55.33 ± 3.48
49.94 ± 2.82
47.04 ± 3.51
zone C
50.60 ± 3.21
50.13 ± 4.49
42.47 ± 2.03

Figure 7

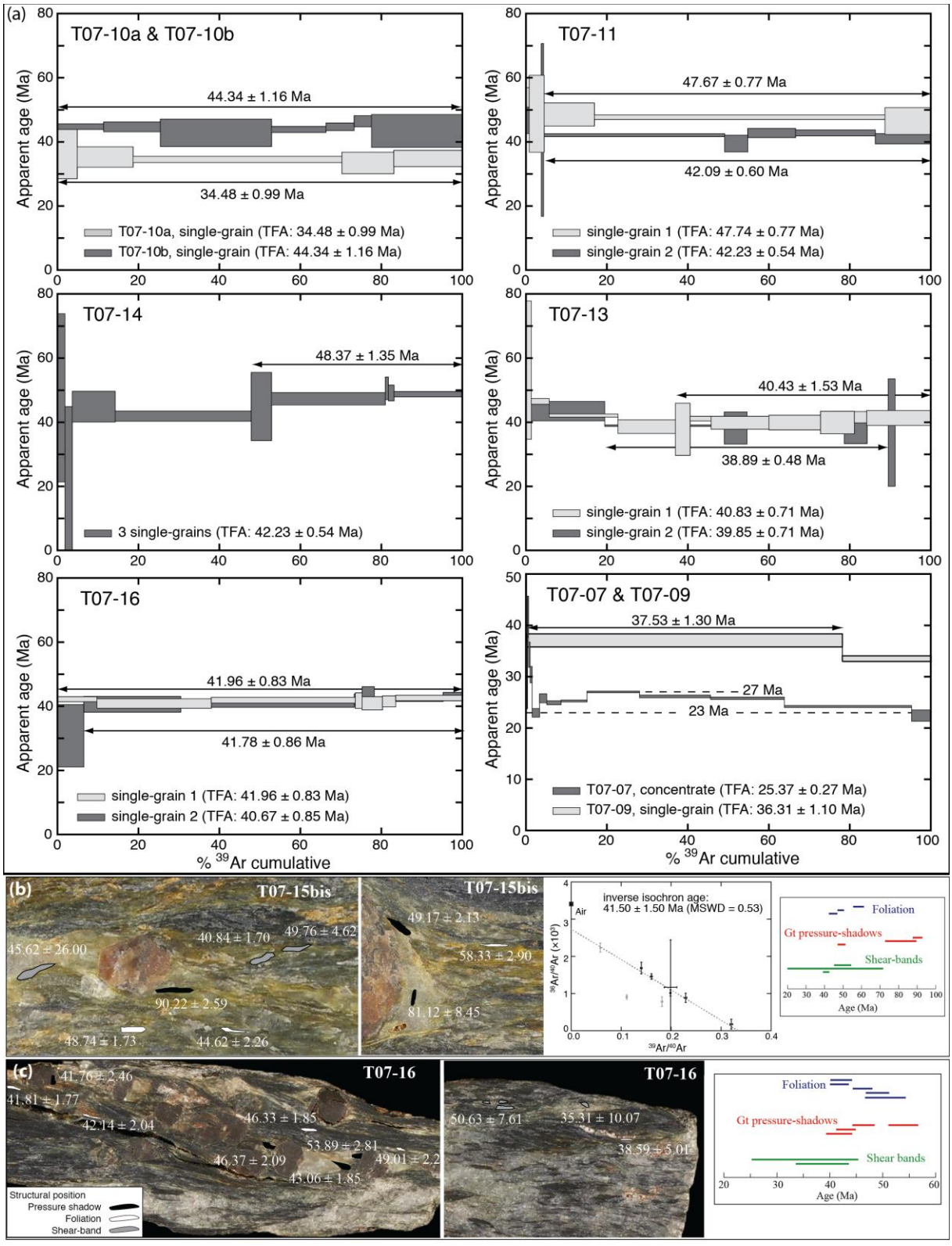
(a)
T07-10a & T07-10b
44.34 ± 1.16 Ma
34.48 ± 0.99 Ma
T07-10a, single-grain (TFA: 34.48 ± 0.99 Ma)
T07-10b, single-grain (TFA: 44.34 ± 1.16 Ma)
T07-11
47.67 ± 0.77 Ma
42.09 ± 0.60 Ma
single-grain 1 (TFA: 47.74 ± 0.77 Ma)
single-grain 2 (TFA: 42.23 ± 0.54 Ma)
T07-14
48.37 ± 1.35 Ma
3 single-grains (TFA: 42.23 ± 0.54 Ma)
T07-13
40.43 ± 1.53 Ma
38.89 ± 0.48 Ma
single-grain 1 (TFA: 40.83 ± 0.71 Ma)
single-grain 2 (TFA: 39.85 ± 0.71 Ma)
T07-16
41.96 ± 0.83 Ma
41.78 ± 0.86 Ma
single-grain 1 (TFA: 41.96 ± 0.83 Ma)
single-grain 2 (TFA: 40.67 ± 0.85 Ma)
T07-07 & T07-09
37.53 ± 1.30 Ma
27 Ma
23 Ma
T07-07, concentrate (TFA: 25.37 ± 0.27 Ma)
T07-09, single-grain (TFA: 36.31 ± 1.10 Ma)
Apparent age (Ma)
% 39Ar cumulative
(b)
T07-15bis
45.62 ± 26.00
40.84 ± 1.70
49.76 ± 4.62
90.22 ± 2.59
48.74 ± 1.73
44.62 ± 2.26
49.17 ± 2.13
58.33 ± 2.90
81.12 ± 8.45
inverse isochron age:
41.50 ± 1.50 Ma (MSWD = 0.53)
Air
36Ar/40Ar (×10³)
39Ar/40Ar
Foliation
Gt pressure-shadows
Shear-bands
Age (Ma)
(c)
T07-16
41.76 ± 2.46
41.81 ± 1.77
42.14 ± 2.04
46.33 ± 1.85
53.89 ± 2.81
46.37 ± 2.09
49.01 ± 2.2
43.06 ± 1.85
50.63 ± 7.61
35.31 ± 10.07
38.59 ± 5.01
Structural position
Pressure shadow
Foliation
Shear-band

Figure 8

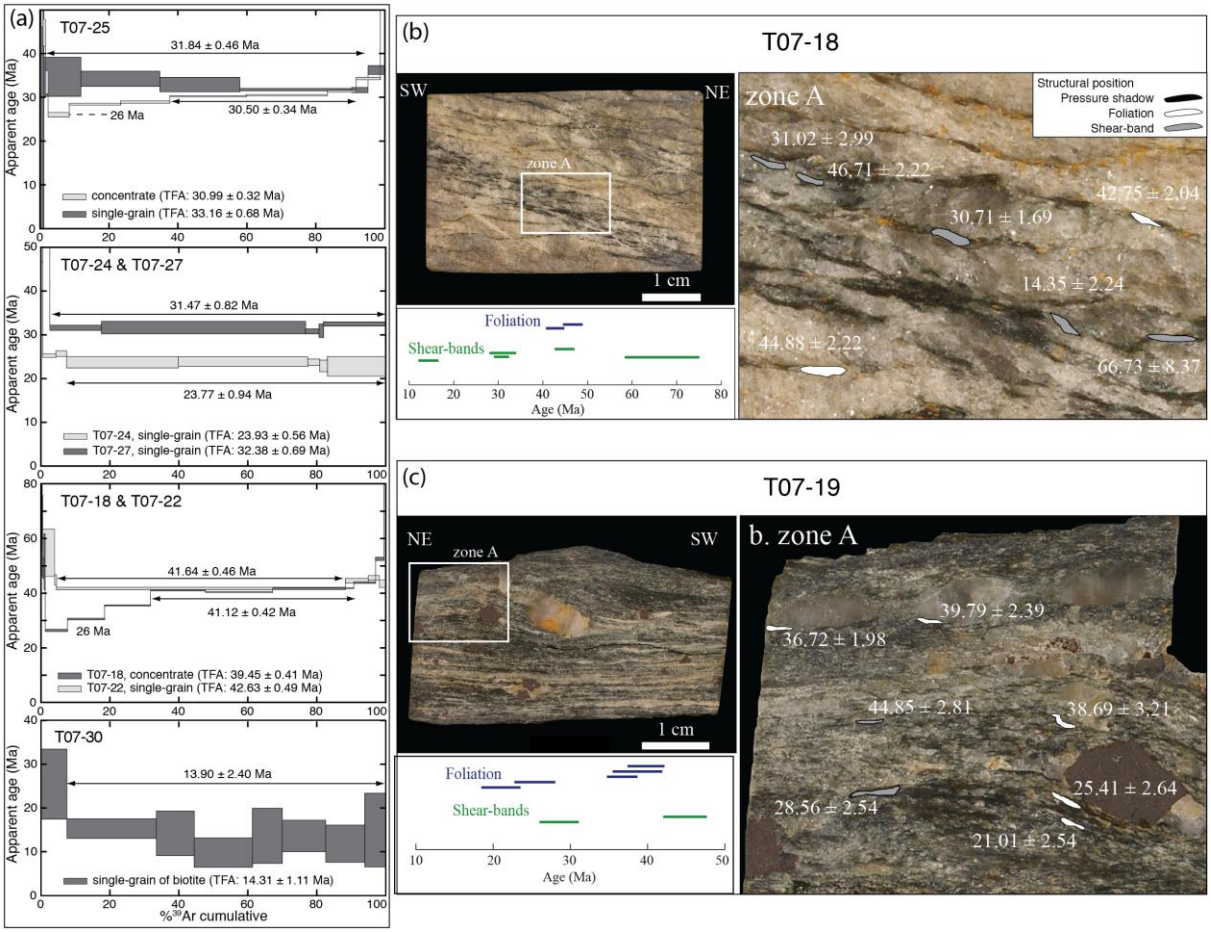

Figure 9

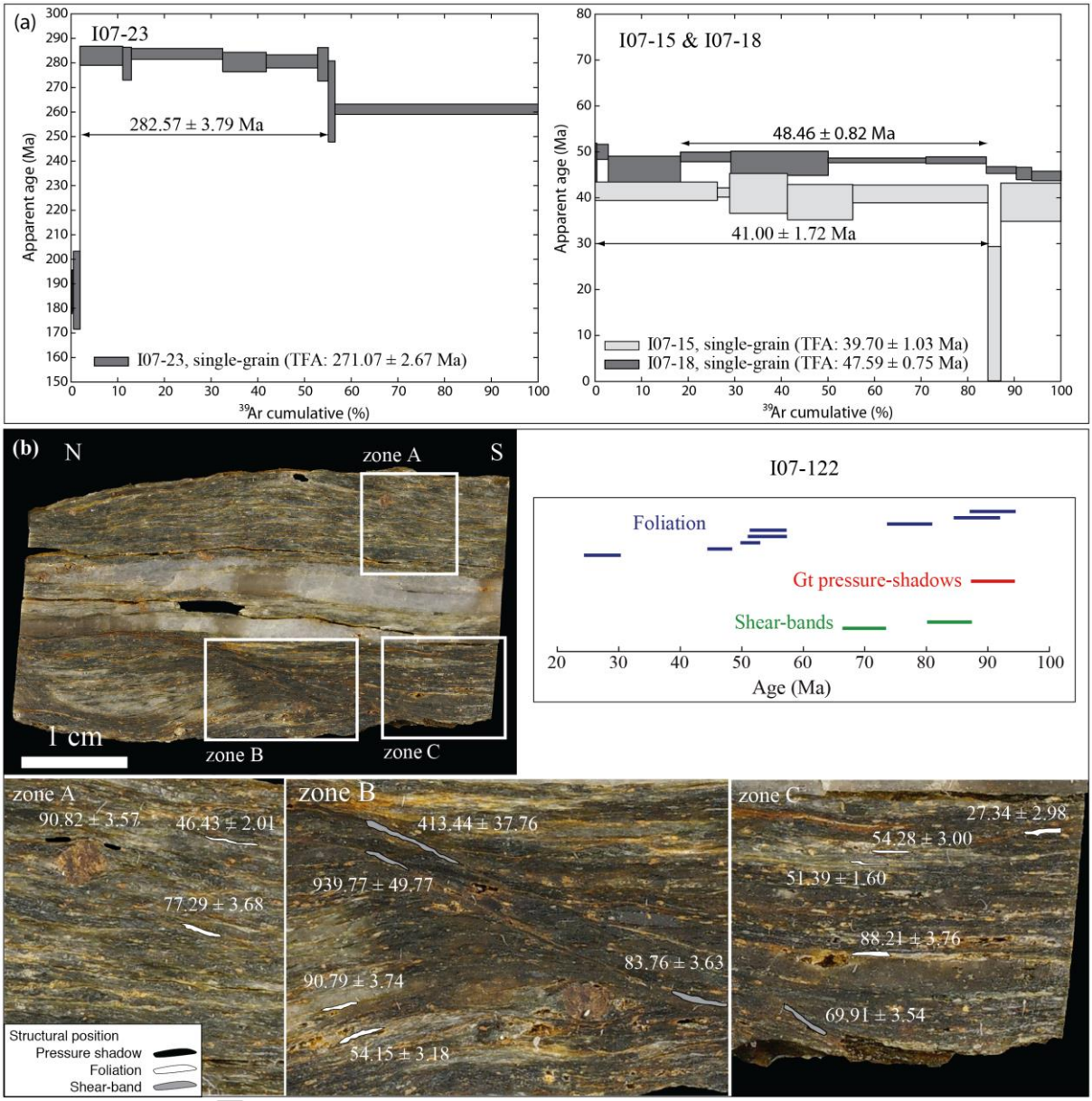

Figure 10

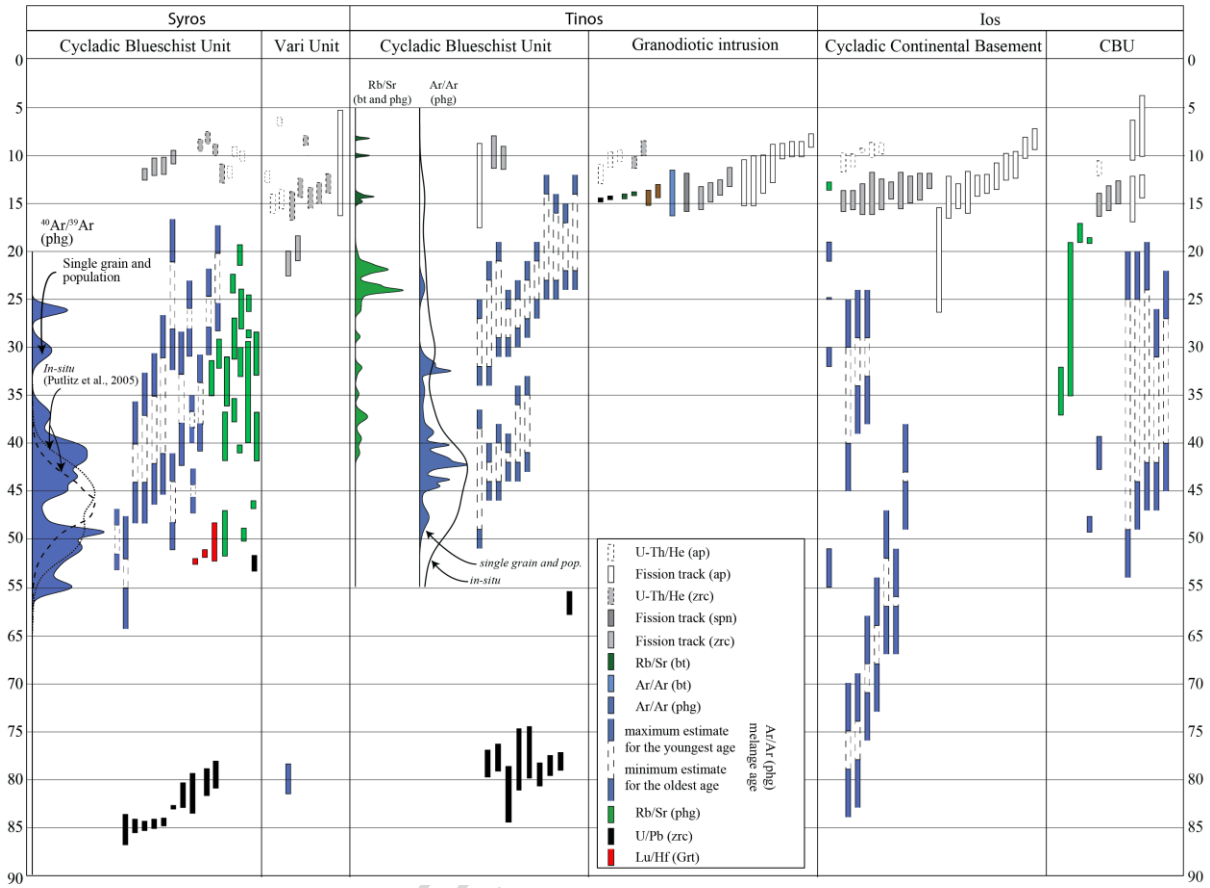

Figure 11

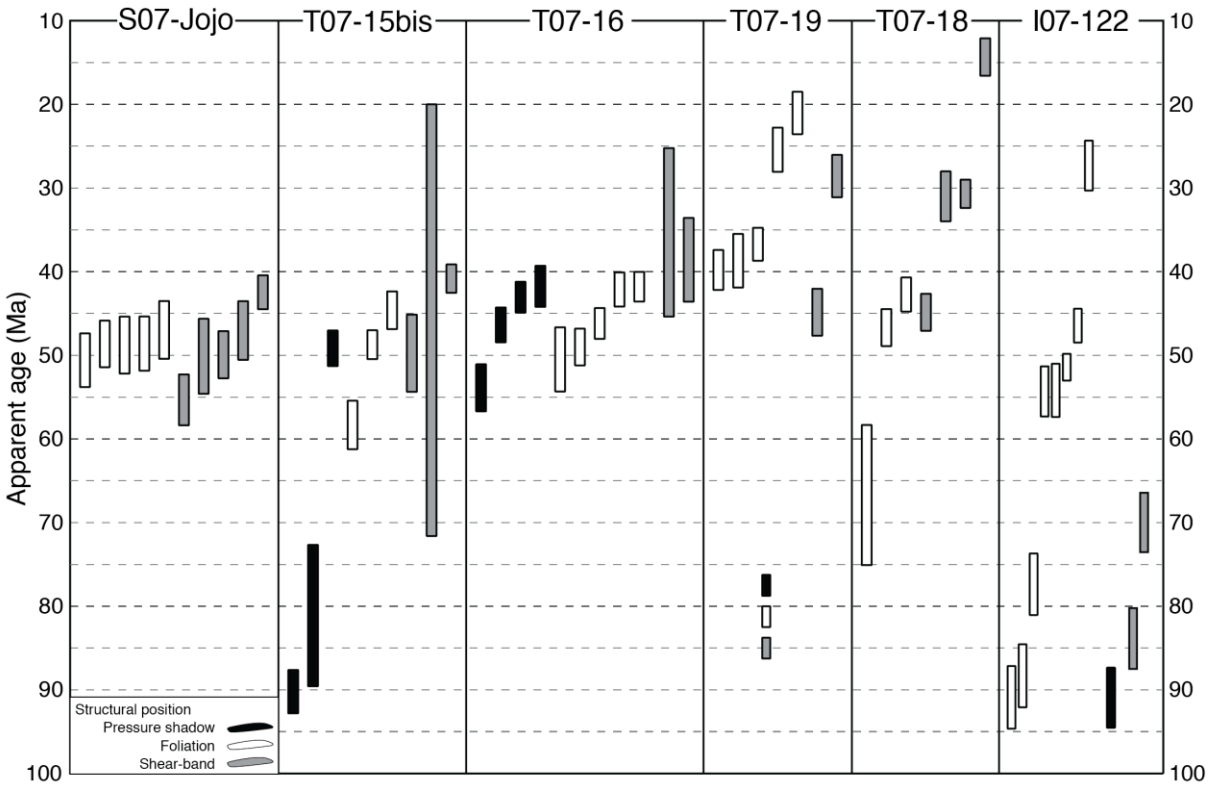

Figure 12

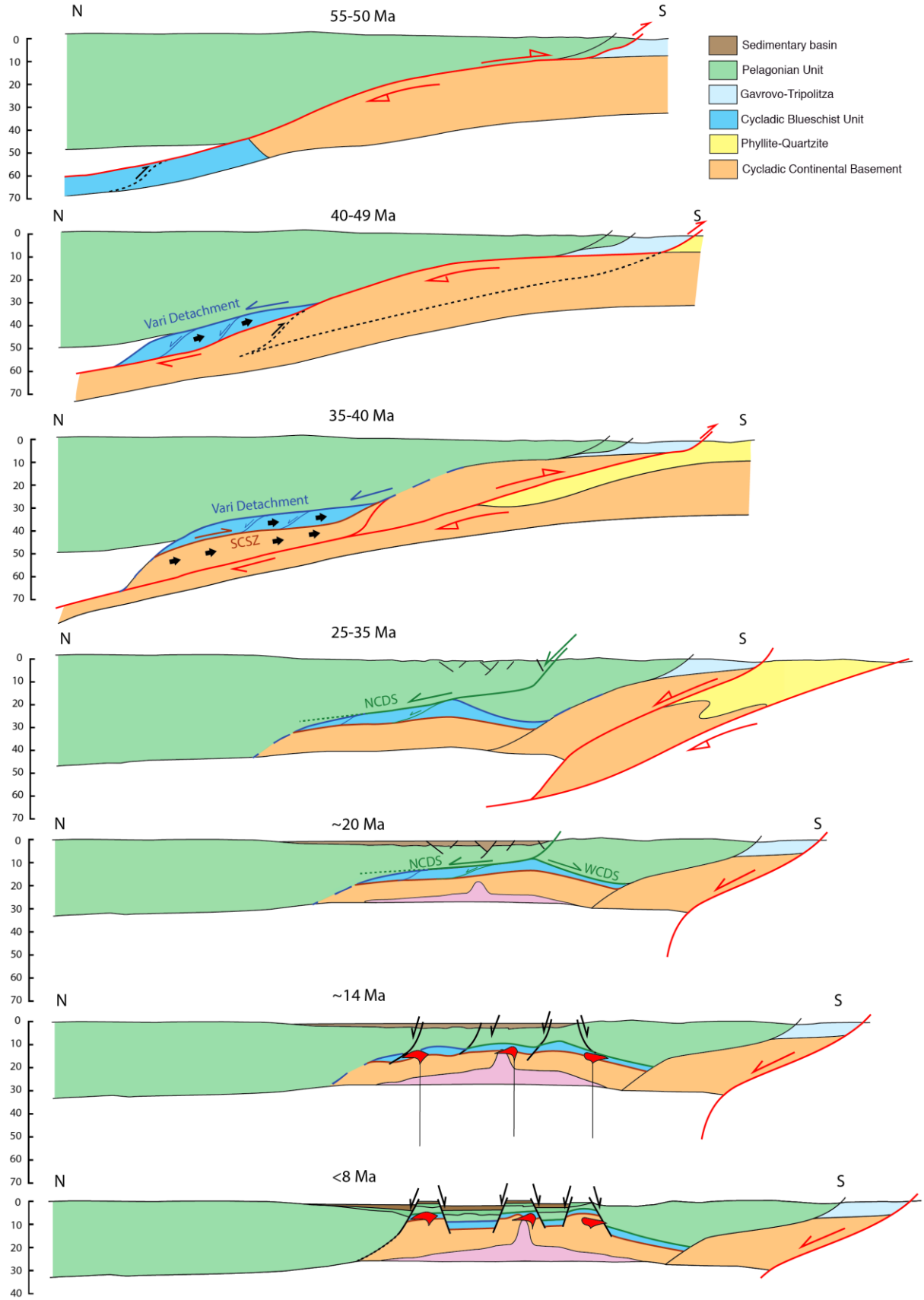

Figure 13

Table 1

Samples	Location	Unit	Mineralogy																Lithology	Lat. N/Lon. E.	$^{40}Ar/^{39}Ar$ analyses
			Ph	Pg	Bt	Omp	Grt	Gln	Cld	Ep	Chl	Ab	Qz	Ank	Cal	Py	Pl	Kfs	Hbl			
S07-14	Syros	CBU	x			x	x	x												Grt-Omp blueschist	37.4992/24.8935	single grain (2)
S07-16	Syros	CBU	x				x				x		x							Grt-Chl micaschist	37.4992/24.8935	concentrate (1)
S07-01	Syros	CBU	x					x		x			x							Gln-Ep micaschist	37.3891/24.9534	single grain (1)
S07-02	Syros	CBU	x					x					x	x						Blueschist	37.3891/24.9534	single grain (2)
S07-04	Syros	CBU	x			x	x	x												Gln eclogite	37.3891/24.9534	single grain (1)
S07-04bis	Syros	CBU	x			x	x	x												Gln eclogite	37.3891/24.9534	single grain (1)
S07-Jojo	Syros	CBU	x			x	x	x		x			x		x					Gln eclogite	37.3891/24.9534	*in situ* (10)
S07-17	Syros	CBU	x								x	x	x							Ab-Chl micaschist	37.3791/24.8819	single grain (1)
T07-07	Tinos	CBU	x								x	x	x							Ab-Chl micaschist	37.6153/25.0414	concentrate (1)
T07-09	Tinos	CBU	x	x							x		x		x					Calcschist	37.6153/25.0414	single grain (1)
T07-10a	Tinos	CBU	x							x			x							Ep-Qz-Phg vein	37.6216/25.0432	single grain (1)
T07-10b	Tinos	CBU	x								x		x							Chl micaschist	37.6216/25.0432	single grain (1)
T07-11	Tinos	CBU	x	x			x	x		x			x							Grt-Ep blueschist	37.6216/25.0432	single grain (2)
T07-13	Tinos	CBU	x				x	x		x			x							Grt-Ep blueschist	37.6216/25.0432	single grain (2)
T07-14	Tinos	CBU	x				x	x			x		x							Grt-Ep blueschist	37.6216/25.0432	single grain (1)
T07-15bis	Tinos	CBU	x				x				x		x							Grt-Chl micaschist	37.6216/25.0432	*in situ* (9)
T07-16	Tinos	CBU	x				x				x		x							Grt-Chl micaschist	37.6270/25.0481	single grain (2), in-situ (11)
T07-25	Tinos	CBU	x								x	x	x							Ab-Chl micaschist	37.6421/25.0408	single grain (1), concentrate (1)
T07-24	Tinos	CBU	x								x		x		x	x				Chl-Cal micaschist	37.6586/25.0560	single grain (1)
T07-22	Tinos	CBU	x							x	x		x		x					Chl-Cal-Qz-Ph vein	37.6604/25.0657	single grain (1)
T07-19	Tinos	CBU	x								x		x			x				Chl micaschist	37.6601/25.0659	*in situ* (7)
T07-18	Tinos	UCU	x								x				x					Chl-Ph marble	37.6596/25.0652	*in situ* (7), concentrate (1)
T07-27	Tinos	CBU	x								x		x							Chl micaschist	37.6230/25.1452	single grain (1)
T07-30	Tinos	Intrusion			x								x				x	x	x	I-type monzogranite	37.6102/25.2363	single grain (1)
I07-23	Ios	CCB	x				x					x	x							Grt micaschist	36.7510/25.3034	single grain (1)
I07122	Ios	CBU	x	x			x		x		x		x							Grt-Cld micaschist	36.7427/25.3297	*in situ* (13)
I07-15	Ios	CBU	x	x				x		x		x	x							Ab-Ep blueschist	36.7480/25.2666	single grain (1)
I07-18	Ios	CBU	x	x			x	x		x										Grt-Ep blueschist	36.7480/25.2666	single grain (1)

Table 2

Temperature	$^{40}Ar/^{39}Ar$	$^{38}Ar/^{39}Ar$	$^{37}Ar/^{39}Ar$	$^{36}Ar/^{39}Ar$ $\times10^{-3}$ mol	^{39}Ar $\times10^{-14}$ mol	$\%^{39}Ar$ released	$\%^{40}Ar^{*}$	$^{40}Ar^{*}/^{39}Ar_K$	Age (Ma)	±1σ (Ma)
SO7-16		Phg		J= 0.009989						
700	35.780	0.199	0.00001	99.931	0.037	0.15	17.41	6.23	108.97	6.91
750	26.521	0.079	0.00005	39.764	0.011	0.20	55.62	14.75	248.09	21.67
800	15.164	0.043	0.04232	11.534	0.021	0.29	77.41	11.74	200.16	6.03
833	12.945	0.004	0.00003	0.006	0.021	0.38	99.83	12.92	219.10	2.12
866	6.498	0.026	0.00001	1.178	0.072	0.68	94.34	6.13	107.28	1.09
900	4.063	0.030	0.00319	1.718	0.178	1.43	87.02	3.54	62.73	0.71
933	4.689	0.021	0.00651	4.125	0.449	3.33	73.58	3.45	61.16	0.64
966	3.796	0.014	0.00167	1.625	1.796	10.89	86.83	3.30	58.54	0.20
1000	3.426	0.013	0.00133	0.660	1.912	18.93	93.73	3.21	56.97	0.15
1033	3.264	0.013	0.00154	0.462	3.668	34.38	95.21	3.11	55.22	0.13
1066	3.235	0.013	0.00157	0.420	5.279	56.60	95.55	3.09	54.87	0.15
1100	3.223	0.013	0.00245	0.350	4.562	75.81	96.18	3.10	55.05	0.14
1200	3.245	0.013	0.00201	0.527	4.948	96.64	94.59	3.07	54.52	0.17
1400	11.845	0.021	0.01214	30.953	0.799	100.00	22.61	2.68	47.69	0.81
T07-07		Phg		J= 0.009989						
700	21.264	0.102	0.00001	64.131	0.077	0.19	10.78	2.29	40.83	6.47
750	8.732	0.036	0.00001	23.757	0.075	0.38	19.37	1.69	30.22	3.24
800	4.475	0.019	0.00000	7.158	0.114	0.67	52.28	2.34	41.71	2.01
833	2.924	0.014	0.00929	3.326	0.150	1.04	65.72	1.92	34.29	1.23
866	2.394	0.016	0.01442	2.294	0.206	1.56	70.90	1.70	30.39	0.79
900	2.097	0.015	0.00617	2.710	0.722	3.37	60.86	1.28	22.93	0.42
933	1.944	0.014	0.00299	1.635	0.717	5.16	74.13	1.44	25.78	0.44
966	1.616	0.013	0.00105	0.686	1.409	8.68	86.23	1.39	24.89	0.20
1000	1.579	0.013	0.00050	0.501	2.569	15.11	89.37	1.41	25.25	0.09
1033	1.667	0.013	0.00108	0.470	5.179	28.07	90.48	1.51	27.02	0.08
1066	1.625	0.013	0.00109	0.484	7.010	45.61	89.98	1.46	26.13	0.13
1100	1.576	0.013	0.00121	0.391	7.277	63.82	91.40	1.44	25.78	0.12
1200	1.482	0.013	0.00123	0.378	12.563	95.25	91.11	1.35	24.18	0.10
1400	4.867	0.016	0.00769	12.173	1.897	100.00	25.68	1.25	22.40	0.55
T07-18		Phg		J= 0.009989						
700	38.043	0.255	0.02595	113.615	0.001	0.21	11.71	4.46	78.56	11.51
750	15.708	0.098	0.00004	21.130	0.001	0.32	60.15	9.45	162.70	9.52
800	6.431	0.034	0.04326	8.679	0.001	0.55	59.93	3.85	68.15	3.84
833	4.043	0.023	0.02410	4.286	0.002	0.94	68.33	2.76	49.12	1.88
866	21.966	0.063	0.39098	64.584	0.002	1.26	13.18	2.90	51.45	5.14
900	2.064	0.014	0.23186	2.006	0.037	7.70	71.37	1.47	26.35	0.20
933	2.249	0.014	0.08909	1.801	0.061	18.48	75.93	1.71	30.51	0.15
966	2.079	0.012	0.00641	0.252	0.076	31.81	95.69	1.99	35.49	0.09
1000	2.353	0.012	0.00194	0.126	0.090	47.71	97.76	2.30	40.98	0.07
1033	2.335	0.012	0.00217	0.190	0.111	67.22	96.93	2.26	40.34	0.06
1066	2.397	0.012	0.00148	0.125	0.134	90.75	97.82	2.35	41.77	0.05
1100	2.523	0.013	0.00661	0.154	0.036	97.07	97.59	2.46	43.84	0.14
1200	3.107	0.014	0.01343	0.456	0.014	99.51	95.19	2.96	52.53	0.30
1400	91.499	0.072	0.09171	287.170	0.003	100.00	7.25	6.63	115.72	11.78
T07-25		Phg		J= 0.009989						
700	10.353	0.021	0.06329	13.823	0.001	0.17	60.44	6.26	109.38	5.61
750	22.200	0.062	0.27173	33.797	0.000	0.20	55.03	12.22	207.77	24.22
800	8.207	0.023	0.08183	3.719	0.001	0.39	86.50	7.10	123.60	2.86
833	5.034	0.019	0.15816	7.479	0.003	0.94	56.02	2.82	50.12	1.99
866	4.016	0.017	0.24385	5.082	0.004	1.64	62.67	2.52	44.80	1.53
900	3.320	0.012	0.30718	4.912	0.004	2.40	56.51	1.88	33.51	1.32
933	2.769	0.015	0.08513	4.407	0.034	8.47	52.63	1.46	26.07	0.28
966	1.976	0.013	0.00325	1.246	0.083	23.35	80.59	1.59	28.48	0.12

1000	1.978	0.013	0.00184	1.155	0.080	37.65	81.96	1.62	28.98	0.14
1033	1.998	0.012	0.00164	0.972	0.123	59.83	84.84	1.69	30.29	0.07
1066	1.962	0.012	0.00209	0.804	0.131	83.40	87.11	1.71	30.55	0.08
1100	1.861	0.013	0.00424	0.292	0.046	91.70	94.53	1.76	31.43	0.10
1200	2.041	0.013	0.01119	0.344	0.039	98.73	94.30	1.92	34.35	0.15
1400	37.342	0.036	0.04928	115.630	0.007	100.00	8.47	3.16	56.09	2.71

Table 3

Step No.	$^{40}Ar/^{39}Ar$	$^{38}Ar/^{39}Ar$	$^{37}Ar/^{39}Ar$	$^{36}Ar/^{39}Ar$ $\times10^{-3}$ mol	^{39}Ar $\times10^{-14}$ mol	$\%^{39}Ar$ released	$\%^{40}Ar^{*}$	$^{40}Ar^{*}/^{39}Ar_K$	Age (Ma)	±1σ (Ma)
S07-01		Phg		J= 0.009901						
1	1.255	0.000	0.00000	0.002	0.002	0.24	98.72	1.24	21.99	2.32
2	1.183	0.009	0.00000	0.002	0.002	0.46	98.63	1.17	20.72	2.19
3	3.348	0.002	0.00000	0.001	0.005	0.98	99.53	3.33	58.56	2.20
4	3.288	0.016	0.22079	0.000	0.014	2.49	99.53	3.29	57.81	1.28
5	2.355	0.029	0.12570	0.001	0.006	3.18	99.34	2.35	41.47	1.18
6	2.374	0.012	0.00000	0.000	0.096	13.44	99.34	2.36	41.64	0.34
7	2.415	0.011	0.00196	0.241	0.426	58.76	96.41	2.33	41.12	0.67
8	2.412	0.011	0.00764	0.000	0.109	70.40	99.35	2.40	42.32	0.39
9	2.395	0.012	0.00000	0.000	0.037	74.35	99.35	2.38	42.01	0.52
10	2.589	0.018	0.00000	0.979	0.039	78.49	88.23	2.28	40.35	6.40
11	2.399	0.010	0.01928	0.211	0.099	89.08	96.81	2.32	41.02	2.57
12	2.446	0.013	0.03059	0.345	0.071	96.60	95.29	2.33	41.17	3.66
13	2.490	0.008	0.06179	0.000	0.032	100.00	99.37	2.48	43.74	0.64
S07-02		Phg		J= 0.009901						
1	2.438	0.012	0.00000	0.000	0.010	1.28	99.36	2.42	42.76	0.91
2	2.487	0.013	0.00000	0.000	0.138	19.68	99.37	2.47	43.62	0.30
3	2.505	0.015	0.00000	0.000	0.027	23.29	99.38	2.49	43.93	0.72
4	2.491	0.013	0.00643	0.000	0.180	47.37	99.37	2.48	43.70	0.25
5	2.475	0.013	0.00000	0.000	0.348	93.81	99.37	2.46	43.41	0.21
6	2.507	0.013	0.00000	0.000	0.046	100.00	99.38	2.49	43.97	0.59
S07-02		Phg		J= 0.009901						
1	2.570	0.013	0.00000	0.372	0.139	17.37	95.12	2.44	43.15	0.94
2	2.471	0.011	0.00140	0.404	0.120	32.35	94.54	2.34	41.24	0.96
3	2.398	0.013	0.00508	0.000	0.123	47.69	99.35	2.38	42.06	0.27
4	2.383	0.012	0.00232	0.000	0.324	88.09	99.35	2.37	41.81	0.40
5	2.515	0.009	0.04594	0.000	0.011	89.41	99.38	2.50	44.16	1.42
6	2.271	0.012	0.02474	0.615	0.085	100.00	91.39	2.08	36.70	1.15
S07-04		Phg		J= 0.009901						
1	3.067	0.020	0.00000	0.000	0.008	0.67	99.49	3.05	53.70	1.35
2	3.677	0.016	0.00000	0.000	0.012	1.64	99.57	3.66	64.23	1.39
3	3.156	0.014	0.01118	0.000	0.067	7.17	99.51	3.14	55.25	0.48
4	2.587	0.013	0.00016	0.000	0.363	37.22	99.40	2.57	45.35	0.54
5	2.557	0.012	0.00908	0.000	0.235	56.73	99.39	2.54	44.84	0.32
6	2.557	0.013	0.02134	0.000	0.241	76.71	99.39	2.54	44.86	0.23
7	2.565	0.011	0.03338	0.000	0.085	83.75	99.39	2.55	45.01	0.45
8	2.573	0.011	0.03871	0.000	0.045	87.47	99.39	2.56	45.16	0.37
9	2.550	0.011	0.00000	0.000	0.151	100.00	99.39	2.53	44.72	0.24
S07-04bis		Phg		J= 0.009901						
1	2.487	0.010	0.02393	0.000	0.026	1.56	99.37	2.47	43.64	1.12
2	2.424	0.014	0.01210	0.000	0.057	4.99	99.36	2.41	42.53	0.61
3	2.313	0.013	0.02968	0.000	0.030	6.79	99.33	2.30	40.62	0.88
4	2.504	0.014	0.00000	0.000	0.060	10.36	99.38	2.49	43.90	0.39
5	2.481	0.019	0.00000	0.000	0.032	12.27	99.37	2.47	43.51	0.89
6	2.306	0.013	0.00000	0.130	0.647	50.92	97.66	2.25	39.78	0.43
7	2.459	0.013	0.00303	0.590	0.372	73.17	92.28	2.27	40.09	0.67
8	2.367	0.012	0.00000	0.306	0.209	85.63	95.52	2.26	39.94	1.16
9	2.319	0.013	0.00000	0.000	0.240	100.00	99.33	2.30	40.68	0.22
S07-14		Phg		J= 0.009901						
1	2.934	0.011	0.00000	0.205	0.162	11.01	97.40	2.86	50.34	1.34
2	2.930	0.009	0.02744	0.023	0.082	16.58	99.31	2.91	51.24	2.53
3	2.977	0.012	0.00000	0.001	0.093	22.88	99.47	2.96	52.13	2.23
4	2.975	0.011	0.05034	0.122	0.071	27.71	98.39	2.93	51.54	3.03
5	3.063	0.013	0.02038	0.926	0.119	35.83	90.60	2.78	48.90	1.87

6	3.035	0.012	0.01433	0.742	0.166	47.11	92.29	2.80	49.35	1.42
7	2.968	0.012	0.00000	0.684	0.227	62.55	92.67	2.75	48.47	1.08
8	3.001	0.014	0.00000	0.146	0.102	69.48	98.04	2.94	51.80	2.31
9	2.991	0.013	0.00557	0.000	0.049	72.85	99.48	2.98	52.39	0.65
10	2.977	0.015	0.00000	0.525	0.133	81.90	94.26	2.81	49.44	1.52
11	2.908	0.024	0.00000	0.000	0.012	82.72	99.46	2.89	50.94	1.41
12	2.932	0.013	0.00000	0.362	0.254	100.00	95.82	2.81	49.49	0.91
S07-14		Phg		J= 0.009901						
1	3.312	0.015	0.00713	1.666	0.083	9.30	84.68	2.80	49.41	1.68
2	2.947	0.013	0.00000	0.161	0.221	34.04	97.85	2.88	50.78	0.62
3	2.929	0.012	0.00918	0.075	0.252	62.31	98.73	2.89	50.92	0.57
4	2.863	0.012	0.00705	0.000	0.141	78.16	99.46	2.85	50.16	0.32
5	3.962	0.026	0.00000	4.608	0.013	79.59	65.24	2.58	45.59	8.92
6	2.940	0.013	0.01448	0.000	0.182	100.00	99.47	2.93	51.52	0.37
S07-17		Phg		J= 0.009901						
1	1.758	0.009	0.01572	1.106	0.021	1.06	80.58	1.42	25.12	11.17
2	2.048	0.013	0.00391	2.352	0.062	4.13	65.32	1.34	23.74	3.91
3	1.524	0.012	0.00051	0.137	0.616	34.67	96.33	1.47	26.03	0.34
4	1.507	0.012	0.00048	0.015	0.732	70.97	98.68	1.49	26.37	0.31
5	1.476	0.012	0.00105	0.000	0.238	82.79	98.94	1.46	25.90	0.19
6	1.378	0.011	0.00000	0.000	0.102	87.83	98.87	1.36	24.16	0.22
7	1.399	0.006	0.04486	0.000	0.041	89.86	98.89	1.39	24.61	0.39
8	1.504	0.010	0.04165	0.000	0.109	95.28	98.96	1.49	26.45	0.23
9	1.508	0.013	0.07146	0.000	0.035	97.03	98.97	1.50	26.55	0.49
10	1.437	0.012	0.03003	0.000	0.060	100.00	98.91	1.42	25.25	0.26
T07-10a		Phg		J= 0.009989						
1	3.895	0.012	0.00036	6.127	0.050	4.87	53.11	2.07	36.90	4.21
2	2.982	0.013	0.00000	3.354	0.143	18.67	66.23	1.98	35.25	1.59
3	2.543	0.012	0.00021	2.016	0.535	70.29	75.96	1.93	34.48	0.49
4	2.547	0.013	0.01504	2.246	0.133	83.10	73.37	1.87	33.36	1.68
5	2.458	0.013	0.01527	1.674	0.175	100.00	79.28	1.95	34.78	1.25
T07-10b		Phg		J= 0.009989						
1	2.527	0.011	0.00000	0.000	0.050	11.43	99.38	2.51	44.69	0.44
2	2.520	0.011	0.02461	0.000	0.061	25.41	99.38	2.51	44.62	0.77
3	2.482	0.014	0.02370	0.224	0.120	52.87	96.78	2.40	42.77	2.14
4	2.475	0.012	0.01746	0.000	0.059	66.30	99.37	2.46	43.82	0.47
5	2.515	0.016	0.10608	0.000	0.031	73.30	99.38	2.51	44.63	0.59
6	2.617	0.018	0.07902	0.000	0.019	77.58	99.40	2.61	46.39	0.87
7	2.575	0.012	0.00000	0.421	0.098	100.00	94.57	2.44	43.37	2.57
T07-11		Phg		J= 0.009989						
1	3.048	0.030	0.00000	0.000	0.008	0.83	99.48	3.03	53.83	1.51
2	3.257	0.015	0.00000	1.701	0.036	4.51	84.09	2.74	48.70	6.00
3	2.884	0.014	0.00000	0.477	0.122	16.91	94.57	2.73	48.49	1.80
4	2.862	0.012	0.00149	0.561	0.709	88.68	93.67	2.68	47.67	0.36
5	2.947	0.012	0.01187	1.092	0.112	100.00	88.55	2.61	46.42	2.09
T07-11		Phg		J= 0.009989						
1	3.706	0.018	0.00000	3.409	0.042	3.41	72.40	2.68	47.71	2.57
2	2.861	0.000	0.69753	0.001	0.005	3.82	99.45	2.90	51.49	1.77
3	3.436	0.019	1.17703	3.577	0.007	4.37	71.35	2.45	43.68	13.48
4	2.474	0.012	0.01475	0.337	0.553	49.09	95.39	2.36	42.04	0.21
5	2.663	0.011	0.00253	1.476	0.071	54.81	83.04	2.21	39.42	1.30
6	2.598	0.011	0.00000	0.624	0.146	66.58	92.30	2.40	42.70	0.71
7	2.595	0.013	0.00000	0.604	0.244	86.31	92.52	2.40	42.76	0.45
8	2.601	0.013	0.00510	0.967	0.169	100.00	88.43	2.30	40.97	0.81
T07-13		Phg		J= 0.009989						
1	4.234	0.024	0.25605	3.624	0.022	1.36	74.80	3.17	56.20	10.79
2	2.624	0.013	0.04159	0.000	0.072	5.76	99.41	2.61	46.46	0.44
3	2.375	0.012	0.00900	0.000	0.277	22.74	99.34	2.36	42.04	0.24

4	2.325	0.013	0.00947	0.496	0.231	36.92	93.06	2.16	38.57	1.07
5	2.362	0.013	0.03607	0.785	0.059	40.56	89.64	2.12	37.75	4.07
6	2.321	0.012	0.01195	0.000	0.085	45.76	99.33	2.31	41.09	0.36
7	2.327	0.012	0.00819	0.268	0.233	60.02	95.95	2.23	39.79	1.00
8	2.354	0.013	0.00000	0.349	0.208	72.78	94.96	2.24	39.84	1.13
9	2.371	0.011	0.00000	0.407	0.136	81.13	94.27	2.23	39.83	1.75
10	2.345	0.008	0.00000	0.000	0.050	84.19	99.33	2.33	41.50	0.88
11	2.377	0.012	0.00000	0.152	0.258	100.00	97.46	2.32	41.27	1.16
T07-13		Phg		J= 0.009989						
1	2.890	0.015	0.00000	1.480	0.411	19.46	84.32	2.44	43.39	1.51
2	2.196	0.012	0.00481	0.000	0.625	49.03	99.29	2.18	38.88	0.11
3	2.295	0.013	0.01343	0.477	0.118	54.62	93.22	2.14	38.14	2.50
4	2.252	0.012	0.00712	0.161	0.507	78.64	97.22	2.19	39.04	0.60
5	2.182	0.011	0.01724	0.120	0.119	84.26	97.72	2.13	38.02	2.37
6	2.252	0.009	0.02209	0.000	0.111	89.49	99.31	2.24	39.88	0.48
7	3.338	0.005	0.06949	4.293	0.036	91.19	61.68	2.06	36.72	8.38
8	2.259	0.012	0.02663	0.000	0.186	100.00	99.31	2.25	40.02	0.29
T07-14		Phg		J= 0.009989						
1	4.255	0.013	0.06358	5.310	0.015	1.83	62.87	2.68	47.58	13.11
2	3.622	0.011	0.07871	9.068	0.015	3.64	25.75	0.93	16.73	14.05
3	3.075	0.013	0.00219	1.833	0.090	14.27	81.89	2.52	44.82	2.40
4	2.569	0.011	0.00428	0.691	0.283	47.86	91.45	2.35	41.84	0.80
5	2.852	0.013	0.00000	1.069	0.042	52.88	88.37	2.52	44.86	5.32
6	2.690	0.013	0.00000	0.057	0.237	80.98	98.79	2.66	47.27	0.95
7	2.859	0.000	0.00000	0.001	0.006	81.73	99.45	2.84	50.52	1.75
8	2.771	0.002	0.05988	0.000	0.012	83.15	99.44	2.76	49.06	1.22
9	2.755	0.014	0.00565	0.000	0.142	100.00	99.43	2.74	48.72	0.42
T07-16		Phg		J= 0.009989						
1	4.414	0.016	0.03339	9.056	0.051	6.51	39.08	1.73	30.82	4.87
2	2.518	0.012	0.00671	0.752	0.186	30.45	90.57	2.28	40.63	1.22
3	2.362	0.012	0.01055	0.149	0.334	73.34	97.51	2.30	41.04	0.66
4	2.387	0.009	0.00000	0.000	0.015	75.24	99.34	2.37	42.24	0.82
5	2.446	0.011	0.01050	0.000	0.024	78.27	99.36	2.43	43.29	1.42
6	2.377	0.013	0.01817	0.000	0.133	95.30	99.34	2.36	42.09	0.27
7	2.429	0.012	0.05951	0.000	0.037	100.00	99.36	2.42	43.06	0.64
T07-16		Phg		J= 0.009989						
1	2.384	0.013	0.02342	0.000	0.069	9.76	99.35	2.37	42.22	0.39
2	2.443	0.012	0.01025	0.452	0.199	38.00	93.93	2.29	40.88	0.73
3	2.384	0.012	0.01250	0.059	0.251	73.56	98.66	2.35	41.90	0.44
4	2.339	0.011	0.27656	0.000	0.012	75.24	99.33	2.34	41.76	1.22
5	2.308	0.013	0.06926	0.000	0.036	80.28	99.32	2.30	40.95	1.03
6	2.347	0.011	0.00953	0.000	0.023	83.54	99.34	2.33	41.54	0.86
7	2.407	0.013	0.00537	0.000	0.116	100.00	99.35	2.39	42.60	0.42
T07-25		Phg		J= 0.009989						
1	3.016	0.001	0.00000	4.233	0.012	1.16	58.01	1.75	31.26	15.83
2	3.639	0.012	0.00000	5.680	0.113	11.86	53.45	1.95	34.72	2.24
3	2.030	0.012	0.00000	0.322	0.242	34.74	94.54	1.92	34.25	0.87
4	2.018	0.013	0.00000	0.529	0.245	57.91	91.48	1.85	32.96	0.84
5	1.795	0.012	0.00000	0.000	0.343	90.41	99.13	1.78	31.78	0.14
6	1.788	0.011	0.02642	0.000	0.050	95.14	99.13	1.77	31.69	0.30
7	2.048	0.014	0.00000	0.000	0.051	100.00	99.24	2.03	36.26	0.52
T07-24		Phg		J= 0.009989						
1	2.835	0.011	0.00000	0.001	0.006	0.59	99.44	2.82	50.10	1.67
2	1.425	0.010	0.03659	0.000	0.040	4.34	98.91	1.41	25.27	0.21
3	1.454	0.013	0.00000	0.000	0.034	7.45	98.93	1.44	25.74	0.32
4	1.467	0.012	0.00187	0.419	0.349	39.82	90.52	1.33	23.78	0.64
5	1.374	0.011	0.00525	0.080	0.405	77.39	97.17	1.34	23.90	0.54
6	1.341	0.009	0.04371	0.000	0.037	80.85	98.84	1.33	23.78	0.36

7	1.296	0.008	0.00699	0.000	0.025	83.14	98.80	1.28	22.94	0.66
8	1.381	0.011	0.00358	0.310	0.182	100.00	92.26	1.27	22.82	1.13
T07-22		Phg		J= 0.009989						
1	4.268	0.011	0.39154	0.001	0.006	0.40	99.63	4.28	75.58	1.82
2	4.039	0.011	0.00011	3.187	0.050	3.96	76.30	3.08	54.69	4.30
3	2.530	0.012	0.00000	0.000	0.008	4.53	99.38	2.51	44.76	0.98
4	2.519	0.012	0.00234	0.562	1.168	88.27	92.80	2.34	41.64	0.23
5	2.516	0.013	0.03125	0.000	0.093	94.93	99.38	2.50	44.54	0.42
6	2.574	0.016	0.04462	0.000	0.045	98.15	99.39	2.56	45.59	0.41
7	2.453	0.016	0.01884	0.000	0.026	100.00	99.36	2.44	43.42	0.71
T07-27		Phg		J= 0.009989						
1	3.123	0.042	0.00000	0.000	0.015	2.58	99.50	3.11	55.15	1.54
2	1.783	0.016	0.00000	0.000	0.085	17.56	99.12	1.77	31.58	0.29
3	1.883	0.013	0.00000	0.326	0.338	76.76	94.05	1.77	31.63	0.70
4	1.735	0.016	0.03445	0.000	0.023	80.71	99.10	1.72	30.76	0.28
5	1.745	0.013	0.00000	0.001	0.007	81.97	99.10	1.73	30.89	0.77
6	1.831	0.013	0.01019	0.000	0.103	100.00	99.15	1.82	32.44	0.24
Tinos-30		Bt		J= 0.009989						
1	6.198	0.024	0.00867	16.106	0.069	7.54	22.97	1.42	25.48	4.01
2	1.132	0.020	0.00000	0.884	0.238	33.44	75.54	0.85	15.34	1.12
3	1.062	0.020	0.00553	0.857	0.101	44.43	74.72	0.79	14.25	2.55
4	0.946	0.019	0.00000	1.291	0.155	61.30	58.02	0.55	9.86	1.67
5	0.881	0.018	0.00471	0.354	0.079	69.93	86.41	0.76	13.67	3.14
6	0.901	0.018	0.01580	0.421	0.116	82.49	84.57	0.76	13.67	1.79
7	0.902	0.018	0.02521	0.764	0.105	93.87	73.45	0.66	11.90	2.13
8	0.937	0.019	0.01951	0.297	0.056	100.00	89.12	0.84	14.99	4.20
I07-18				J= 0.009901						
1	2.710	0.025	0.00000	0.001	0.003	0.35	99.41	2.69	47.48	2.34
2	2.865	0.007	0.07786	0.000	0.022	2.80	99.46	2.86	50.30	0.82
3	2.840	0.012	0.00000	0.777	0.141	18.30	91.37	2.60	45.77	1.79
4	2.807	0.014	0.00000	0.000	0.099	29.13	99.44	2.79	49.18	0.52
5	2.832	0.013	0.00000	0.355	0.190	49.99	95.75	2.71	47.79	1.32
6	2.762	0.013	0.00000	0.000	0.191	70.96	99.44	2.75	48.40	0.25
7	2.765	0.013	0.00000	0.000	0.118	83.94	99.44	2.75	48.45	0.36
8	2.642	0.011	0.00000	0.000	0.058	90.37	99.41	2.63	46.31	0.38
9	2.597	0.018	0.03105	0.000	0.030	93.67	99.40	2.58	45.56	0.67
10	2.568	0.012	0.01693	0.000	0.058	100.00	99.39	2.55	45.04	0.52
I07-15				J= 0.009901						
1	2.540	0.011	0.00385	0.605	0.239	26.26	92.36	2.35	41.43	1.01
2	2.346	0.004	0.00000	0.000	0.024	28.89	99.33	2.33	41.15	0.50
3	2.491	0.012	0.00730	0.536	0.113	41.30	93.04	2.32	40.94	2.17
4	2.476	0.012	0.00044	0.850	0.128	55.32	89.22	2.21	39.03	1.92
5	2.518	0.011	0.00868	0.644	0.264	84.34	91.85	2.31	40.84	0.96
6	2.252	0.010	0.01853	5.719	0.025	87.11	24.32	0.55	9.76	9.81
7	2.442	0.013	0.00000	0.734	0.117	100.00	90.48	2.21	39.04	2.08
I07-23				J= 0.009901						
1	11.026	0.020	0.00000	0.001	0.006	0.26	99.86	11.01	186.67	4.40
2	11.069	0.000	0.00000	0.001	0.006	0.54	99.86	11.05	187.36	4.15
3	11.802	0.012	0.00000	2.474	0.030	1.93	93.67	11.06	187.40	7.95
4	17.163	0.012	0.00861	0.000	0.199	11.07	99.91	17.15	282.91	1.94
5	16.954	0.013	0.00000	0.000	0.041	12.94	99.91	16.94	279.71	3.35
6	17.224	0.013	0.00979	0.037	0.426	32.48	99.85	17.20	283.68	1.10
7	16.994	0.012	0.00223	0.000	0.203	41.80	99.91	16.98	280.33	1.98
8	17.013	0.013	0.01301	0.000	0.240	52.83	99.91	17.00	280.63	1.32
9	16.935	0.017	0.00000	0.000	0.050	55.11	99.91	16.92	279.42	3.41
10	15.977	0.016	0.00000	0.089	0.031	56.53	99.74	15.94	264.30	8.25
11	15.746	0.012	0.00113	0.000	0.947	100.00	99.90	15.73	261.14	1.04

Table 4

Analyse No.	$^{40}Ar/^{39}Ar$	$^{38}Ar/^{39}Ar$	$^{37}Ar/^{39}Ar$	$^{36}Ar/^{39}Ar$ $\times10^{-3}$ mol	^{39}Ar $\times10^{-14}$ mol	$\%^{40}Ar^{*}$	$^{40}Ar^{*}/^{39}Ar_K$	Age (Ma)	±1σ (Ma)
S07-Jojo		Phg		J= 0.009758					
1	2.972	0.095	0.00000	0.527	0.071	94.23	2.80	48.65	2.79
2	3.275	0.052	0.00000	1.882	0.053	82.55	2.70	46.98	3.46
3	3.656	0.167	0.06754	2.830	0.054	76.84	2.81	48.79	3.40
4	3.992	0.046	0.00892	3.987	0.058	70.12	2.80	48.61	3.24
5	4.386	0.027	0.01433	5.060	0.077	65.58	2.88	49.94	2.82
6	3.262	0.022	0.04950	0.199	0.055	97.83	3.19	55.33	3.48
7	3.788	0.026	0.09397	3.628	0.056	71.47	2.71	47.04	3.51
8	4.536	0.037	0.02412	5.532	0.044	63.66	2.89	50.13	4.49
9	3.353	0.018	0.05614	1.445	0.060	86.93	2.92	50.60	3.21
10	3.367	0.022	0.03595	3.090	0.102	72.50	2.44	42.47	2.03
T07-15bis		Phg		J= 0.009758					
1	4.029	0.034	0.00000	4.641	0.008	65.58	2.64	45.62	26.00
2	2.502	0.015	0.00000	0.419	0.122	94.42	2.36	40.84	1.70
3	7.203	0.020	0.03301	6.429	0.079	73.45	5.29	90.22	2.59
4	4.031	0.015	0.01014	4.031	0.110	70.08	2.83	48.74	1.73
5	3.499	0.020	0.00504	3.048	0.086	73.83	2.58	44.62	2.26
6	5.708	0.020	0.00871	9.503	0.045	50.54	2.89	49.76	4.62
7	4.986	0.020	0.01547	7.176	0.114	57.18	2.85	49.17	2.13
8	13.733	0.021	0.05281	30.376	0.026	34.55	4.75	81.12	8.45
9	4.407	0.024	0.00000	3.388	0.067	76.93	3.39	58.33	2.90
T07-16		Phg		J= 0.009758					
1	5.677	0.027	0.08906	11.631	0.037	39.30	2.23	38.59	5.01
2	3.803	0.035	0.00000	5.915	0.021	53.63	2.04	35.31	10.07
3	3.467	0.016	0.01456	2.067	0.077	81.96	2.84	49.01	2.20
4	3.573	0.018	0.00201	1.451	0.061	87.57	3.13	53.89	2.81
5	2.561	0.012	0.00000	0.178	0.093	97.33	2.49	43.06	1.85
6	3.066	0.014	0.00000	1.234	0.083	87.60	2.69	46.37	2.09
7	2.862	0.021	0.00000	0.550	0.095	93.78	2.68	46.33	1.85
8	2.852	0.014	0.00000	1.412	0.103	84.82	2.42	41.81	1.77
9	3.004	0.018	0.00986	1.863	0.096	81.18	2.44	42.14	2.04
10	2.862	0.021	0.00000	1.457	0.078	84.41	2.42	41.76	2.46
11	3.715	0.047	0.11295	2.610	0.026	79.04	2.94	50.63	7.61
T07-19		Phg		J= 0.009758					
1	1.931	0.020	0.00000	1.530	0.074	75.78	1.46	25.41	2.64
2	2.357	0.023	0.00092	2.351	0.078	69.86	1.65	28.56	2.54
3	2.974	0.037	0.00017	1.222	0.073	87.33	2.60	44.85	2.81
4	2.195	0.025	0.00000	3.285	0.079	55.06	1.21	21.01	2.54
5	2.365	0.032	0.01104	0.385	0.062	94.57	2.24	38.69	3.21
6	2.530	0.030	0.06742	1.348	0.093	83.84	2.12	36.72	1.99
7	2.671	0.025	0.00000	1.200	0.074	86.14	2.30	39.79	2.39
T07-18		Phg		J= 0.009758					
1	4.446	0.018	0.03794	6.208	0.110	58.45	2.60	44.88	2.22
2	4.848	0.016	0.02992	10.305	0.066	36.91	1.79	31.02	2.99
3	2.537	0.015	0.01001	2.539	0.111	69.83	1.77	30.71	1.69
4	3.382	0.015	0.00000	8.604	0.090	24.36	0.82	14.35	2.24
5	4.155	0.021	0.00000	0.851	0.114	93.57	3.89	66.73	8.37
6	2.574	0.017	0.05904	0.301	0.098	96.11	2.47	42.75	2.04
7	2.958	0.014	0.00000	0.799	0.080	91.49	2.71	46.71	2.22
I07-122				J= 0.009758					
1	3.799	0.114	0.00000	7.508	0.064	41.19	1.56	27.34	2.98
2	3.486	0.062	0.03792	1.160	0.063	89.80	3.13	54.28	3.00
3	3.364	0.025	0.00000	1.310	0.126	88.03	2.96	51.39	1.60
4	14.19	0.039	0.00123	30.589	0.130	36.19	5.14	88.22	3.76

5	4.743	0.040	0.00000	2.296	0.059	85.37	4.05	69.91	3.54
6	5.562	0.084	0.00000	2.289	0.061	87.56	4.87	83.76	3.63
7	56.951	0.384	0.00000	103.353	0.009	46.35	26.39	413.44	37.76
8	79.283	0.159	0.00000	31.187	0.022	88.36	70.05	939.77	49.78
9	3.558	0.035	0.26399	1.488	0.053	87.76	3.12	54.15	3.18
10	6.226	0.047	0.04896	3.130	0.052	84.95	5.29	90.79	3.74
11	5.457	0.035	0.00000	0.510	0.061	96.95	5.29	90.82	3.57
12	5.621	0.029	0.25356	3.855	0.063	79.79	4.49	77.29	3.68
13	3.336	0.020	0.13477	2.232	0.098	80.07	2.67	46.43	2.01

Table 5

Unit	Sample	Lithology	Method	Analyzed fractions	Age (Ma)	Uncertainty (Ma)	Reference
CBU	Ag31	Gln-Ep-Ph-eclogite	Lu/Hf	WR-Grt	52.2	0.3	Lagos et al., 2007
CBU	Ag85	Gln-Ep-Ph-eclogite	Lu/Hf	WR-Grt-Omp	51.4	0.4	Lagos et al., 2007
CBU	Ap21	Gln-Ep-Ph-eclogite	Lu/Hf	WR-Grt-Omp	50.2	2	Lagos et al., 2007
CBU	1081	omphacitite	Rb/Sr	WR-Ph	49.4	0.7	Brocker & Enders, 2001
CBU	1083	omphacitite	Rb/Sr	WR-Ph	46.3	0.4	Brocker & Enders, 2001
CBU	5243	calcschist	Rb/Sr	WR-Ph-Cal	28.7	2.4	Bröcker et al., 2013
CBU	5244	greenschist	Rb/Sr	WR-Ph-Ep-Ab	20.5	1.3	Bröcker et al., 2013
CBU	5246	greenschist	Rb/Sr	WR-Ph-Ep-Ab	25.3	0.9	Bröcker et al., 2013
CBU	5267	calcschist	Rb/Sr	WR-Ph-Cal	33.5	3.2	Bröcker et al., 2013
CBU	5831	greenschist	Rb/Sr	Ph-Ab-Cal-Ep	39.2	3.2	Bröcker et al., 2013
CBU	SYR015	greenschist in marble	Rb/Sr	Pg-Ph-Ep-Ab	30.8	2.9	Bröcker et al., 2013
CBU	63287a	calcschist	Rb/Sr	Ph	52.5	0.2	Cliff et al., 2016
CBU	63287a	calcschist	Rb/Sr	Ph	28.5	0.6	Cliff et al., 2016
CBU	63287a	calcschist	Rb/Sr	Ph	52.1	1.1	Cliff et al., 2016
CBU	63287a	calcschist	Rb/Sr	Ph	46.9	2.3	Cliff et al., 2016
CBU	63287b	calcschist	Rb/Sr	Ph	48.6	0.5	Cliff et al., 2016
CBU	63287b	calcschist	Rb/Sr	Ph	47.1	0.6	Cliff et al., 2016
CBU	63287b	calcschist	Rb/Sr	Ph	46.2	1.3	Cliff et al., 2016
CBU	63286	calcschist	Rb/Sr	Ph	35.2	1	Cliff et al., 2016
CBU	63286	calcschist	Rb/Sr	Ph	26	2.3	Cliff et al., 2016
CBU	63286	calcschist	Rb/Sr	Ph	37.4	0.8	Cliff et al., 2016
CBU	63286	calcschist	Rb/Sr	Ph	37.4	0.8	Cliff et al., 2016
CBU	63286	calcschist	Rb/Sr	Ph	37.5	1.7	Cliff et al., 2016
CBU	63297	calcschist	Rb/Sr	Ph	40.5	1.1	Cliff et al., 2016
CBU	63297	calcschist	Rb/Sr	Ph	35.6	0.5	Cliff et al., 2016
CBU	63297	calcschist	Rb/Sr	Ph	32.2	0.3	Cliff et al., 2016
CBU	63297	calcschist	Rb/Sr	Ph	34.6	1.1	Cliff et al., 2016
CBU	63297	calcschist	Rb/Sr	Ph	34.4	0.5	Cliff et al., 2016
CBU	63300	calcschist	Rb/Sr	Ph	37.1	0.4	Cliff et al., 2016
CBU	63300	calcschist	Rb/Sr	Ph	40.5	0.4	Cliff et al., 2016

CBU	63300	calcschist	Rb/Sr	Ph	41.8	2	Cliff et al., 2016
CBU	63300	calcschist	Rb/Sr	Ph	40.9	1.3	Cliff et al., 2016
CBU	63310	blueschist	Rb/Sr	Ph	31.3	0.4	Cliff et al., 2016
CBU	63310	blueschist	Rb/Sr	Ph	29.5	1.2	Cliff et al., 2016
CBU	63314	blueschist	Rb/Sr	Ttn	40.9	4.9	Cliff et al., 2016
CBU	63314	blueschist	Rb/Sr	Ttn	38.7	2.9	Cliff et al., 2016
CBU	63314	blueschist	Rb/Sr	Ph	29.2	0.7	Cliff et al., 2016
CBU	63314	blueschist	Rb/Sr	Ph	34	1.7	Cliff et al., 2016
CBU	63314	blueschist	Rb/Sr	Ph	39.5	3.1	Cliff et al., 2016
CBU	63314	blueschist	Rb/Sr	Ph	33.9	1.2	Cliff et al., 2016
CBU	63314	blueschist	Rb/Sr	Ph	29.7	0.7	Cliff et al., 2016
CBU	63314	blueschist	Rb/Sr	Ph	36.3	1.3	Cliff et al., 2016
CBU	63314	blueschist	Rb/Sr	Ph	34.3	1.2	Cliff et al., 2016
CBU	63314	blueschist	Rb/Sr	Ph	33.7	0.6	Cliff et al., 2016
CBU	S97/234	greenschist	Rb/Sr	Ph	33.6	0.4	Cliff et al., 2016
CBU	S97/234	greenschist	Rb/Sr	Ph	29.4	2.3	Cliff et al., 2016
CBU	S97/234	greenschist	Rb/Sr	Ph	23	1.1	Cliff et al., 2016
CBU	S97/234	greenschist	Rb/Sr	Ph	34	0.5	Cliff et al., 2016
CBU	63301	greenschist	Rb/Sr	Ph	30.1	0.7	Cliff et al., 2016
CBU	63301	greenschist	Rb/Sr	Ph	33.7	0.6	Cliff et al., 2016
CBU	1081	omphacitite	U/Pb	Zrn	77.86	0.2	Bröcker & Enders, 1999
CBU	4017	plagiogranite	U/Pb	Zrn	76.6	1.3	Bröcker & Keasling, 2006
CBU	3148	jadeitite	U/Pb	Zrn	79.8	0.7	Bröcker & Keasling, 2006
CBU	3149	omphacitite	U/Pb	Zrn	79.8	0.5	Bröcker & Keasling, 2006
CBU	3148	glaucophanite	U/Pb	Zrn	79.6	0.5	Bröcker & Keasling, 2006
CBU	3152	Chl-Act greenschist	U/Pb	Zrn	79.4	0.4	Bröcker & Keasling, 2006
CBU	BSY261	metagabbro	U/Pb	Zrn	80.2	1.6	Tomaschek et al., 2003
CBU	BSY260	metAplagiogranite	U/Pb	Zrn	76.4	2.1	Tomaschek et al., 2003
CBU	AG144	metAplagiogranite	U/Pb	Zrn	52.4	0.8	Tomaschek et al., 2003
CBU	S27.2.1	Chlorite-schist	U/Pb	Zrn	80.1	1.4	Bulle et al., 2010
CBU	S29.1.2	Chlorite-schist	U/Pb	Zrn	79.7	1.2	Bulle et al., 2010
CBU	S07-17	Quartzschist	Ar/Ar single grain	Ph	26.1	0.5	this study
CBU	S07-14	Grt-blueschist	Ar/Ar single grain	Ph	49.44	2.62	this study

CBU	S07-14	Grt-blueschist	Ar/Ar single grain	Ph	50.84	0.84	this study
CBU	S07-01	Gln-micaschist	Ar/Ar single grain	Ph	41.65	0.95	this study
CBU	S07-02	blueschist	Ar/Ar single grain	Ph	43.51	0.56	this study
CBU	S07-02	blueschist	Ar/Ar single grain	Ph	41.95	0.77	this study
CBU	S07-04	Gln-eclogite	Ar/Ar single grain	Ph	44.89	0.65	this study
CBU	S07-04bis	Gln-eclogite	Ar/Ar single grain	Ph	40.29	0.73	this study
CBU	AG144	metAplagiogranite	Ar/Ar concentrate	Pg	51.8	1.2	Tomaschek et al., 2003
CBU	SY89642	eclogite	Ar/Ar concentrate	Ph	49.2	0.2	Balwin, 1996
CBU	SY 01	metachert	Ar/Ar concentrate	Ph	53.5	1.3	Maluski et al., 1987
CBU	SY 7	calcschist	Ar/Ar concentrate	Ph	37	1	Maluski et al., 1987
CBU	SY 8	calcschist	Ar/Ar concentrate	Pg	49.7	1.2	Maluski et al., 1987
CBU	SY 66	Omp-metagabbro	Ar/Ar concentrate	Ph	45.3	3.4	Maluski et al., 1987
CBU	SY 30 F	Omp-Grt-metagabbro	Ar/Ar concentrate	Ph	40.2	1.1	Maluski et al., 1987
CBU	SY 501	Omp-metagabbro	Ar/Ar concentrate	Ph	30.3	0.9	Maluski et al., 1987
CBU	S07-16	Gln-micaschist	Ar/Ar concentrate	Ph	55.04	0.56	this study
Vari Unit	SY 20	metagranite	Ar/Ar concentrate	Ph	75	3	Maluski et al., 1987
CBU	BSY260	metAplagiogranite	Ar/Ar concentrate	Pg	37-44		Tomaschek et al., 2003
CBU	SY89644	Gln-schist	Ar/Ar concentrate	Ph	52-55		Baldwin, 1996
CBU	SY89645	blueschist	Ar/Ar concentrate	Ph	35-42		Baldwin, 1996
CBU	SY89647	-	Ar/Ar concentrate	Ph	21-28		Baldwin, 1996
CBU	SY89646	quartzite	Ar/Ar concentrate	Ph	31-41		Baldwin, 1996
CBU	SY89649	blueschist	Ar/Ar concentrate	Ph	40-44		Baldwin, 1996
CBU	5243	calcschist	Ar/Ar concentrate	Ph	28-42		Bröcker et al., 2013
CBU	5246	greenschist	Ar/Ar concentrate	Ph	22-31		Bröcker et al., 2013
CBU	5267	calcschist	Ar/Ar concentrate	Ph	35-40		Bröcker et al., 2013
CBU	SYR015	greenschist in marble	Ar/Ar concentrate	Pg-Ph	31-41		Bröcker et al., 2013
CBU	HR	marble	Ar/Ar concentrate	Ph	40.2	1.6	Rogowitz et al., 2015
CBU	SZ	marble	Ar/Ar concentrate	Ph	37.4	1.3	Rogowitz et al., 2015
CBU	AG10-31	eclogite	Ar/Ar concentrate	Ph	47-53		Lister and Forster, 2016
CBU	AG10-14	eclogite	Ar/Ar concentrate	Ph	41-51		Lister and Forster, 2016
CBU	AG10-15	blueschist	Ar/Ar concentrate	Ph	43-47		Lister and Forster, 2016
CBU	AG10-16	blueschist	Ar/Ar concentrate	Ph	47.3	0.4	Lister and Forster, 2016
CBU	AG10-26S	greenschist	Ar/Ar concentrate	Ph	22-31		Lister and Forster, 2016

CBU	AG10-26C	greenschist	Ar/Ar concentrate	Ph	17-28		Lister and Forster, 2016
CBU	SY-7	eclogite	Ar/Ar *in situ*	Ph	49.8	2.3	Pulitz et al., 2005
CBU	SY-7	eclogite	Ar/Ar *in situ*	Ph	45.9	3.1	Pulitz et al., 2005
CBU	SY-7	eclogite	Ar/Ar *in situ*	Ph	47.9	4.00	Pulitz et al., 2005
CBU	SY-7	eclogite	Ar/Ar *in situ*	Ph	45.4	2.6	Pulitz et al., 2005
CBU	SY-7	eclogite	Ar/Ar *in situ*	Ph	46.1	2.3	Pulitz et al., 2005
CBU	SY-7	eclogite	Ar/Ar *in situ*	Ph	43.9	2.8	Pulitz et al., 2005
CBU	SY-7	eclogite	Ar/Ar *in situ*	Ph	48.8	2.5	Pulitz et al., 2005
CBU	SY-7	eclogite	Ar/Ar *in situ*	Ph	47.7	0.9	Pulitz et al., 2005
CBU	SY-7	eclogite	Ar/Ar *in situ*	Ph	46.5	1.4	Pulitz et al., 2005
CBU	SY-7	eclogite	Ar/Ar *in situ*	Ph	49.6	2.4	Pulitz et al., 2005
CBU	SY-7	eclogite	Ar/Ar *in situ*	Ph	47.6	2.00	Pulitz et al., 2005
CBU	SY-7	eclogite	Ar/Ar *in situ*	Ph	45.2	1.2	Pulitz et al., 2005
CBU	SY-7	eclogite	Ar/Ar *in situ*	Ph	44.5	1.5	Pulitz et al., 2005
CBU	SY-7	eclogite	Ar/Ar *in situ*	Ph	45.7	0.9	Pulitz et al., 2005
CBU	SY-7	eclogite	Ar/Ar *in situ*	Ph	42.9	1.2	Pulitz et al., 2005
CBU	SY-7	eclogite	Ar/Ar *in situ*	Ph	46.00	0.6	Pulitz et al., 2005
CBU	SY-7	eclogite	Ar/Ar *in situ*	Ph	47.8	1.3	Pulitz et al., 2005
CBU	SY-7	eclogite	Ar/Ar *in situ*	Ph	47.4	0.9	Pulitz et al., 2005
CBU	SY-7	eclogite	Ar/Ar *in situ*	Ph	47.00	1.00	Pulitz et al., 2005
CBU	SY-7	eclogite	Ar/Ar *in situ*	Ph	44.3	0.8	Pulitz et al., 2005
CBU	SY-7	eclogite	Ar/Ar *in situ*	Ph	44.9	1.4	Pulitz et al., 2005
CBU	SY-7	eclogite	Ar/Ar *in situ*	Ph	43.3	1.9	Pulitz et al., 2005
CBU	SY-7	eclogite	Ar/Ar *in situ*	Ph	47.9	0.9	Pulitz et al., 2005
CBU	SY-7	eclogite	Ar/Ar *in situ*	Ph	49.8	1.4	Pulitz et al., 2005
CBU	SY-7	eclogite	Ar/Ar *in situ*	Ph	49.4	1.6	Pulitz et al., 2005
CBU	SY-7	eclogite	Ar/Ar *in situ*	Ph	44.5	2.3	Pulitz et al., 2005
CBU	SY-7	eclogite	Ar/Ar *in situ*	Ph	43.6	2.00	Pulitz et al., 2005
CBU	SY-25	Omp-metagabbro	Ar/Ar *in situ*	Ph	52.4	3.5	Pulitz et al., 2005
CBU	SY-25	Omp-metagabbro	Ar/Ar *in situ*	Ph	45.1	1.6	Pulitz et al., 2005
CBU	SY-25	Omp-metagabbro	Ar/Ar *in situ*	Ph	44.4	2.6	Pulitz et al., 2005
CBU	SY-25	Omp-metagabbro	Ar/Ar *in situ*	Ph	41.9	1.2	Pulitz et al., 2005
CBU	SY-25	Omp-metagabbro	Ar/Ar *in situ*	Ph	49.3	1.3	Pulitz et al., 2005

CBU	SY-25	Omp-metagabbro	Ar/Ar *in situ*	Ph	50.5	1.1	Pulitz et al., 2005
CBU	SY-25	Omp-metagabbro	Ar/Ar *in situ*	Ph	43.2	2.4	Pulitz et al., 2005
CBU	SY-25	Omp-metagabbro	Ar/Ar *in situ*	Ph	48.3	2.5	Pulitz et al., 2005
CBU	SY-25	Omp-metagabbro	Ar/Ar *in situ*	Ph	41.5	1.5	Pulitz et al., 2005
CBU	SY-25	Omp-metagabbro	Ar/Ar *in situ*	Ph	46.2	1.2	Pulitz et al., 2005
CBU	SY-25	Omp-metagabbro	Ar/Ar *in situ*	Ph	44.3	1.2	Pulitz et al., 2005
CBU	SY-25	Omp-metagabbro	Ar/Ar *in situ*	Ph	43.9	3.4	Pulitz et al., 2005
CBU	SY-25	Omp-metagabbro	Ar/Ar *in situ*	Ph	43.9	1.6	Pulitz et al., 2005
CBU	SY-25	Omp-metagabbro	Ar/Ar *in situ*	Ph	46.00	3.00	Pulitz et al., 2005
CBU	SY-25	Omp-metagabbro	Ar/Ar *in situ*	Ph	47.6	2.7	Pulitz et al., 2005
CBU	SY-25	Omp-metagabbro	Ar/Ar *in situ*	Ph	45.1	2.00	Pulitz et al., 2005
CBU	SY-25	Omp-metagabbro	Ar/Ar *in situ*	Ph	46.8	1.8	Pulitz et al., 2005
CBU	SY-25	Omp-metagabbro	Ar/Ar *in situ*	Ph	51.6	1.8	Pulitz et al., 2005
CBU	SY-25	Omp-metagabbro	Ar/Ar *in situ*	Ph	46.5	1.9	Pulitz et al., 2005
CBU	SY-25	Omp-metagabbro	Ar/Ar *in situ*	Ph	45.2	2.3	Pulitz et al., 2005
CBU	SY-25	Omp-metagabbro	Ar/Ar *in situ*	Ph	48.6	2.00	Pulitz et al., 2005
CBU	SY-25	Omp-metagabbro	Ar/Ar *in situ*	Ph	43.00	1.1	Pulitz et al., 2005
CBU	SY-25	Omp-metagabbro	Ar/Ar *in situ*	Ph	49.00	2.8	Pulitz et al., 2005
CBU	SY-25	Omp-metagabbro	Ar/Ar *in situ*	Ph	49.00	1.5	Pulitz et al., 2005
CBU	SY-25	Omp-metagabbro	Ar/Ar *in situ*	Ph	51.4	1.1	Pulitz et al., 2005
CBU	SY-25	Omp-metagabbro	Ar/Ar *in situ*	Ph	45.5	1.4	Pulitz et al., 2005
CBU	SY-25	Omp-metagabbro	Ar/Ar *in situ*	Ph	48.9	1.00	Pulitz et al., 2005
CBU	SY-25	Omp-metagabbro	Ar/Ar *in situ*	Ph	52.1	1.5	Pulitz et al., 2005
CBU	SY-25	Omp-metagabbro	Ar/Ar *in situ*	Ph	45.1	1.9	Pulitz et al., 2005
CBU	SY-25	Omp-metagabbro	Ar/Ar *in situ*	Ph	52.00	1.6	Pulitz et al., 2005
CBU	S07-Jojo	Gln-eclogite	Ar/Ar *in situ*	Ph	48.65	2.79	this study
CBU	S07-Jojo	Gln-eclogite	Ar/Ar *in situ*	Ph	46.98	3.46	this study
CBU	S07-Jojo	Gln-eclogite	Ar/Ar *in situ*	Ph	48.79	3.4	this study
CBU	S07-Jojo	Gln-eclogite	Ar/Ar *in situ*	Ph	48.61	3.24	this study
CBU	S07-Jojo	Gln-eclogite	Ar/Ar *in situ*	Ph	49.94	2.82	this study
CBU	S07-Jojo	Gln-eclogite	Ar/Ar *in situ*	Ph	55.33	3.048	this study
CBU	S07-Jojo	Gln-eclogite	Ar/Ar *in situ*	Ph	47.04	3.51	this study
CBU	S07-Jojo	Gln-eclogite	Ar/Ar *in situ*	Ph	50.13	4.49	this study

CBU	S07-Jojo	Gln-eclogite	Ar/Ar *in situ*	Ph	50.6	3.21	this study
CBU	S07-Jojo	Gln-eclogite	Ar/Ar *in situ*	Ph	42.47	2.03	this study
Vari Unit	Syr5	orthogneiss	FT	Ap	10.7	5.5	Ring et al., 2003
Vari Unit	Syr5	orthogneiss	FT	Zrn	21.2	1.3	Ring et al., 2003
Vari Unit	Syr6	orthogneiss	FT	Zrn	19.6	1.3	Ring et al., 2003
CBU	1078	jadeitite	FT	Zrn	10.1	0.7	Ring et al., 2003
CBU	1081	omphacitite	FT	Zrn	11.9	0.6	Ring et al., 2003
CBU	1083	omphacitite	FT	Zrn	11.00	0.9	Ring et al., 2003
CBU	1085	omphacitite	FT	Zrn	11.1	0.9	Ring et al., 2003
CBU	zGr2	gneiss-schist	(U-Th)/He	Zrn	9.0	0.7	Soukis and Stöckli, 2013
CBU	zGr3	gneiss-schist	(U-Th)/He	Zrn	8.8	0.7	Soukis and Stöckli, 2013
CBU	zGr6	gneiss-schist	(U-Th)/He	Zrn	9.2	0.7	Soukis and Stöckli, 2013
CBU	zGr8	gneiss-schist	(U-Th)/He	Zrn	12.4	1.0	Soukis and Stöckli, 2013
CBU	Gr5	gneiss-schist	(U-Th)/He	Ap	12.0	0.72	Soukis and Stöckli, 2013
CBU	Gr6	gneiss-schist	(U-Th)/He	Ap	9.6	0.58	Soukis and Stöckli, 2013
CBU	Gr8	gneiss-schist	(U-Th)/He	Ap	10.0	0.6	Soukis and Stöckli, 2013
Vari Unit	zGr12	gneiss	(U-Th)/He	Zrn	15.8	1.3	Soukis and Stöckli, 2013
Vari Unit	zGr14	gneiss	(U-Th)/He	Zrn	8.1	0.6	Soukis and Stöckli, 2013
Vari Unit	zGr15	gneiss	(U-Th)/He	Zrn	13.7	1.1	Soukis and Stöckli, 2013
Vari Unit	zGr16	gneiss	(U-Th)/He	Zrn	14.4	1.2	Soukis and Stöckli, 2013
Vari Unit	zGr17	quartzite	(U-Th)/He	Zrn	14.1	1.1	Soukis and Stöckli, 2013
Vari Unit	zGr18	granitic gneiss	(U-Th)/He	Zrn	13.3	1.1	Soukis and Stöckli, 2013
Vari Unit	Gr12	gneiss	(U-Th)/He	Ap	14.5	0.9	Soukis and Stöckli, 2013
Vari Unit	Gr14	gneiss	(U-Th)/He	Ap	15.0	0.9	Soukis and Stöckli, 2013
Vari Unit	Gr15	gneiss	(U-Th)/He	Ap	12.4	0.74	Soukis and Stöckli, 2013
Vari Unit	Gr18	granitic gneiss	(U-Th)/He	Ap	6.3	0.4	Soukis and Stöckli, 2013

Table 6

Unit	Sample	Lithology	Method	Analyzed fractions	Age (Ma)	Uncertainty (Ma)	Reference
CBU	3513	impure marble	Rb/Sr	Ph-Cal	24.2	0.2	Brocker & Franz, 2005
CBU	3514	impure marble	Rb/Sr	Ph-Cal	25	0.3	Brocker & Franz, 2005
CBU	3515	impure marble	Rb/Sr	Ph-Cal	23.5	0.2	Brocker & Franz, 2005
CBU	3519	calcschist	Rb/Sr	Ph-Cal	22	0.2	Brocker & Franz, 2005
CBU	3520	impure marble	Rb/Sr	Ph-Cal	22.9	0.9	Brocker & Franz, 2005
CBU	3522	calcschist	Rb/Sr	Ph-Cal	21.9	0.2	Brocker & Franz, 2005
CBU	3521	impure marble	Rb/Sr	Ph-Cal	24	0.2	Brocker & Franz, 2005
CBU	2016	calcschist	Rb/Sr	Ph-Cal	21.5	0.2	Brocker & Franz, 2005
CBU	1221	phyllite	Rb/Sr	Ph-WR	23.3	0.4	Brocker & Franz, 2005
CBU	1222	quartzite	Rb/Sr	Ph-WR	23.8	0.3	Brocker & Franz, 2005
CBU	1418	phyllite	Rb/Sr	Ph-WR	24.1	0.2	Brocker & Franz, 2005
CBU	1421	phyllite	Rb/Sr	Ph-WR	24.1	0.2	Brocker & Franz, 2005
CBU	3518	quartzite	Rb/Sr	Ph-Cal	24	0.2	Brocker & Franz, 2005
CBU	1076	greenschist-facies calcschist	Rb/Sr	WR-Ph	21.7	0.2	Brocker & Franz, 1998
CBU	318	metasediment	Rb/Sr	WR-Ph	22.00	0.2	Bröcker & Franz, 2000
CBU	305	metasediment	Rb/Sr	WR-Ep-Ph	26.2	0.3	Bröcker & Franz, 2000
CBU	461	metasediment	Rb/Sr	WR-Ph	21.2	0.2	Bröcker & Franz, 2000
CBU	1163	metasediment	Rb/Sr	WR-Ph	21.8	0.3	Bröcker & Franz, 2000
CBU	526	metasediment	Rb/Sr	WR-Ph	25.6	0.3	Bröcker & Franz, 2000
CBU	348	metasediment	Rb/Sr	WR-Ph	32.1	0.3	Bröcker & Franz, 2000
CBU	348	metasediment	Rb/Sr	WR-Bt	14.1	0.2	Bröcker & Franz, 2000
CBU	28	metasediment	Rb/Sr	WR-Bt	8.2	0.1	Bröcker & Franz, 2000
CBU	275	metasediment	Rb/Sr	WR-Bt	14.8	0.2	Bröcker & Franz, 2000
CBU	453	metasediment	Rb/Sr	WR-Bt	14.3	0.1	Bröcker & Franz, 2000
CBU	492	metasediment	Rb/Sr	WR-Bt	10.00	0.1	Bröcker & Franz, 2000
CBU	3008	impure marble	Rb/Sr	Ph-Cal	41.1	0.4	Bröcker et al., 2004
CBU	3009	impure marble	Rb/Sr	Ph-Cal	37.2	0.5	Bröcker et al., 2004
CBU	3012	impure marble	Rb/Sr	Ph-Cal	24.2	0.3	Bröcker et al., 2004
CBU	3013	impure marble	Rb/Sr	Ph-Cal	23.9	0.3	Bröcker et al., 2004
CBU	3014	impure marble	Rb/Sr	Ph-Cal	24.5	0.3	Bröcker et al., 2004

CBU	3016	impure marble	Rb/Sr	Ph-Cal	34.9	0.4	Bröcker et al., 2004
CBU	47	blueschist-facies metabasite	Rb/Sr	WR-Ph	36.9	0.4	Brocker & Franz, 1998
CBU	61	blueschist-facies metabasite	Rb/Sr	WR-Ph-Ep	39.00	1.6	Brocker & Franz, 1998
CBU	223	blueschist-facies metabasite	Rb/Sr	WR-Ph	37.4	0.4	Brocker & Franz, 1998
CBU	14	greenschist-facies metabasite	Rb/Sr	WR-Ph	28.9	0.3	Brocker & Franz, 1998
CBU	221	blueschist-facies micaschist	Rb/Sr	WR-Ph	32.5	0.6	Brocker & Franz, 1998
CBU	10	blueschist-facies micaschist	Rb/Sr	WR-Ph	39.5	0.4	Brocker & Franz, 1998
CBU	1192	greenschist-facies micaschist	Rb/Sr	WR-Ph	37.4	0.4	Brocker & Franz, 1998
CBU	1193	greenschist-facies micaschist	Rb/Sr	WR-Ph	39.9	0.7	Brocker & Franz, 1998
CBU	91	greenschist-facies calcschist	Rb/Sr	WR-Ph	22.4	0.2	Brocker & Franz, 1998
CBU	128	greenschist-facies calcschist	Rb/Sr	WR-Ph	23.5	0.2	Brocker & Franz, 1998
CBU	90	greenschist-facies meta-acidite	Rb/Sr	WR-Ph-Ep	21.00	0.9	Brocker & Franz, 1998
CBU	155	greenschist-facies meta-acidite	Rb/Sr	WR-Ph	20.9	0.8	Brocker & Franz, 1998
CBU	340	greenschist-facies meta-acidite	Rb/Sr	WR-Ph	22.5	1.5	Brocker & Franz, 1998
Upper Unit	1096	phyllite	Rb/Sr	WR-Ph-WR	20.8	2.1	Brocker & Franz, 1998
Upper Unit	1060	mafic phyllite	Rb/Sr	WR-Ph-WR	28.3	1.00	Brocker & Franz, 1998
Upper Unit	1054	metagabbro	Rb/Sr	WR-Ph	39.00	0.4	Brocker & Franz, 1998
Upper Unit	1157	phyllite	Rb/Sr	WR-Ph	16.6	0.5	Brocker & Franz, 1998
Upper Unit	1059	phyllite	Rb/Sr	Ph-Pl	92.4	1.4	Brocker & Franz, 1998
intrusion	T3	I-type granite	Rb-Sr	WR-Bt	13.98	0.2	Altherr et al. , 1982
intrusion	T13	I-type granite	Rb-Sr	WR-Bt	14.25	0.26	Altherr et al. , 1982
intrusion	T9-T10-T11-T16	S-type granite	Rb-Sr	WR	14.01	0.11	Altherr et al. , 1982
CBU	85-32	meta-tuff	Ar/Ar concentrate	Ph	41-42		Brocker et al., 1993
CBU	85-531	omphacitite	Ar/Ar concentrate	Ph	42-44		Brocker et al., 1993
CBU	85-39	omphacitite	Ar/Ar concentrate	Ph	36-42		Brocker et al., 1993
CBU	85-204	Cld-schist	Ar/Ar concentrate	Ph+Pg	38-48		Brocker et al., 1993
CBU	85-103	meta-acidite	Ar/Ar concentrate	Ph	23-32		Brocker et al., 1993
CBU	85-558	Chl-Ab-Ep gneiss	Ar/Ar concentrate	Ph	27-32		Brocker et al., 1993
CBU	85-145	schist	Ar/Ar concentrate	Ph	21-29		Brocker et al., 1993
CBU	85-155	Ep-Ab-gneiss	Ar/Ar concentrate	Ph	21-25		Brocker et al., 1993
CBU	85-90	meta-acidite	Ar/Ar concentrate	Ph	14-22		Brocker et al., 1993
CBU	85-168	meta-tuff	Ar/Ar concentrate	Ph	16-23		Brocker et al., 1993
CBU	85-400x	meta-acidite	Ar/Ar concentrate	Ph	14-23		Brocker et al., 1993

CBU	85-340	meta-acidite	Ar/Ar concentrate Ph	17-22		Brocker et al., 1993
CBU	3008	impure marble	Ar/Ar concentrate Ph	40-44		Bröcker et al., 2004
CBU	3013	impure marble	Ar/Ar concentrate Ph	25.5-28.5		Bröcker et al., 2004
CBU	3014	impure marble	Ar/Ar concentrate Ph	24.5-28		Bröcker et al., 2004
CBU	3016	impure marble	Ar/Ar concentrate Ph	34.5-41		Bröcker et al., 2004
Upper Unit	S-5	phyllite	Ar/Ar concentrate Ph	8-31.3		Zeffren et al., 2005
Upper Unit	S-6	phyllite	Ar/Ar concentrate Ph	21-27		Zeffren et al., 2005
Upper Unit	S-48	phyllite	Ar/Ar concentrate Ph	6.3-31		Zeffren et al., 2005
Upper Unit	S-14	phyllite	Ar/Ar concentrate Ph	16-118		Zeffren et al., 2005
Upper Unit	S-40	phyllite	Ar/Ar concentrate Ph	10.5-53		Zeffren et al., 2005
CBU	T07-07-pop	quartzschist	Ar/Ar concentrate Ph	23-27		This study
Upper Unit	T07-18-pop	marble	Ar/Ar concentrate Ph	26-41		This study
CBU	T07-25-pop	quartzschist	Ar/Ar concentrate Ph	26-31		This study
CBU	85-47	glaucophanite	Ar/Ar concentrate Ph	43.8	0.2	Brocker et al., 1993
CBU	85-61	glaucophanite	Ar/Ar concentrate Ph	42.3	0.2	Brocker et al., 1993
CBU	85-221	Gln-micaschist	Ar/Ar concentrate Ph+Pg	44.5	0.3	Brocker et al., 1993
CBU	87-9	Gln-Cld-micaschist	Ar/Ar concentrate Ph+Pg	40.2	0.2	Brocker et al., 1993
CBU	87-14	greenschist	Ar/Ar concentrate Ph	32.5	0.2	Brocker et al., 1993
Upper Unit	S-54	phyllite	Ar/Ar concentrate Ph	32.4	0.38	Zeffren et al., 2005
intrusion	T3	I-type granodiorite	Ar/Ar concentrate hb	13.7	0.7	Brichau et al., 2007
intrusion	T4	I-type granodiorite	Ar/Ar concentrate hb	14.4	0.8	Brichau et al., 2007
CBU	T07-09	calcschist	Ar/Ar single grain Ph	37.53	1.3	This study
CBU	T07-10alpha	Ep-vein	Ar/Ar single grain Ph	34.48	0.99	This study
CBU	T07-10beta	Chl-schist	Ar/Ar single grain Ph	44.34	1.16	This study
CBU	T07-11-1	Grt-blueschist	Ar/Ar single grain Ph	47.67	0.77	This study
CBU	T07-11-2	Grt-blueschist	Ar/Ar single grain Ph	42.09	0.6	This study
CBU	T07-13-1	Grt-blueschist	Ar/Ar single grain Ph	40.43	1.53	This study
CBU	T07-13-2	Grt-blueschist	Ar/Ar single grain Ph	38.89	0.48	This study
CBU	T07-14-2	Grt-blueschist	Ar/Ar single grain Ph	48.37	1.35	This study
CBU	T07-16-1	Grt-micaschist	Ar/Ar single grain Ph	41.78	0.86	This study
CBU	T07-16-2	Grt-micaschist	Ar/Ar single grain Ph	41.96	0.83	This study
CBU	T07-22	Ep-vein	Ar/Ar single grain Ph	41.64	0.46	This study
CBU	T07-24	quartzschist	Ar/Ar single grain Ph	23.77	0.94	This study

CBU	T07-25	quartzschist	Ar/Ar single grain	Ph	31.84	0.46	This study
CBU	T07-27	quartzschist	Ar/Ar single grain	Ph	31.47	0.82	This study
intrusion	T07-30	granodiorite	Ar/Ar single grain	Bt	13.9	2.4	This study
CBU	T07-15bis	Grt-micaschist	Ar/Ar *in situ*	Ph	40.84	1.7	This study
CBU	T07-15bis	Grt-micaschist	Ar/Ar *in situ*	Ph	48.74	1.73	This study
CBU	T07-15bis	Grt-micaschist	Ar/Ar *in situ*	Ph	44.62	2.26	This study
CBU	T07-15bis	Grt-micaschist	Ar/Ar *in situ*	Ph	49.76	4.62	This study
CBU	T07-15bis	Grt-micaschist	Ar/Ar *in situ*	Ph	49.17	2.13	This study
CBU	T07-16	Grt-micaschist	Ar/Ar *in situ*	Ph	38.59	5.01	This study
CBU	T07-16	Grt-micaschist	Ar/Ar *in situ*	Ph	35.31	10.07	This study
CBU	T07-16	Grt-micaschist	Ar/Ar *in situ*	Ph	49.01	2.2	This study
CBU	T07-16	Grt-micaschist	Ar/Ar *in situ*	Ph	53.89	2.81	This study
CBU	T07-16	Grt-micaschist	Ar/Ar *in situ*	Ph	43.06	1.85	This study
CBU	T07-16	Grt-micaschist	Ar/Ar *in situ*	Ph	46.37	2.09	This study
CBU	T07-16	Grt-micaschist	Ar/Ar *in situ*	Ph	46.33	1.85	This study
CBU	T07-16	Grt-micaschist	Ar/Ar *in situ*	Ph	41.81	1.77	This study
CBU	T07-16	Grt-micaschist	Ar/Ar *in situ*	Ph	42.14	2.04	This study
CBU	T07-16	Grt-micaschist	Ar/Ar *in situ*	Ph	41.76	2.46	This study
Upper Unit	T07-18	marble	Ar/Ar *in situ*	Ph	44.88	2.22	This study
Upper Unit	T07-18	marble	Ar/Ar *in situ*	Ph	31.02	2.99	This study
Upper Unit	T07-18	marble	Ar/Ar *in situ*	Ph	30.71	1.69	This study
Upper Unit	T07-18	marble	Ar/Ar *in situ*	Ph	14.35	2.24	This study
Upper Unit	T07-18	marble	Ar/Ar *in situ*	Ph	42.75	2.04	This study
Upper Unit	T07-18	marble	Ar/Ar *in situ*	Ph	46.71	2.22	This study
CBU	T07-19	Chl-schist	Ar/Ar *in situ*	Ph	25.41	2.64	This study
CBU	T07-19	Chl-schist	Ar/Ar *in situ*	Ph	28.56	2.54	This study
CBU	T07-19	Chl-schist	Ar/Ar *in situ*	Ph	44.85	2.81	This study
CBU	T07-19	Chl-schist	Ar/Ar *in situ*	Ph	21.01	2.54	This study
CBU	T07-19	Chl-schist	Ar/Ar *in situ*	Ph	38.69	3.21	This study
CBU	T07-19	Chl-schist	Ar/Ar *in situ*	Ph	36.72	1.98	This study
CBU	T07-19	Chl-schist	Ar/Ar *in situ*	Ph	39.79	2.39	This study
intrusion	T3	I-type granodiorite	U/Pb	Zrn	14.63	0.22	Brichau et al., 2007
intrusion	-	S-type granite	U/Pb	Zrn	14.4	0.2	Keay, 1998

CBU	18.2	Eclogite	U/Pb	Zrn	78.2	1.4	Bulle et al., 2010
CBU	20.1.7	Meta-gabbro	U/Pb	Zrn	77.3	1.4	Bulle et al., 2010
CBU	19.9.3a	Glaucophanite	U/Pb	Zrn	81.8	2.7	Bulle et al., 2010
CBU	19.13	Blackwall	U/Pb	Zrn	77.5	3.2	Bulle et al., 2010
CBU	5224	Chlorite schist	U/Pb	Zrn	77.0	2.4	Bulle et al., 2010
CBU	29.1.2	Chlorite schist	U/Pb	Zrn	79.7	1.2	Bulle et al., 2010
CBU	T29	Quartz mica schist	U/Pb	Zrn	78.9	1.3	Bulle et al., 2010
CBU	5220a	Quartz mica schist	U/Pb	Zrn	78.5	0.9	Bulle et al., 2010
CBU	5220b	Quartz mica schist	U/Pb	Zrn	56.8	1.2	Bulle et al., 2010
intrusion	T3	I-type granite	FT	Spn	13.8	2.0	Altherr et al. , 1982
CBU	GR56	Ab-gneiss	FT	Ap	13.1	4.4	Hejl et al., 2002
intrusion	T3	I-type granite	FT	Ap	10.8	2.0	Altherr et al. , 1982
intrusion	T2	I-type granodiorite	FT	Ap	11.9	2.0	Brichau et al., 2007
intrusion	T3	I-type granodiorite	FT	Ap	12.6	2.6	Brichau et al., 2007
intrusion	T4	I-type granodiorite	FT	Ap	12.8	2.4	Brichau et al., 2007
intrusion	GR51	I-type monzogranite	FT	Ap	9.3	0.8	Hejl et al., 2002
intrusion	GR52	I-type monzogranite	FT	Ap	9.3	0.8	Hejl et al., 2002
intrusion	GR53	I-type monzogranite	FT	Ap	9.5	0.8	Hejl et al., 2002
intrusion	GR54	I-type monzogranite	FT	Ap	8.4	0.7	Hejl et al., 2002
CBU	1047	eclogite	FT	Zrn	9.6	1.7	Ring et al., 2003
CBU	1048	eclogite	FT	Zrn	10.2	1.2	Ring et al., 2003
intrusion	T2	I-type granodiorite	FT	Zrn	12.2	1.00	Brichau et al., 2007
intrusion	T3	I-type granodiorite	FT	Zrn	13.3	0.8	Brichau et al., 2007
intrusion	T4	I-type granodiorite	FT	Zrn	13.8	1.0	Brichau et al., 2007
intrusion	T5	S-type granite	FT	Zrn	14.4	1.2	Brichau et al., 2007
intrusion	T2	I-type granodiorite	U-Th/He	Ap	10.00	0.6	Brichau et al., 2007
intrusion	T3	I-type granodiorite	U-Th/He	Ap	10.4	0.8	Brichau et al., 2007
intrusion	T4	I-type granodiorite	U-Th/He	Ap	11.9	1.0	Brichau et al., 2007
intrusion	T2	I-type granodiorite	U-Th/He	Zrn	9.2	0.8	Brichau et al., 2007
intrusion	T4	I-type granodiorite	U-Th/He	Zrn	10.7	0.6	Brichau et al., 2007

Table 7

Unit	Sample	Lithology	Method	Analyzed fractions	Age (Ma)	Uncertainty (Ma)	Reference
CCB	77-227	orthogneiss	Rb/Sr	WR-Ph	13.2	0.4	Henjes-Kunst & Kreuzer, 1982
CCB	IOS04-1	orthogneiss	Rb/Sr	Fsp-Ap-Ph	18	1	Thomson, et al., 2009
CBU	IOS03-2	impure marble	Rb/Sr	Ph-Cal	34.5	2.5	Thomson, et al., 2009
CBU	IOS04-6	impure marble	Rb/Sr	Ph-Cal	18.8	0.3	Thomson, et al., 2009
CBU	IOS04-7	quartzite	Rb/Sr	Ph-Fsp	27	8.0	Thomson, et al., 2009
CCB	AG03-10	Grt-micaschist	Ar/Ar concentrate	Ph	30-40		Forster & Lister, 2009
CCB	AG03-08	Grt-micaschist	Ar/Ar concentrate	Ph	29-33.5		Forster & Lister, 2009
CCB	AG03-09	Grt-micaschist	Ar/Ar concentrate	Ph	29-32		Forster & Lister, 2009
CCB	AG03-01	leucogranite	Ar/Ar concentrate	Ph	42.5-44		Forster & Lister, 2009
CCB	AG03-03	orthogneiss	Ar/Ar concentrate	Ph	70-74		Forster & Lister, 2009
CCB	AG03-04	orthogneiss	Ar/Ar concentrate	Ph	62.5-65.5		Forster & Lister, 2009
CCB	AG03-05	orthogneiss	Ar/Ar concentrate	Ph	68.5-73		Forster & Lister, 2009
CCB	AG03-06	orthogneiss	Ar/Ar concentrate	Ph	55.5-57		Forster & Lister, 2009
CCB	88607	orthogneiss	Ar/Ar concentrate	Ph	59-63		Baldwin & Lister, 1998
CCB	90368	orthogneiss	Ar/Ar concentrate	Ph	52-57		Baldwin & Lister, 1998
CBU	88606	schiste à q-Ph	Ar/Ar concentrate	Ph	30.5-42		Baldwin, 1996
CBU	88610	Gln-schist	Ar/Ar concentrate	Ph	25.6-39.8		Baldwin, 1996
CBU	88638	Gln-schist	Ar/Ar concentrate	Ph	25-44		Baldwin, 1996
CBU	88639	Gln-schist	Ar/Ar concentrate	Ph	23.5-42		Baldwin, 1996
CBU	88641	Gln-Grt-schist	Ar/Ar concentrate	Ph	25.3-49.3		Baldwin, 1996
CCB	90350	Grt-micaschist	Ar/Ar concentrate	Ph+Pg	53	2	Baldwin & Lister, 1998
CCB	90354	orthogneiss	Ar/Ar concentrate	Ph	31	1	Baldwin & Lister, 1998
CCB	88609	orthogneiss	Ar/Ar concentrate	Ph	20	1	Baldwin & Lister, 1998
CCB	AG03-07	orthogneiss	Ar/Ar concentrate	Ph	24.9	0.1	Forster & Lister, 2009
CBU	I07-15	Ab-Ep-blueschist	Ar/Ar single grain	Ph	41	1.72	this study
CBU	I07-18	Grt-blueschist	Ar/Ar single grain	Ph	48.46	0.82	this study
CBU	I07-122	Grt-Cld-micaschist	Ar/Ar *in situ*	Ph	46.4	2	this study
CBU	I07-122	Grt-Cld-micaschist	Ar/Ar *in situ*	Ph	77.3	3.7	this study
CBU	I07-122	Grt-Cld-micaschist	Ar/Ar *in situ*	Ph	90.8	3.6	this study
CBU	I07-122	Grt-Cld-micaschist	Ar/Ar *in situ*	Ph	90.8	3.7	this study

CBU	I07-122	Grt-Cld-micaschist	Ar/Ar *in situ*	Ph	54.2	3.2	this study
CBU	I07-122	Grt-Cld-micaschist	Ar/Ar *in situ*	Ph	939.8	79.8	this study
CBU	I07-122	Grt-Cld-micaschist	Ar/Ar *in situ*	Ph	413.4	37.8	this study
CBU	I07-122	Grt-Cld-micaschist	Ar/Ar *in situ*	Ph	83.8	3.6	this study
CBU	I07-122	Grt-Cld-micaschist	Ar/Ar *in situ*	Ph	69.91	3.5	this study
CBU	I07-122	Grt-Cld-micaschist	Ar/Ar *in situ*	Ph	88.2	3.8	this study
CBU	I07-122	Grt-Cld-micaschist	Ar/Ar *in situ*	Ph	51.4	1.6	this study
CBU	I07-122	Grt-Cld-micaschist	Ar/Ar *in situ*	Ph	54.3	3	this study
CBU	I07-122	Grt-Cld-micaschist	Ar/Ar *in situ*	Ph	27.3	3	this study
CCB	83	orthogneiss	FT	Ap	13.2	1.1	Hejl et al., 2008
CCB	85	orthogneiss	FT	Ap	11.2	1.4	Hejl et al., 2008
CCB	87	orthogneiss	FT	Ap	9.2	1.1	Hejl et al., 2008
CCB	88	orthogneiss	FT	Ap	8.3	1.1	Hejl et al., 2008
CCB	116	orthogneiss	FT	Ap	21	5.5	Hejl et al., 2008
CCB	I2	orthogneiss	FT	Ap	12.2	1.4	Brichau, 2004
CCB	I8	orthogneiss	FT	Ap	11	1.4	Brichau, 2004
CCB	IOS03-6	orthogneiss	FT	Ap	14	1.3	Thomson, et al., 2009
CCB	IOS03-7	orthogneiss	FT	Ap	14.4	2.2	Thomson, et al., 2009
CCB	IOS04-1	orthogneiss	FT	Ap	13.9	2.2	Thomson, et al., 2009
CCB	IOS04-2	orthogneiss	FT	Ap	13	1	Thomson, et al., 2009
CBU	IOS03-2	carbonate	FT	Ap	8.4	2.1	Thomson, et al., 2009
CBU	IOS03-3	-	FT	Ap	14.6	2.4	Thomson, et al., 2009
CBU	IOS03-4	Grt-Ep-blueschist	FT	Ap	6.9	3.2	Thomson, et al., 2009
CBU	IOS03-5	-	FT	Ap	13.3	1.2	Thomson, et al., 2009
CCB	I11	orthogneiss	FT	Zrn	14.5	1.6	Brichau, 2004
CCB	I2	orthogneiss	FT	Zrn	14	1.6	Brichau, 2004
CCB	I8	orthogneiss	FT	Zrn	13.2	1.4	Brichau, 2004
CCB	IOS03-6	orthogneiss	FT	Zrn	13.9	2.2	Thomson, et al., 2009
CCB	IOS03-7	orthogneiss	FT	Zrn	14.7	1.1	Thomson, et al., 2009
CCB	IOS03-7	orthogneiss	FT	Zrn	12.6	0.8	Thomson, et al., 2009
CCB	IOS03-7	orthogneiss	FT	Zrn	13.5	1.4	Thomson, et al., 2009
CCB	IOS04-1	orthogneiss	FT	Zrn	14.6	1	Thomson, et al., 2009
CCB	IOS04-2	orthogneiss	FT	Zrn	13.6	1.9	Thomson, et al., 2009

CCB	IOS04-4	orthogneiss	FT	Zrn	13.6	0.9	Thomson, et al., 2009
CBU	IOS03-4	Grt-Ep-blueschist	FT	Zrn	15.1	1.2	Thomson, et al., 2009
CBU	IOS03-5	-	FT	Zrn	14.4	1.3	Thomson, et al., 2009
CBU	IOS04-9	-	FT	Zrn	13.8	1.2	Thomson, et al., 2009
CCB	I8	orthogneiss	U-Th/He	Ap	9.5	0.8	Brichau, 2004
CCB	I2	orthogneiss	U-Th/He	Ap	10.8	1	Brichau, 2004
CCB	I0S03-6	orthogneiss	U-Th/He	Ap	10.58	0.68	Thomson, et al., 2009
CCB	I0S04-1	orthogneiss	U-Th/He	Ap	9.31	0.59	Thomson, et al., 2009
CCB	I0S04-2	orthogneiss	U-Th/He	Ap	9.52	0.23	Thomson, et al., 2009
CCB	I0S03-5	-	U-Th/He	Ap	11.4	0.78	Thomson, et al., 2009

Highlights

1) Extraneous argon is heterogeneously distributed in the CBU and of minor importance

2) Extraneous argon in the CBU is correlated to the vicinity of the Cycladic Basement

3) Clear evidence of excess argon in microstructures where fluid circulation is enhanced

4) A minimum closure temperature of 550°C is proposed for phengites of the CBU

5) Recrystallization is the main process controlling $^{40}Ar/^{39}Ar$ ages in HP rocks